FIBER-REINFORCED POLYMER STRENGTHENING OF WAR MEMORIAL

BRIDGE—INSTALLATION, LOAD TESTING, AND ANALYSIS

Except where reference is made to the work of others, the work described in this thesis is my own or was done in collaboration with my advisory committee. This thesis does not include proprietary or classified information.

_____

Benjamin Mark Carmichael

Certificate of Approval

_____	_____
Anton K. Schindler Assistant Professor Civil Engineering	Robert W. Barnes, Chair Associate Professor Civil Engineering
_____	_____
G. Ed Ramey Professor Civil Engineering	Stephen L. McFarland Dean Graduate School

FIBER-REINFORCED POLYMER STRENGTHENING OF WAR MEMORIAL BRIDGE—INSTALLATION, LOAD TESTING, AND ANALYSIS

Benjamin Mark Carmichael

A Thesis

Submitted to

the Graduate Faculty of

Auburn University

in Partial Fulfillment of the

Requirements for the

Degree of

Master of Science

Auburn, Alabama
December 16, 2005

FIBER-REINFORCED POLYMER STRENGTHENING OF WAR MEMORIAL

BRIDGE—INSTALLATION, LOAD TESTING, AND ANALYSIS

Benjamin Mark Carmichael

_____

Signature of Author

_____

Date of Graduation

THESIS ABSTRACT

FIBER-RINFORCED POLYMER STRENGTHENING OF WAR MEMORIAL BRIDGE—INSTALLATION, LOAD TESTING, AND ANALYSIS

Benjamin Mark Carmichael
Master of Science, December 16, 2005
(B.E.E., Auburn University, 2000)

151 Typed Pages

Directed by Robert W. Barnes

An assessment of the rehabilitation of a reinforced-concrete bridge using carbon fiber reinforced polymer (FRP) laminate materials is presented. The installation of FRP strips to girder bottoms in the positive moment section of a three-span, continuous bridge is detailed, as well as a summary of the load testing procedure. Comparisons and evaluations are made between load tests performed before strengthening and after strengthening. A finite-element model was created, and data generated from analysis was utilized in a cracked section analysis to determine analytical bridge characteristics. These findings are compared to experimental data and presented to aid in assessing post-strengthened bridge behavior and examine its viability as a design and evaluation aid. A strength capacity increase was achieved, and no significant performance degradation was observed in six months' service use. The results are given in order to help the reader evaluate the benefit of FRP as a rehabilitation method for aging infrastructure.

Style Manual: Kate L. Turabian, *A Manual for Writers of Term Papers, Theses, and Dissertations,* Sixth Edition

Software Used: Microsoft Word

TABLE OF CONTENTS

LIST OF TABLES

LIST OF FIGURES

CHAPTER 1: INTRODUCTION

1.1 BACKGROUND

As of the year 2000, of the nearly 600,000 bridges in the National Bridge Inventory Database, 87,801 are classified as structurally deficient and 79,860 are classified as functionally obsolete (NBI 2005). Efforts to compensate for deficiencies and rehabilitate these bridges range from posting load limits for traffic usage to minor repair to complete replacement. Faster and more cost-effective repair methods will be needed in the future to provide and maintain adequate service with existing inventory. In an effort to examine the feasibility of repair for many of these structures, the rehabilitation of a reinforced concrete bridge using fiber-reinforced composite materials was proposed and studied.

In 1999, the Alabama Department of Transportation (ALDOT) selected the War Memorial Bridge in Macon County, Alabama for flexural strengthening. Completed in 1945, this eighteen-span reinforced concrete bridge is located on Alabama State Highway 81 and crosses the Uphapee Creek approximately 0.3 miles north of Interstate 85 (Figure 1.1). Over the years of its service life, typical truck loads have increased, resulting in greater stresses and deflections than those for which the bridge was designed. This necessitated posting load limits for certain types of trucks (Figure 1.2). ALDOT had the need to lift the load limit due to the amount of heavy traffic desiring to use the bridge. Auburn University researchers proposed bonding fiber-reinforced polymer (FRP) material to the bridge girders to supply the additional positive moment capacity and

permit removal of the existing load restriction (Barnes and Swenson 2003). FRP use promises many benefits to the construction industry and particularly to highway infrastructure. These advantages may include reduced installation time and expense, resistance to typical corrosive agents like salt, and greater service life cycles (Nystrom et al. 2003). In the future, FRP composites may be used as the sole material in different types of new construction or rehabilitation, but in its current state as a developing technology, lack of experience, familiarity, and uniform construction standards retard its advancement in use. From this study, ALDOT hopes to gain insight into whether FRP materials can play a role in rehabilitating Alabama's ailing bridge inventory.

Figure 1.1: Location of War Memorial Bridge (Mapquest 2005)

A team comprised of ALDOT bridge maintenance personnel and Auburn University researchers performed the design and installation of the FRP material. Additionally this team further conducted load tests to evaluate the resulting benefit of the FRP. One load test of the unstrengthened bridge and three load tests of the strengthened structure were performed. The design of the FRP strengthening system is outlined in a separate report (Swenson and Barnes 2002). Reed and Barnes (2004) describe a related experimental study to assess the ramifications of live loads experienced during the installation of the FRP strengthening system.

Figure 1.2: ALDOT Load Posting Sign for War Memorial Bridge

1.2 OBJECTIVES

The objective of the experiment performed on the War Memorial Bridge was to evaluate the use of an FRP strengthening system for use by ALDOT for rehabilitating Alabama's reinforced concrete bridge inventory. Specifically, researchers hoped to better understand the FRP installation process, work with ALDOT maintenance personnel to become proficient in installation techniques, develop a method to efficiently test the effectiveness and integrity of the repair, create a computer model that can validate the field evaluation of the repair, and make recommendations to ALDOT regarding the potential usefulness of repairs with FRP materials.

1.3 SCOPE

This report will examine and evaluate the steps taken to meet the project objectives and expand a discussion of the results of the research. It will discuss at length the application and evaluation of carbon-FRP laminates to an in-situ structure, the War Memorial Bridge. To preface the work at hand, Chapter 2 presents a review of previous relevant work. Chapter 3 presents a description of the War Memorial Bridge and the repair issues challenging researchers, while Chapter 4 describes the design and installation of the FRP strengthening system. Chapter 5 discusses bridge testing, including descriptions of data collecting methods and load test procedures. Chapter 6 examines the finite-element computer model that was created to analyze the effectiveness of the repair. Chapter 7 presents findings and results of the bridge testing, while Chapter 8 presents conclusions drawn from the experiment.

CHAPTER 2: LITERATURE REVIEW

2.1 GENERAL

Fiber reinforced polymer (FRP) laminate materials are engineered materials comprised of polymer matrices incorporating a high-performance fiber reinforcing material of a sufficient aspect ratio to provide measurable reinforcing in one or more directions. This composite material technology is less than a century old and was initially developed in Switzerland. Swiss engineers built upon the work of French engineers in bonded steel plate rehabilitation by substituting both stronger and lighter carbon FRP plates for the cumbersome steel plates (Petrou, Harries, and Papakonstantinou 1999). FRP composites are anisotropic and have begun to revolutionize many industries (Nystrom et al. 2003). Typically, carbon, aramid, or glass fibers are used and are oriented directionally in long strands. The resulting laminate material, typically in a pliable sheet or strip, possesses high tensile strength in the direction parallel to the fiber orientation but has insignificant strength along axes perpendicular to the fiber and also along all axes in compression. FRP laminate materials offer several advantages such as high strength-to-weight performance, resistance to corrosion, nonconductivity, and relative ease of installation. Studies have been performed to evaluate the properties of FRP materials as well as the performance of traditional construction elements enhanced with FRP materials. However, studies lag in areas of design analysis of FRP systems and evaluation of in-situ elements—rather than laboratory specimens—enhanced with FRP (Petrou, Harries, and

Papakonstantinou 1999; Vecchio and Bucci 1999). As a part of the research performed on the War Memorial Bridge, design analysis has been performed and discussed at length in another report (Swenson and Barnes 2002). This chapter includes a review of literature describing the use of externally bonded FRP to strengthen existing concrete structures as well as the testing and analysis of such strengthened structures.

2.2 Utilizing FRP Laminates for Reinforced Concrete Repair

Although more than 1500 structures worldwide have been retrofitted with FRP materials for strengthening, their use in the United States has lagged applications in Japan and Europe. However, FRP is being utilized more use in the United States as transportation departments are beginning to specify FRP for rehabilitation projects, engineers and contractors are becoming more familiar with these systems and their installation, and design codes are becoming more rigorous, especially with respect to seismic constraints (Petrou, Harries, and Papakonstantinou 1999; Vecchio and Bucci 1999). FRP materials can be used for strengthening all components of reinforced concrete bridges, including piers, decks, and flexural members.

Nystrom et al. (2003) note that recent studies conducted by the Federal Highway Administration report 29% of the United States bridge infrastructure is structurally deficient or functionally obsolete, and an estimated $87.3 billion is required to eliminate the backlog of improvements and repairs. Advancing technology in composite materials may provide a solution to this problem at a significantly reduced expense. Though many benefits are associated with their use—such as fast and easy installation, reliability gained through pre-engineering exercises, corrosion resistance, and increased service life—a relative unfamiliarity with the material and lack of standards hinder their

advancement. Material costs are an additional obstacle to wider acceptance. Though manufacturers are working to bring costs down, repairs utilizing FRP laminate materials can be as much as 200% the cost of a traditional steel rehabilitative method (Petrou, Harries, and Papakonstantinou 1999).

Of the three primary types of fibers, carbon fibers have been used almost exclusively in Europe and Japan. In the United States, glass fibers were initially used, due to the facts that (1) the glass fiber industry in the U.S. was very mature, (2) the carbon fiber industry was a niche industry catering primarily to military applications, and (3) glass fibers are cheaper (Petrou, Harries, and Papakonstantinou 1999). However, as the superiority of carbon fibers is being noted and the costs are coming down, more carbon FRP is being used in the United States (Petrou, Harries, and Papakonstantinou 1999). Mayo et al.(1999) and Petrou, Harries, and Papakonstantinou (1999) summarize the differences between the three types of fibers.

Carbon produces the strongest, stiffest, and most durable fiber. Carbon fibers have an upper range of tensile strength of approximately 350 ksi and modulus of elasticity of 24,000 ksi. Commercial carbon fibers are obtained by processing polyacrylonitrile, rayon, or pitch. Resins will not easily wet carbon fibers, and this has subsequently led to the development of surface treatments for some resins that will increase the amount of active chemical groups on the surface of the fiber or actually roughen the fiber surface. Often an epoxy size treatment is applied for shipping in order to prevent fiber abrasion and provide an epoxy-resin matrix-compatible interface.

Glass had been the most widely used fiber in the United States for FRP materials. Four main types of glass fibers are readily available and offer different characteristics for

specific applications. E-Glass, or electrical-grade glass, is the most widely used glass fiber. S2-Glass is a high-strength grade of fiber. ECR-Glass is a type of E-Glass that offers acid resistance. AR-Glass is an alkali-resistant glass fiber. Monofilament E-Glass has a modulus of elasticity of approximately 10,600 ksi. The upper range of tensile strength for E-Glass is around 250 ksi. It is theorized that glass fiber contains sub-microscopic voids at the surface of the material that create localized stress concentrations. As a result, glass fibers exhibit a phenomenon called creep rupture, meaning that when held under a constant load at a stress below the instantaneous static strength, the fibers will fail as long as the stress remains above some minimum value. The glass fibers are extremely hydrophilic, and water vapor is very damaging to the fibers. Moist air containing weakly acidic carbon dioxide may cause failure. Glass fibers can be easily damaged during handling, and a protective film is applied immediately after fiber forming in order to prevent damage.

Aramid, which is commonly sold under the trade name Kevlar, is an organic fiber. It offers tremendous impact resistance, attested by its use in bulletproof vests. The upper range of aramid fiber tensile strength is approximately 300 ksi and modulus of elasticity is 11,000 ksi.

Mayo et al. (1999) also describe the polymers that comprise the binder for the fibers. The binder resins are thermosetting materials and serve to protect the fibers from environmental effects and spread loads evenly among the individual fibers. Three resin types are common: epoxy, vinyl ester, and phenolic resins. Epoxy resins are the most commonly used matrix material. Their safe-use temperature threshold is approximately 200^{o}F. Though more expensive than the other common binder materials, they offer

superior adhesive and structural properties. Epoxies are available in varying viscosities and allow for different cure states which give rise to the prepreg condition, a partial- or advanced-cure condition. Prepreg epoxies containing the fibers can be molded or wound at room temperature. Vinyl ester resins offer good durability but compromise structural performance and are more susceptible to heat damage. Phenolic resins also offer good durability with higher heat resistance than vinyl ester resins. Neither vinyl ester nor phenolic resins are as expensive as epoxy resins.

Fiber laminates and fabrics used for rehabilitating reinforced concrete structures can be categorized into eight different groups of systems following the prescription of *ACI440R-96 – State of the Art Report of Fiber Reinforced Plastic Reinforcement for Concrete Structures* (ACI 440 1996):

- unidirectional fiber tow and stitched or woven fabrics, bonded to the substrate in a wet lay-up method,
- multidirectional stitched or woven fabric, bonded to the substrate in a wet lay-up method,
- resin pre-impregnated, uncured (prepreg) sheets or fabrics bonded to the substrate with or without additional resin,
- fiber tows wound or mechanically placed on the substrate while resin is applied during the placement in a wet lay-up method,
- resin pre-impregnated uncured (prepreg) fiber tows wound or mechanically placed on the substrate with or without additional resin,

- pre-cured laminates and shells manufactured at an off-site facility and bonded to the substrate at the jobsite with an adhesive and possibly requiring additional prepreg or wet lay-up materials,
- pre-cured laminate sheets in strip or grid form bonded to the substrate with a prescribed adhesive and method, and
- pre-cured curved or shaped shells, in segments or otherwise pieced that they may be opened, fitted in single or multiple layers and bonded to the substrate with a prescribed adhesive and method.

When utilizing any FRP system for installation, proper substrate preparation is crucial. Sand-blasting or another means of removing dirt, spalled concrete, and any other laitance is necessary to provide a clean surface for bonding. After blasting, a thin portion of the concrete cover should be stripped, exposing small to medium sized aggregate (Rahimi and Hutchinson 2001). Also crucial is cleaning and degreasing of the bonding surface of the FRP material, as it has been shown that the joint strength of treated components is dependent on the degree that contaminants are removed from the bonding surfaces, and not on the extent of abrasion (Quantrill, Hollaway, and Thorne 1996).

Bond strength plays a vital role in FRP strengthening applications. Many investigations have demonstrated new brittle failure modes of FRP-strengthened reinforced concrete beams, mostly due to premature debonding of the FRP material as the bonding agent fails (Aprile, Spacone, and Limkatanyu 2001). At the plate-to-beam interface, shear stresses act parallel to the interface and peeling stresses act normal to the interface; shear stresses are zero at the end of the plate and reach their maximum at a distance approximately equal to the thickness of the resin before decreasing at increasing

distance from the end. Peeling stresses are also at a maximum at the same distance of the resin thickness and decrease to nearly zero at a distance of three to four times the resin thickness from the end of the plate (Aprile, Spacone, and Limkatanyu 2001). Ziraba et al. (1994) note that for thin plates, failure of the reinforced beam is primarily controlled by flexural concrete cracking, yielding of internal reinforcement, yielding of the FRP reinforcement, and crushing of the concrete in the compression zone. However, as the plate thickness increases, the failure mode increasingly becomes debonding of the plate as the interface stresses increase. Weak adhesive or improper adhesive application and/or curing may result in a failure distinguished by delamination that emanates from the plate ends and proceeds to a point along the FRP section where peeling stresses increase to a level where shear-critical cracking develops and leads to sudden failure. If the bond itself is not compromised, failure for thicker plates is characterized by cracking emanating from the plate end and propagating in a nearly horizontal direction at a level just below the internal reinforcement. When this horizontal crack intersects an existing shear critical crack, failure will result. Ziraba et al. (1994) propose three steps for design of a beam with FRP plates to account for the potential failure described, which can be extended to a checklist for reinforced-concrete beams to be strengthened with FRP laminates as follows:

- check the design of the reinforced-concrete beam for flexure, assuming plate yielding and concrete crushing on the compression side,
- calculate interface stresses to insure that they are within the limits to avoid plate delamination, and

- check the shear capacity of the beam to ensure that adequate capacity is present in the reinforced concrete to avoid failure due to concrete cover rip-off.

Wong and Vecchio (2003) found that bonding vertically oriented FRP material, acting in much the same manner as stirrups, would prevent the brittle shear failure of the beams, and therefore could be used in a retrofit to mitigate failure due to propagation of shear-critical cracks.

2.3 Analysis and Design of FRP-Retrofitted Reinforced Concrete Structures

The increased use of FRP materials for rehabilitation and strengthening necessitates analysis and design techniques that adequately encompass the unique condition of the union of materials exhibiting different behavioral properties, the effects of age on reinforced concrete, and the other peculiarities that stem from the marriage of the technology of reinforced concrete and composite fibers. Guidelines for the design of FRP retrofit systems have been standardized in the last few years, notably through publications such as the American Concrete Institute Committee 440 *Design and Construction of Externally Bonded FRP Systems for Strengthening Concrete Structures* (ACI 440 2002). As design procedures become more prescribed, researchers are still pushing to develop accurate ways to model the behavior of the reinforced concrete/FRP systems more efficiently and accurately. Notable are several methods that employ non-linear finite element analysis programs to model the bond interface and the nonlinearity that exists in the cracked reinforced concrete simultaneous with the linear FRP (Rahimi and Hutchinson 2001; Tedesco, Stallings, and El-Mihilmy 1999).

ACI Committee 440 (2002) formally outlines design procedures for rehabilitative design for reinforced concrete structures. The design for the FRP flexural reinforcement of the War Memorial Bridge was accomplished in part using the recommendations delineated in Chapter Nine of the ACI report and as described by Swenson and Barnes (2002). Based on ultimate strength design, the nominal amount of FRP required for external reinforcement was calculated using force equilibrium, strain compatibility, and constitutive material relationships of concrete, steel, and FRP. The ACI Committee 440 procedure outlined requires certain assumptions to be valid for proper design:

- all member dimensions, material properties, and locations of reinforcing steel are correct,
- concrete and reinforcing steel strains are directly proportional to their distance from the neutral axis,
- maximum concrete compressive strain is 0.003, and concrete tensile stresses are neglected,
- FRP material exhibits linear elastic behavior until failure, while steel behavior is linear elastic until yielding and plastic thereafter (strain hardening is neglected),
- a perfect bond exists between the reinforcing steel and concrete and the concrete and the FRP reinforcement (prior to debonding), and
- concrete compressive stress at failure is represented by the rectangular stress distribution defined by ACI 318-02 Section 10.2.7.

Other investigations have suggested that neglecting concrete tensile stresses can lead to discrepancies in calculations due to the conservativeness of the method, and likewise, neglecting strain hardening can lead to similar discrepancies (Quantrill, Hollaway, and

Thorne 1996). Assuming a partially cracked section model will reduce these issues (Quantrill, Hollaway, and Thorne 1996). For the War Memorial Bridge rehabilitation design, failure through FRP delamination was predicted to occur well before a concrete compressive strain of 0.003 was reached. Consequently, compressive stresses at failure could not be represented by the rectangular stress distribution as defined by ACI 318-02 Section 10.2.7.

Swenson and Barnes (2002) performed two design variations utilizing the procedure outlined by ACI Committee 440. One variation modeled the compressive concrete stresses as linear elastic while the other variation used the rectangular stress distribution from ACI 318-99 Section 10.2.7. Both variations incorporated alterations to the equations given by ACI Committee 440 (2002) to account for compression reinforcement. Additionally, Swenson and Barnes (2002) performed a second design to determine the most efficient amount of FRP required for adequate flexural strengthening of the girders and to check the validity of the method outlined by ACI Committee 440 in Chapter Nine of their report. This design modeled the concrete stress-strain behavior as nonlinear based on a function reported by Collins and Mitchell (1991), enabling a more accurate calculation of moment-curvature behavior of the design cross sections. This second design method was further extended to include design criteria that limited allowable strain in the FRP material. By limiting the allowable FRP strain in design, the FRP reinforcement scheme designed should more conservatively predict the actual non-ductile failure mode.

Tedesco, Stallings, and El-Mihilmy (1999) investigated a reinforced concrete bridge consisting of seven simple spans, 10.36 m each, by flexurally reinforcing the girders

using externally bonded FRP laminates. Carbon fiber reinforced polymer (CFRP) plates were applied to the bottoms of the girders and glass fiber reinforced polymer (GFRP) plates were applied to the sides of the stems of the T-beams, with one girder serving as a reference for GFRP performance. A three-dimensional finite-element analysis was performed to compare field results to analytical performance. A reduced modulus of elasticity was used to more accurately reflect the bridge's cracked state. Static and dynamic analyses were performed, which included frequency analysis to verify the accuracy of the finite-element model by comparison of fundamental frequency and free vibration response of the model to that observed in the field. Results indicated an excellent agreement between the model and actual conditions. Transient analysis was performed on the finite-element model as a succession of moving concentrated nodal loads. Again, when compared to the field results, the model was found to agree. Static analysis indicated that the model predicted slightly lower steel stresses than observed in the field. This was attributed to the simplification of reinforcement bars into one bar at the centroid of the tension steel while the field gauge was physically located at the bottom of the bottom reinforcing bar. A parametric study was also undertaken to assess how changing cross-sectional area and modulus of elasticity would affect the performance of the rehabilitated bridge. It was found that, though increasing either parameter would result in enhanced load-carrying performance, tensile strength was the critical parameter at the ultimate load stage (Tedesco, Stallings, and El-Mihilmy 1999).

El-Mihilmy and Tedesco (2000) proposed a method for evaluating the deflection of reinforced concrete members strengthened with FRP bonded to the tension face. A procedure for estimating deflection in the pre-cracking, cracking, and post-cracking stage

of loading is presented. Where the ultimate deflection of a conventionally reinforced concrete beam typically ranges from five to twelve times the deflection at first yield of the reinforcing steel, values only range up to five times the yield deflection in a FRP-reinforced concrete beam. The extent of cracking presents the particular challenge to accurately estimating the deflection. In the precracked stage, the FRP reinforcement simply needs to be accounted for in the gross uncracked moment of inertia and calculated as outlined by ACI 318. For the cracking stage, calculations using the Branson effective moment of inertia equations tend to overestimate the effective moment of inertia and therefore underestimate the deflections. By noting that the effective moment of inertia at yielding of the steel is approximately equal to the cracked-section moment of inertia, an equation was proposed which more closely predicts the effective moment of inertia and leads to more accurate predictions of the deflection. In the cracking stage, the conventional ACI calculations overestimate deflection as the equations assume that a post-cracked beam cannot carry much additional moment, and therefore do not account for the fact that an FRP-reinforced beam can carry a service load well into the post-cracking stage. A procedure is presented based on integrating the curvature along the beam length. A simplification is made by assuming two idealized linear sections for the curvature. The maximum curvature at the location of the beam's maximum moment can be obtained through interpolation and then used in the conventional elastic equations to obtain the effective moment of inertia. As with the proposed equation given for the cracking stage, experimental results prove that this equation will more satisfactorily estimate beam deflection (El-Mihilmy and Tedesco 2000).

Recognizing the inaccuracy of results not incorporating bond-slip effects, Spacone and Limkatanyu (2000) developed a beam fiber model to account for the bond-slip phenomena which can be used for the bond-slip effects between concrete and the reinforcing bars or externally bonded CFRP applied for flexural reinforcement. Prior fiber models largely assumed that plane sections remain plane, therefore ignoring the effects of bond slip. While this basis accurately predicted strength in models, initial stiffness was larger in modeling than in practice, while hysteretic energy of reinforced concrete members was larger also than in practice. Previous attempts to model bond-slip effects have led to fairly inefficient results. A simple modeling approach is to add nonlinear springs at ends of the element, though this approach necessitates an ad-hoc moment-rotation law and disrupts inter-fiber continuity. Monti and Spacone (2000) developed an element from a force-based fiber beam element and a bar element model that incorporates bond-slip. This element, though precise, is difficult to implement. Spacone and Limkatanyu (2000) propose a displacement-based fiber model utilizing separate displacement fields for the concrete and reinforcing bars, FRP, or both. They formulated and tested the model on both a reinforced concrete column previously studied for verification of a fiber model and a reinforced concrete beam strengthened with a CFRP plate in flexure and loaded to failure. The model is comprised of a two-node concrete beam and any number of two-node bars representing the reinforcing bars or CFRP that slip with respect to the beam. Differing degrees of freedom between the concrete beam and the bars allow slipping. Analytical and experimental results were found to be in close agreement in both test cases.

2.4 Load Testing of FRP-Retrofitted Reinforced Concrete Structures

A truly representative assessment of the effect FRP materials have on strengthening reinforced concrete members has been difficult. This is primarily due to the fact that those members for which rehabilitation is required and study is prudent are those members currently in use in the transportation infrastructure, building inventory, or other service use; therefore, they cannot be readily decommissioned nor easily duplicated in the laboratory for thorough study. Design guidelines have been primarily written based on investigations in the laboratory with newly cast, small-scale, reinforced concrete test specimens (Shahrooz, Boy, and Baseheart 2002; Arduini, Nanni, Romagnolo 2002). It is necessary to investigate the effectiveness of FRP repairs to members in field conditions, including concrete deterioration and cracking, corrosion of internal reinforcing steel, and geometrical nonuniformities, to properly assess the effectiveness of FRP strengthening.

In the Tedesco, Stallings, and El-Mihilmy (1999) study discussed in the previous section, field load tests were conducted before and after FRP laminate plates had been applied to the bridge. Static and dynamic tests were performed using two identical ALDOT test trucks having a three-axle configuration and weighing 346 kN. For static testing, the trucks were positioned in four different transverse positions, with the center axle positioned at midspan in all four tests. Transverse positions were determined by selecting the locations in which the most extreme loadings possible were generated. These positions used spacings which were significantly less than those prescribed by the American Association of State Highway and Transportation Officials (AASHTO) for design. Dynamic tests were conducted by driving the test trucks at 80 km/h side-by-side across the bridge, centered in the traffic lanes. Electrical resistance foil strain gauges

were affixed to the steel reinforcing bars, to the surface of the FRP plates, and to the surfaces of the concrete girders to measure the strain response during testing. Vertical deflections were measured with linear variable differential transformers (LVDT) at the midspan of each girder. Measurements were taken before and after FRP laminate installation. Experimental data was utilized for comparison with a three dimensional finite-element model for performance validation.

Schiebel et al. (2002) evaluated three bridges in Boone County, Missouri that were strengthened using CFRP laminates for flexural and shear strengthening. Three bridges were strengthened and diagnostically tested—one bridge comprised seven channel sections with one solid slab section on either side and a span of 6.13 m, and two bridges comprised eight channel sections with span lengths of 5.92 m and 11.84 m. A high-strength, unidirectional, carbon fiber laminate was utilized for design loads based on AASHTO guidelines for an HS20 truck for precast multigirder bridge decks. A manual lay-up system was employed to affix the FRP material to girder soffits for flexural strengthening and to channel legs for shear strengthening. The system was allowed to cure before load testing began. Testing was conducted only on the seven-channel bridge and one of the eight-channel bridges due to similarities of the two eight-channel bridges. The test sought to evaluate service-load response. Strain gauges and LVDTs were installed at the girder soffits and at top and bottoms of the channel legs, respectively, of one side of the bridge. LVDTs were used to record deformations, which were used to calculate a smeared strain value. Deflections were measured, and strains were recorded on reinforcing steel in pre-strengthened tests and for steel and FRP in the post-strengthened tests. Load trucks were positioned at five transverse positions on the

bridges. Moments were back-calculated from strain data for comparison with AASHTO-prescribed applied-load distributions, and deflections were compared with values calculated from Branson's classical procedure. In both cases for the prestrengthened tests, the experimental deformations were smaller than analytical predictions. This was explained in one respect as the analytical methods are conservative. Additionally, the experimental values include effects of the non-homogenous nature of concrete and the rotational complexities that exist at the real supports, which may lead to experimental values being lower than the analytical values. For the post-strengthened tests, deflection and moment values were less than for the values measured in pre-strengthened tests. This suggests some additional stiffness was added to the bridge due to the FRP preventing existing cracks from opening under load (Schiebel et al. 2002).

Arduini, Nanni, and Romagnolo (2002) procured the five girders of a decommissioned bridge taken from a highway viaduct in Italy for laboratory tests to failure in order to study the effects of FRP repair specimens on aged and deteriorated reinforced concrete members. The girders had experienced varying degrees of cover spalling and reinforcement corrosion. One girder was left unrepaired; the remaining four girders were repaired to a condition simulating a field repair and providing an adequate surface to install FRP. This included mechanical scarification to remove deteriorated concrete followed by treatment to remove remaining reinforcement corrosion. A welded wire mesh was installed over the entire web as a substrate for shotcrete application to replace original cover. A flange was cast on the tops of the girders to essentially simulate the removed bridge deck. After curing and cleaning, FRP was installed onto the shotcrete in various configurations. All the girders received two sets of soffit plies and U-wraps on

the web at the ends of the plies. Two of the girders received additional U-wraps, and one girder further received an additional length of plies at the web bottoms. Two different types of FRP were used—one a dry fiber system and one a prepreg fiber system. Analysis was performed with a model previously developed and presented by the researchers and based on the assumptions that plane sections remain plane, a perfect bond exists between all material, small displacements, and constituent material laws. The analytical results were compared with the experimental findings, and good predictive ability was found in the model. Experimental values of the ultimate FRP strain were significantly lower than the analytical values, but the behavioral trend was the same. Shear stresses at the FRP-concrete interface were observed to be much higher at girder discontinuities, such as the FRP terminations, the stumps remaining from the transverse beam at girder midpoint that was in place on the bridge, or cracks in the concrete. As common in design, the practice of considering only the beam cross section subjected to the maximum bending moment may not be sufficient to account for areas of interfacial shear stress higher than the design strength that may exist along the cross section of the girder at those discontinuities. Designers must take into account any discontinuities along the entire length of the cross section and consider that in design, even if the design becomes more complex (Arduini, Nanni, and Romagnolo 2002).

CHAPTER 3: BRIDGE DESCRIPTION

3.1 GENERAL

The War Memorial Bridge is of north-south orientation and consists of eighteen, 38-ft simple spans and a three-span continuous section of 161-ft length. Figure 3.1 shows the continuous span portion of the War Memorial Bridge, the section of concern to this report. The roadway is 26 ft wide. Spans are numbered incrementally from south to north, and girders are numbered incrementally from west to east. Bents, or piers, are numbered incrementally from south to north.

Figure 3.1: Continuous Span Portion of the War Memorial Bridge

The three-span continuous superstructure was selected for rehabilitation. The simple spans have been rated as adequate by current ALDOT bridge rating standards. Therefore, for the purposes of this study and report, the term “bridge” will be limited to only include the three continuous spans—Spans 9, 10, and 11. Spans 9 and 11 are 48-ft end spans. Span 10 is the center span and is 65 ft in length. The superstructure is symmetric about the midspan of the center span and about the centerline of the roadway, creating four sections exhibiting symmetrical properties. Four variable-depth, reinforced concrete T-beams support each span. Diaphragms are located at midspan of the outer spans and at the one-third points of the center span. The depth of a typical exterior girder varies from 30.5 in. at the simply supported end and midspan of the center span to 61 in. where the girders rest on the interior bents. The interior girders have a similar profile, but they are 1-5/16 in. deeper than the exterior girders throughout. A typical end span and center span are shown in Figure 3.2 and Figure 3.3, respectively.

At the time of construction, high early strength concrete as defined by the 1939 Alabama State Highway Department Standard Specifications was used. Due to the age of the structure, a concrete compressive strength was estimated from compressive testing of cores taken from various locations in the bridge deck in accordance with test method AASHTO T 22. Based on these test results, a conservative value of 5000 psi was taken as the concrete compressive strength for the purpose of assessing the existing bridge capacity.

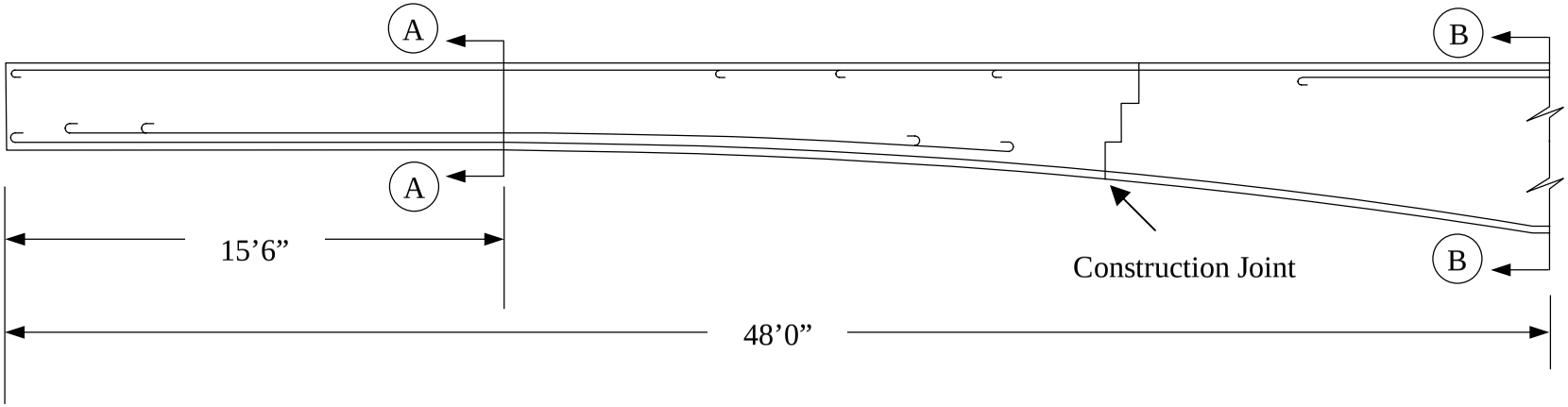

Figure 3.2: Typical End Span

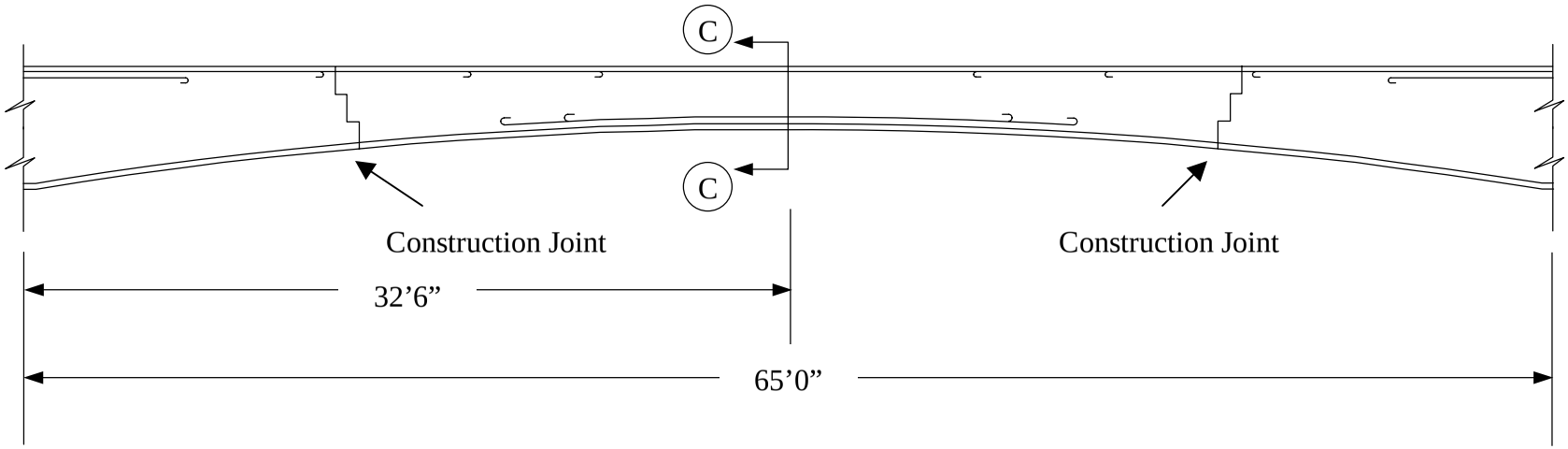

Figure 3.3: Typical Center Span

The four variable-depth T-beams are spaced at 88 in. center-to-center and support a 6-in. thick bridge deck. Positive moment reinforcement consists of one to two layers of deformed steel bars. For a typical exterior girder, the bottom layer consists of four 1-1/8 in. or 1-1/4 in. square bars depending on location. For a typical interior girder, the bottom layer consists of four 1-1/8 in. square bars. For both exterior and interior girders, the top layer of steel consists of up to four 1 in. or 1-1/8 in. square bars, depending on location within the span. Half cross sections for Sections A, B, and C (as located in Figure 3.2 and Figure 3.3) are shown in Figure 3.4 and Figure 3.5. All reinforcing steel bars are deformed bars. The yield stress, f_y, of the steel was taken from the Manual for Condition Evaluation of Bridges (AASHTO 1994) as 33,000 psi for bridges built prior to 1954.

3.2 FLEXURAL CRACKING

In its pre-strengthened condition, the War Memorial Bridge exhibited significant cracking. That cracking was distinctively apparent after mechanical abrasion from sandblasting was performed during summer of 2000. While a small percentage of cracks may be a result of shear, the majority of all cracks are vertical cracks caused by positive and negative moments. Vertical cracks extending upward from the girder soffit are produced by positive moment; vertical cracks extending downward from the deck are produced by negative moment.

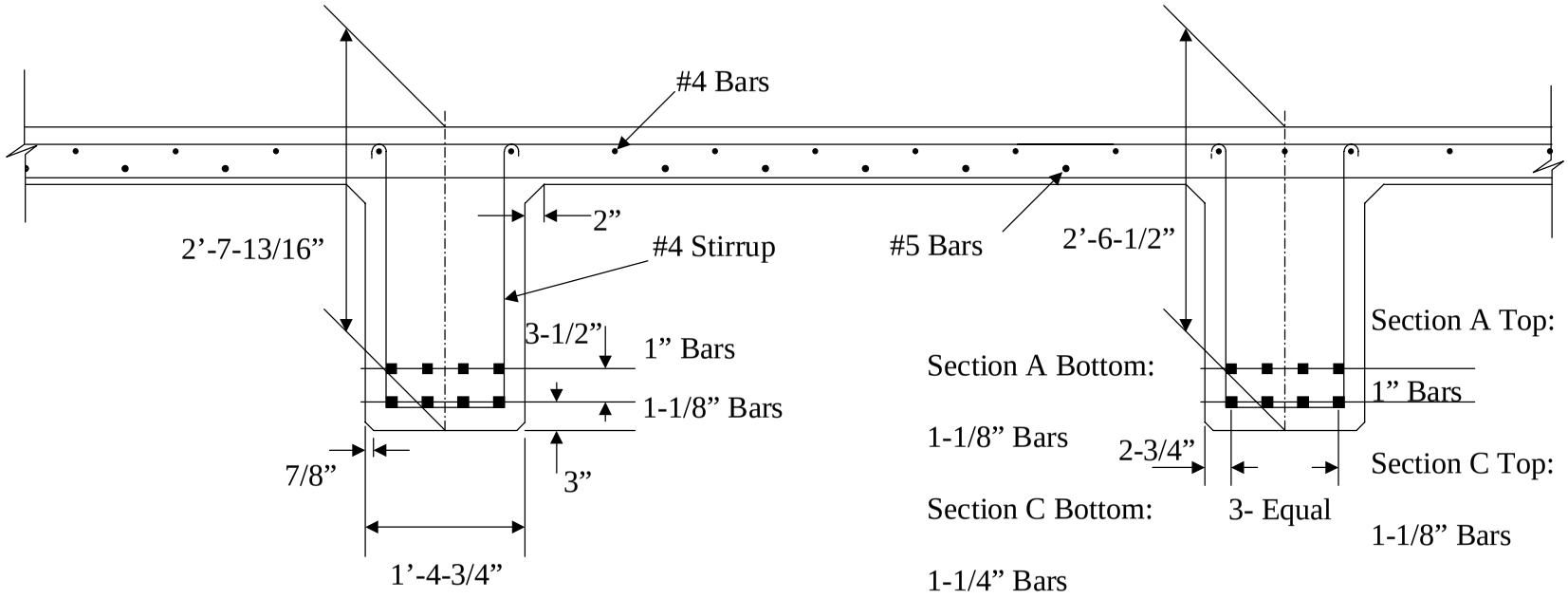

Figure 3.4: Cross Sections A and C
(Refer to Figures 3.2 and 3.3 for Cross Section Locations)

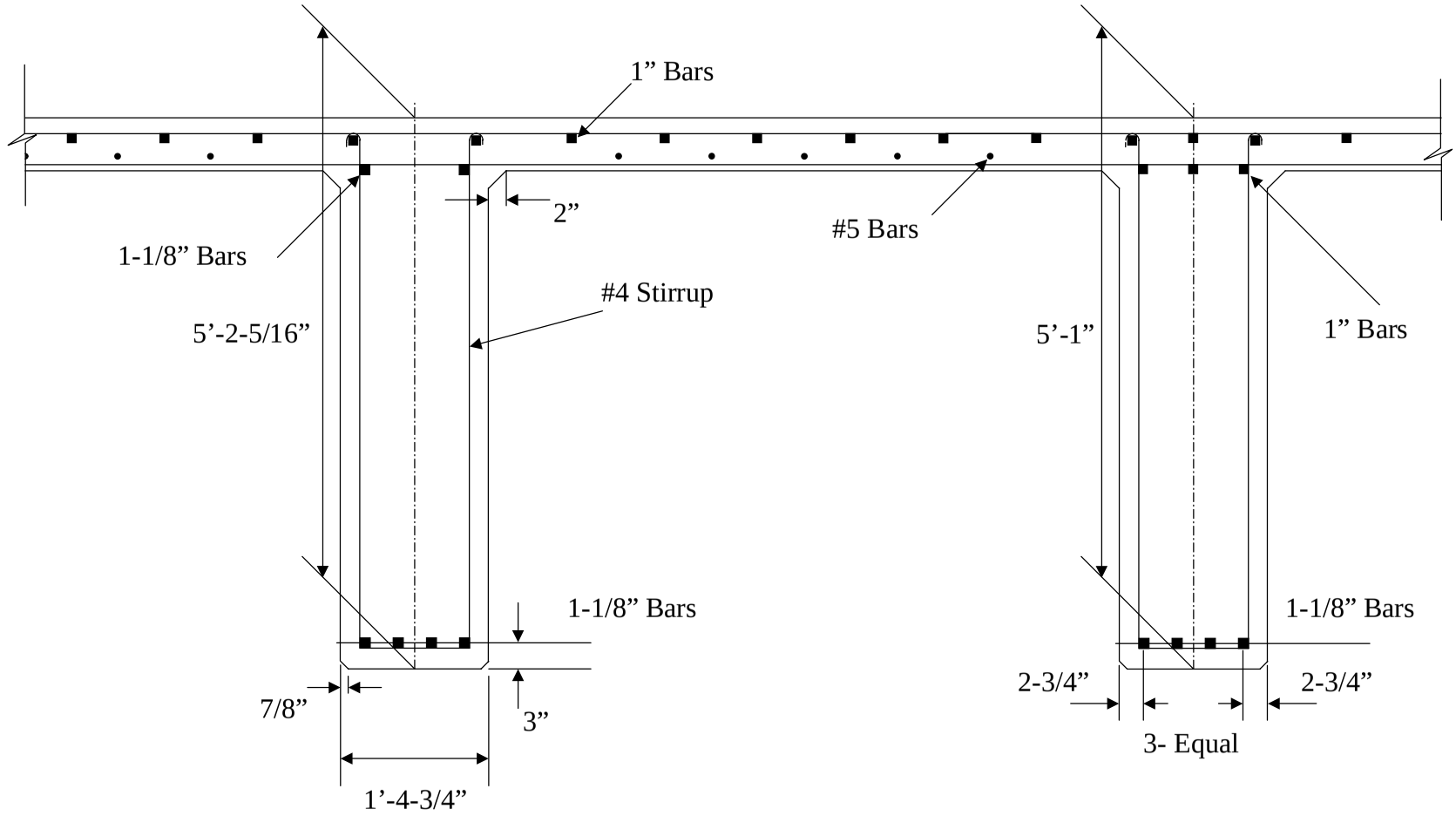

Figure 3.5: Cross Section B
(Refer to Figure 3.2 for Cross Section Location)

According to the American Concrete Institute (ACI) Committee 224 (1993) the location and extent of cracking should be identified before repairing those cracks in the concrete. Additionally, ACI Committee 440 (2002) reports that cracks 0.010 in. and wider can affect the performance of externally bonded FRP through fiber crushing or by promoting delamination. Consequently, ACI 440 suggests that epoxy be pressure injected into cracks wider than 0.010 in. before FRP is applied. Since FRP was only to be used for positive moment strengthening of the bridge, only those cracks in the portions of the bridge subjected to positive moment were mapped and evaluated for epoxy pressure injection.

Crack locations and widths were mapped onto a sketch of the bridge. Crack widths were measured with an accuracy of 0.001 in. using a crack comparator or a hand-held microscope designed for crack comparison. Crack widths appearing less than 0.003 in. were not recorded due to the negligible effect they would have on the performance of FRP. Overall, approximately 25% of all cracks were measured precisely. Specific crack locations and corresponding crack widths are included in Appendix A. A typical end span and center span with corresponding positive moment crack patterns are shown in Figure 3.6 and Figure 3.7, respectively.

Cracks in the end spans exhibited similar patterns on both exterior and interior girders. Cracks in these spans are located within a region of approximately 3 ft to 33 ft from the simply supported end of the girders (Figure 3.6). In these regions, the average horizontal spacing between cracks on each girder ranges from roughly 9 in. to 12 in.

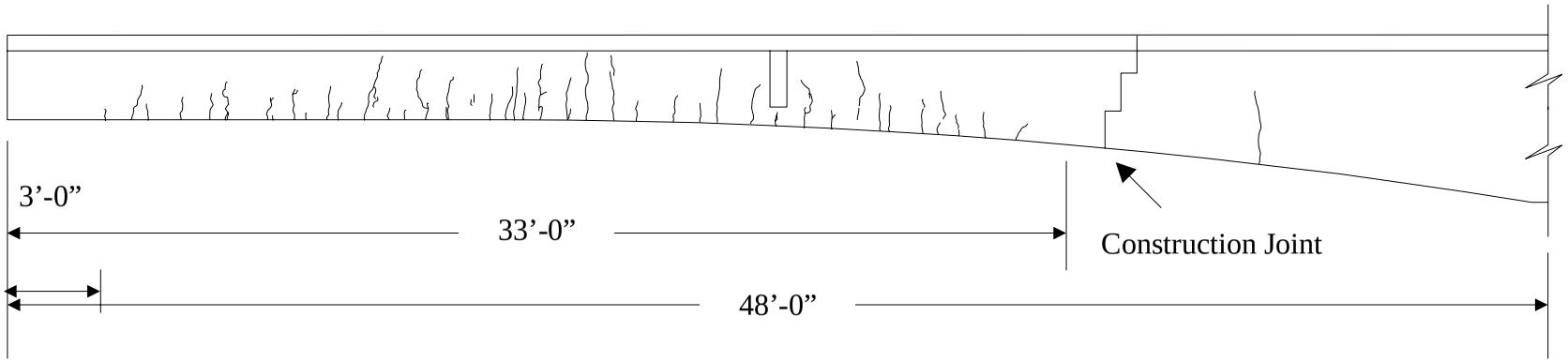

Figure 3.6: Crack Pattern for Typical End Girder

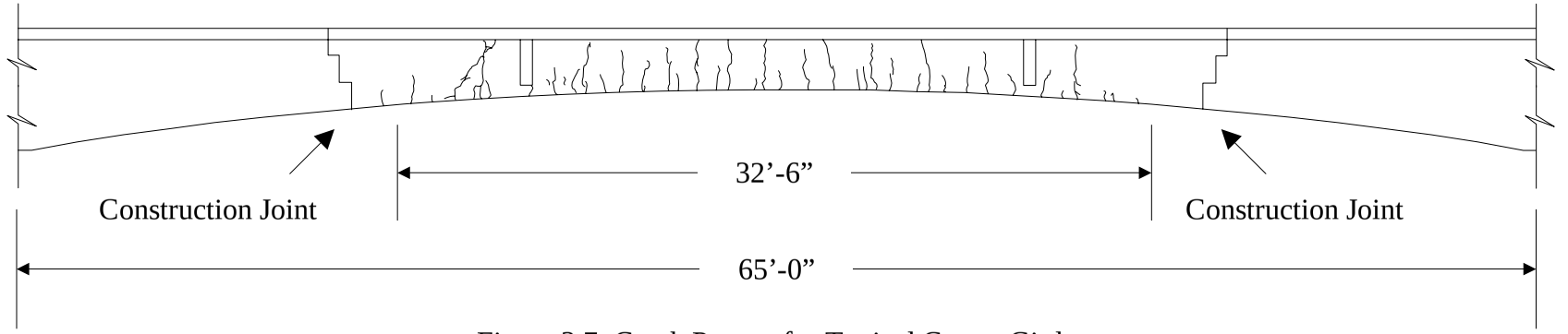

Figure 3.7: Crack Pattern for Typical Center Girder

Cracks in the center span exhibited similar patterns on both exterior and interior girders. Cracks in this span are primarily located in the middle 50 percent of the span with the average distance between horizontal cracks ranging from approximately 8 in. to 10 in. (Figure 3.7).

Typical construction joints can be seen in the girders in Figure 3.6 and Figure 3.7. Cracking was present at the construction joints, and they were epoxy injected in order to prevent further introduction of contaminants through those cracks.

Cracking of concrete in tension is an accepted design assumption used in reinforced concrete design. Design procedures used by ACI 318 (2002) and AASHTO *Standard Specifications for Highway Bridges* (1996) rely on the reinforcing steel not only to carry the full tensile force but also to limit crack widths and control crack distribution. Consequently, abnormally large cracks suggest possible structural problems, possibly caused by an overload, or may point to future problems. Overload is defined as a load sufficient to yield the reinforcing steel, which can cause permanent plastic deformation. Because cracking may indicate a structural problem, a comparative measure of the degree of cracking is desirable. An equation based on the physical model of cracking is given in Equation 3.1 (Frosch 1994),

$$w_c = \beta \varepsilon_s S_c \qquad \text{Equation 3.1}$$

where w_c is the crack width at the extreme tension face (in.), β is the ratio of distances to neutral axis from extreme tension face and from centroid of reinforcement, ε_s is the reinforcing steel strain, and S_c is the crack spacing (in.). This equation is based the assumption that plane sections remain plane, and that the reinforcing steel is uniformly strained within a crack spacing. Contributions from the concrete in tension are neglected.

The crack map showing locations and widths of cracks along the span for all girders was used to evaluate the integrity of the structure in its existing state. For crack widths measured in the field, Equation 3.1 was used to estimate the reinforcing steel strain indicated by this crack width. This estimated strain was compared to an estimated sustained dead load strain and the yield strain of the reinforcing steel. From ACI Committee 224 (1993), flexural crack widths can be expected to increase with time up to two times their widths for members subjected to sustained or repetitive loading. In the case of a bridge, long-term loading is the dead load while repetitive loading is traffic loading. At the time of crack measurement, there were no live loads on the bridge. Therefore, a crack width that is measured at less than two times the crack width obtained using Equation 3.1 that corresponds to the estimated dead load strain would not indicate abnormal structural degradation. On the other hand, crack widths larger than twice than the crack width expected from the dead load would indicate that the bridge had experienced transient loads larger than the original design live loads.

The majority of cracks recorded in the end spans satisfy the criteria outlined above for structural integrity. However, several cracks near the midspan of the center span are nearly 4 times as large as the crack width corresponding to the estimated dead load strain. Several recorded cracks located in the outer thirds of the center span indicate a strain level significantly larger than that estimated from the physical model. A few, less than 5% of the total, of these cracks indicate a strain that exceeds the yield strain of the reinforcing steel. An explanation for this occurrence is not easily found. Due to the continuous nature of the bridge, the outer thirds of the center span girders can be subjected to significant positive and negative moments in rapid succession when exposed

to large truck traffic. Over time, this repetitive load reversal has possibly caused a bond degradation or breakdown between the reinforcing steel and contiguous concrete. Because of this deficiency, the cracks may not completely close after opening. The sizeable cracks measured in the midspan region indicate a residual strain in the reinforcing steel due to overload at some point in the bridge's history. FRP laminates can add stiffness, and thus capacity, to a structure by restraining crack opening under applied loads (Schiebel et al. 2002).

3.3 STRUCTURAL DEFICIENCIES

The War Memorial Bridge was designed in accordance with the AASHTO truck loading H 15. Present minimum design specifications for highway bridges carrying heavy truck traffic require AASHTO HS 20-44 loading for design purposes (AASHTO 1996). Depending on the particular span and girder, the live load moment at the critical sections on the girders due to the H-15 truck loading can be as little as 54–56% of the live load effect produced by the current design HS 20-44 truck loading.

Highway bridges are rated at two levels—inventory and operating levels (AASHTO 1994). The inventory rating level corresponds to a design loading level, which allows comparison of existing structures with new structures. An inventory rating results in a loading that can be safely supported by a structure for an indefinite period of time. The operating rating level is a critical load rating method that yields the maximum allowable load to which a structure may be safely exposed. ALDOT posts weight restrictions on bridges according to the operating level. A rating factor indicating the remaining capacity of the structure in accordance with AASHTO (1994) was determined by ALDOT for both

inventory and operating ratings. The rating factor (RF) may be calculated as shown in Equation 3.2,

$$RF = \frac{C - A_1 D}{A_2 L(1+I)} \qquad \text{Equation 3.2}$$

where C is the capacity of the member, D is the dead load effect on the member, L is the live load effect on the member due to the truck being considered, I is the impact factor to be used, A_1 is the dead load factor, and A_2 is the live load factor. For the load-factor rating method used by ALDOT in the evaluation of the capacity of members, $A_1 = 1.3$. For the operator rating, $A_2 = 1.3$, and for inventory rating, $A_2 = 2.17$.

The impact factor used in Equation 3.2 was determined from AASHTO Design Specification as follows in Equation 3.3,

$$I = \frac{50}{L + 125} \qquad \text{Equation 3.3}$$

where I is the impact factor not greater than 0.30 and L is the length (in feet) of the portion of the span that is loaded to produce the maximum stress in the member. For continuous spans under positive moment, the actual length of the span is used for L. After obtaining the rating factor, the load rating is equal to the product of the rating factor times the nominal weight of the truck considered.

Capacity calculations for the variable depth members were determined by ALDOT using the Bridge Analysis and Rating Software (BARS) package. Additionally, the dead load effect and live load effect for ALDOT-specific posting truck types used for exterior and interior girders were determined with BARS. Load effects due to standard HS loading were also determined using BARS.

It was determined that the bridge had sufficient capacity in both negative moment and shear, and that the positive moment capacity of the exterior girder controls the load rating of the bridge. The tri-axle dump truck used by ALDOT for posting produced the largest positive moment for both exterior and interior girders; similarly, the tandem-axle concrete truck produced significant positive moment. Table 3.1 summarizes typical exterior girder load ratings for positive moment due to loadings from HS 20-44 and other trucks used by ALDOT for posting by the load factor method. The ratings are rounded down to the nearest ½ ton. For a typical interior girder, the load rating follows the same pattern with the tri-axle posting truck producing the largest load effect.

Table 3.1: Bridge Load Ratings for Exterior Girders

Truck Loading	Gross Weight (Tons)	Inventory Rating (Tons)	Operator Rating (Tons)
HS 20-44	36.0	29.5	29.5
Tri-axle Dump Truck	37.5	15.0	25.5
Concrete Truck	33.0	15.0	25.5
Tandem Axle Truck	29.5	16.0	27.0
6 Axle Tractor Trailor	42.0	24.0	40.0
18 Wheeler	40.0	23.0	39.0
School Bus	12.5	16.0	27.0

Since ALDOT restricts truck weights according to operator ratings, an occurrence in which the gross weight of the vehicle is larger than the operator rating signifies a need for posting of weight restrictions. For posting, the assumption is made that the individual axle loads are in constant proportion to the gross vehicle weight.

As previously mentioned, the vehicle that produces the largest live load effect and thus has the most critical load rating in Table 3.1 above is the tri-axle dump truck. A comparison between the positive-moment capacity and positive-moment demand due to

dead load effects and live load effects from the tri-axle dump truck for a typical exterior girder is presented in Figure 3.8. Since the load ratings for an interior girder differ from that for an exterior girder, a capacity-demand curve is also presented for an interior girder in Figure 3.9. The jagged portions of the capacity curves correspond to locations of tension reinforcement termination.

The locations at which load effects exceed the capacity in Figure 3.8 and Figure 3.9 indicate deficient regions. Thus, these regions require positive moment strengthening. The design and application of the FRP composite to the deficient regions is presented in Chapter Four.

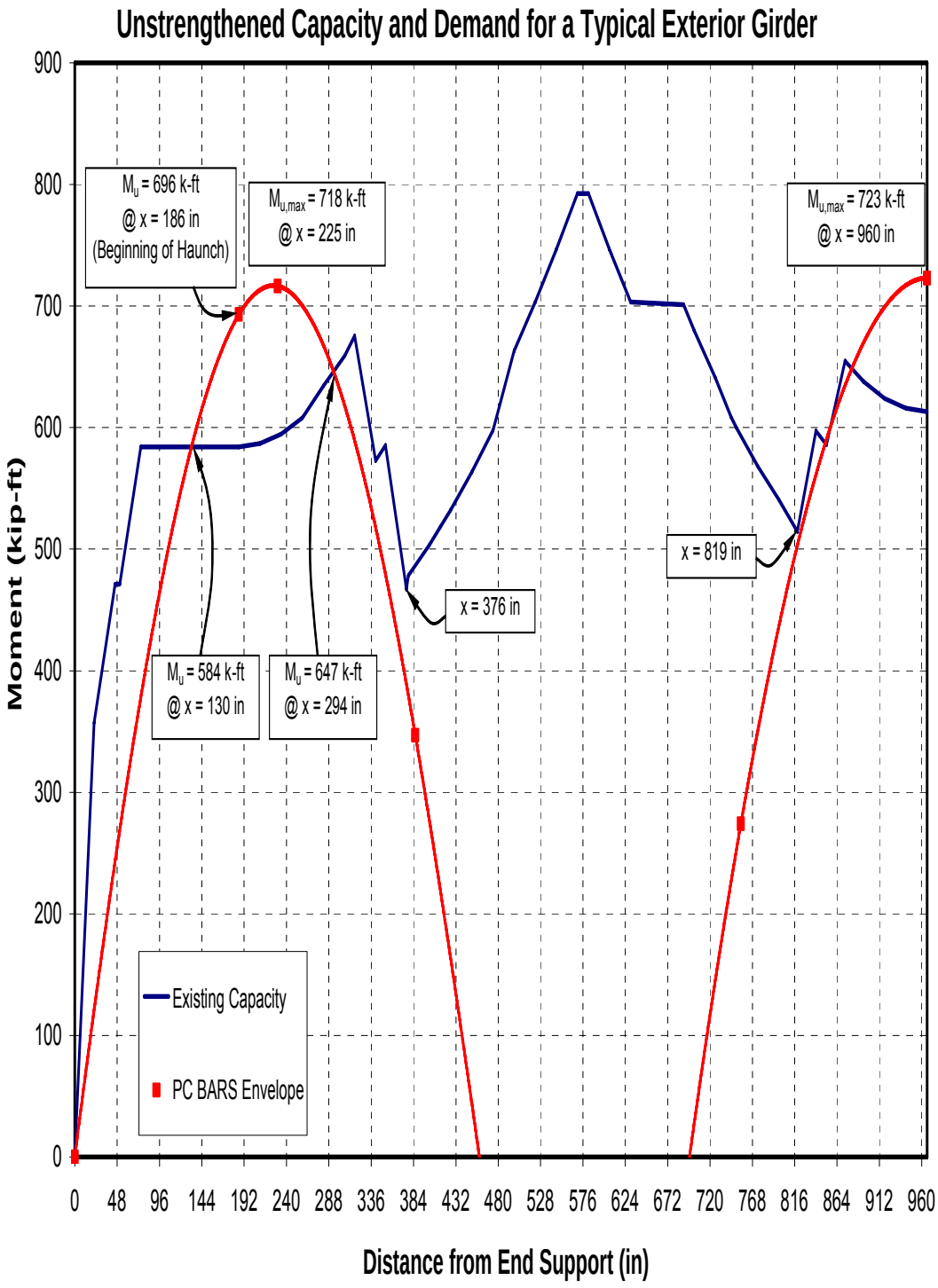

Figure 3.8: Unstrengthened Capacity and Demand for a Typical Exterior Girder

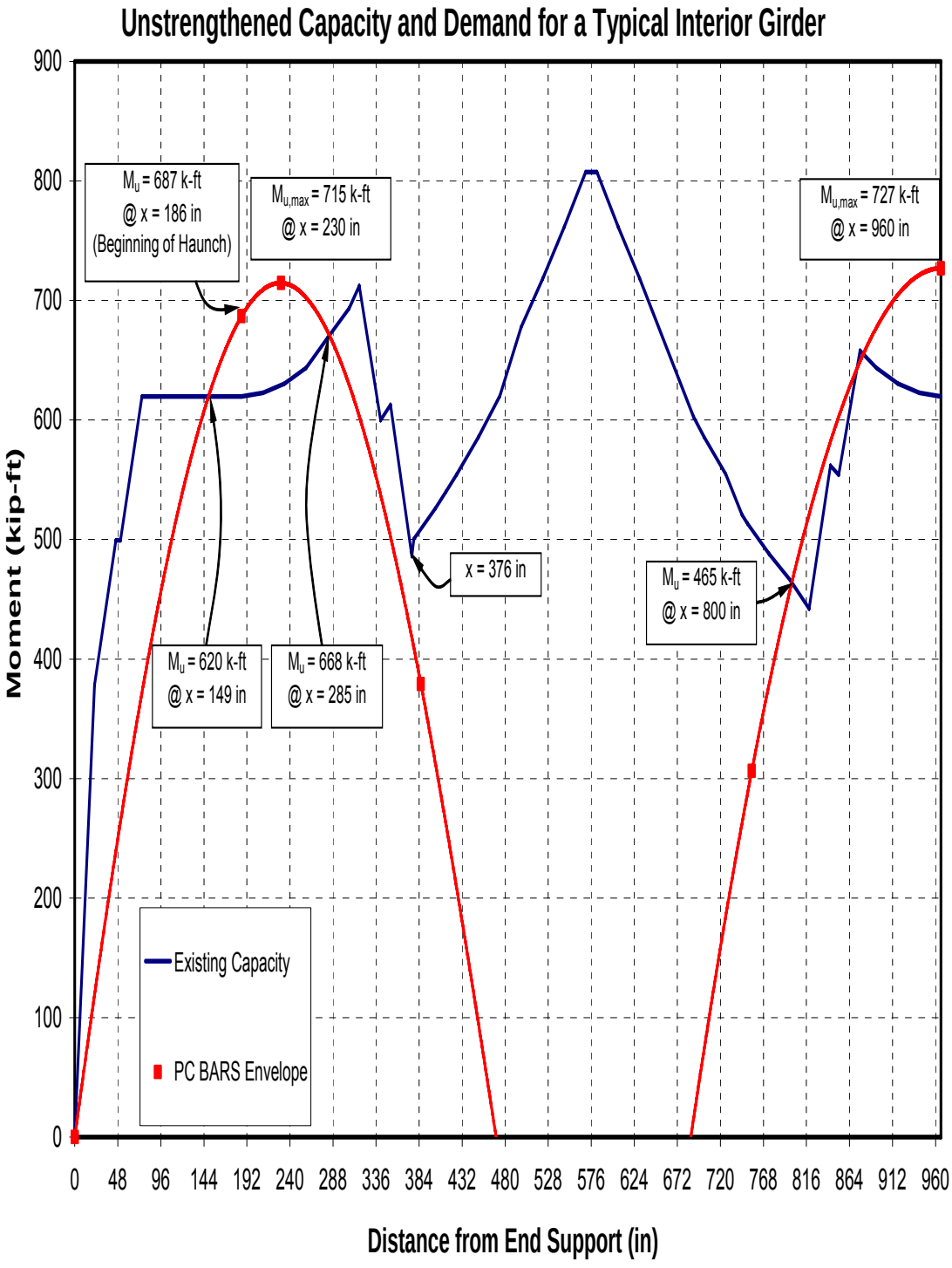

Figure 3.9: Unstrengthened Capacity and Demand for a Typical Interior Girder

CHAPTER 4: DESIGN AND INSTALLATION OF FRP STRENGTHENING SYSTEM

4.1 GENERAL

Following the design process and load testing of the unstrengthened structure, the installation phase began in late October 2001 and lasted approximately one month. The key elements of FRP application to the deficient positive moment regions can be summarized as follows:

- surface preparation and crack injection in accordance with ACI 440 guidelines,
- preparation of the FRP composite system,
- epoxy application to the surface of the composite and girder soffits,
- application of the composite to the surface of the concrete, and
- inspection of the composite installation.

Performance of the FRP composite strip system under service load conditions was evaluated by comparing unstrengthened load tests performed in August 2001 to strengthened load tests of the bridge performed in December 2001 and June 2002. The experimental load testing procedures, data, and corresponding results will be presented and evaluated in Chapters Five and Six.

4.2 DESIGN SUMMARY

Positive moment capacity of the War Memorial Bridge had become deficient during its service life and necessitated load posting for certain types of truck traffic. Negative

moment and shear capacity remained adequate for all girders. Therefore, designers needed to only consider strengthening positive moment regions to adequately repair the bridge. FRP was chosen as the material for repair for its speed of installation, high performance-to-weight ratio, and cost efficiency, among other factors. Capacity increases due to FRP systems can be as high as three times the original ultimate strength depending on factors such as reinforcement steel and FRP ratios, FRP properties, and existing concrete properties and damage (El-Mihilmy and Tedesco 2000). The flexural strengthening design procedure used was based on recommendations given outlined in the then-draft version of ACI Committee 440 *Design and Construction of Externally Bonded FRP Systems for Strengthening Concrete Structures* (2002). Auburn University researchers completed three designs, with different functions used to model the concrete compressive stress distribution in each design (Swenson and Barnes 2002). The first design modeled the concrete compressive stresses as a rectangular stress distribution. The second design modeled the concrete compressive stress as linear elastic. The third design modeled the nonlinear nature of the stress-strain relationship for concrete. Design was assisted through use of a computer spreadsheet program. Anchorage and serviceability issues were considered. A complete explanation of the design procedure can be found in a previous report (Swenson and Barnes 2002).

The material chosen for reinforcement was the Tyfo UC Composite Laminate Strip System from Fyfe Company, LLC. This product utilizes a carbon composite material with high tensile modulus and strength. Tyfo TC epoxy is used to bond the composite strips to the substrate—the positive moment regions of the RC girders—that have been primed with Tyfo S Epoxy. When the epoxy is cured, the composite system maintains

desirable properties over a wide temperature range. Tyfo UC strips contain at least 60% content of fiber by volume and come in standard thicknesses of 0.055 in. and 0.075 in. and widths of 2 in. or 4 in., but can be adjusted to meet specific project criteria. The manufacturer guarantees property values for the composite laminate material as listed in Table 4.1 below.

Table 4.1: Tyfo UC Composite Laminate Properties

Tyfo UC Composite Laminate Properties	
Property	Nominal Value
Ultimate tensile strength in primary fiber direction	405,000 psi
Ultimate tensile strength 90º to primary fiber direction	0 psi
Tensile Modulus	22.5×10^6 psi

The Tyfo S and TC epoxies cure as a function of time and temperature. Fyfe Company, LLC., specifies a minimum application temperature of 40°F for both epoxies. For the Tyfo TC epoxy, temperature is more critical to the life of the product. Similar to most products with a curing time required, colder temperatures will increase cure time while warmer temperatures will decrease cure time. At temperatures over 90°F, careful attention should be given to the mixed epoxy as curing time may decrease rapidly. Ambient temperatures of approximately 70°F should result in a pot life of around two

hours. The curing reaction is exothermic, and its rate of reaction increases as more heat is added. Both epoxies are toxic, and caution should be exercised when handling these materials. Respirators or other types of air filtration devices should be used to avoid breathing the fumes, especially indoors. Contact with the skin, eyes, etc., should be avoided. Use of eye protection, a chemical suit, and heavy-duty gloves is recommended.

The system design utilizing Tyfo UC composite was completed based on ultimate strength design, anchorage, and serviceability concerns. The locations requiring installation of FRP composite are shown in Figures 4.1 and 4.2 for an exterior and interior girder, respectively. A thickness of 0.055 in. was used for each critical section while the width was varied.

For an exterior girder, a 10-in.-wide section comprised of two 4-in. strips and one 2-in. strip was required. For end spans, the strips extended between points located 96 in. and 336 in. from the end of the bridge. For the center span, the exterior girder strips extended 180 in. on each side of midspan. For each interior girder, an 8-in.-wide section comprised of two 4-in. strips was required. For end spans, the strips extended between points located 116 in. and 320 in. from the end of the bridge. For the center span, interior girder strips extended 204 in. on each side of midspan. The installation of the composite is discussed in the following sections.

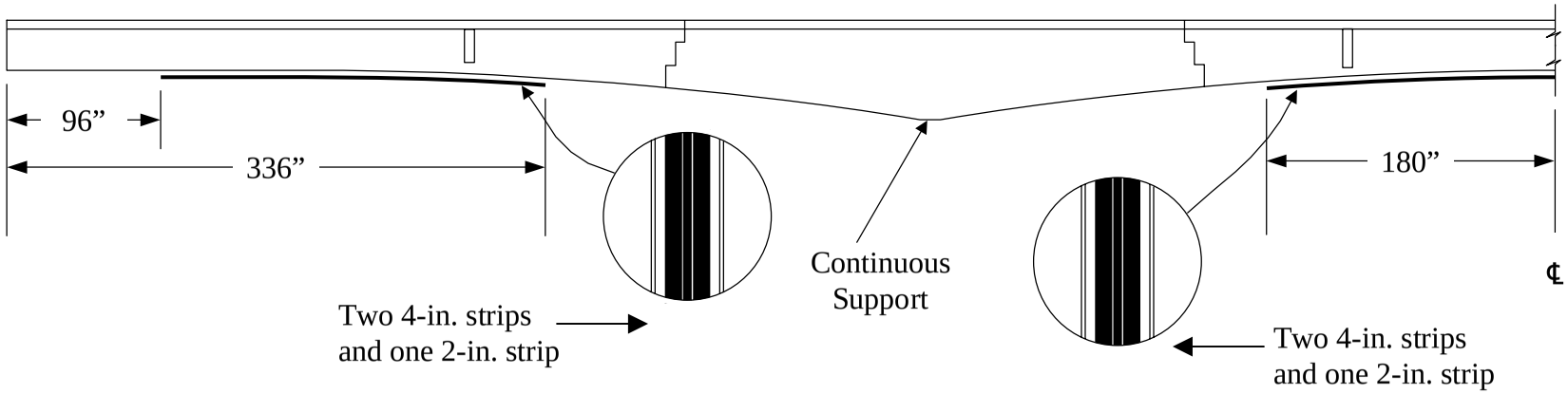

Figure 4.1: Location of Composite on Typical Exterior Girder

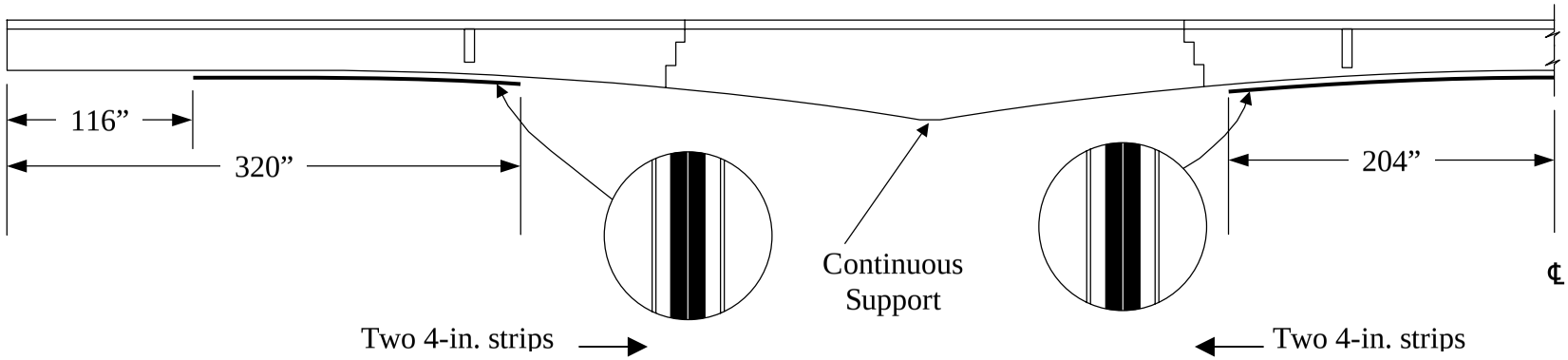

Figure 4.2: Location of Composite on Typical Interior Girder

4.3 CONCRETE SURFACE PREPARATION

Preparation of the concrete surface was necessary before priming the girder soffit for application of the FRP. Dust, dirt, and laitance were removed by sandblasting. Form lines and surface imperfections were removed by a hand-held grinder. After grinding was complete, a profile inspection of the girder soffit was performed, which involved observing contact continuity between the girder surface and a yardstick. Surface protrusions were noted and grinding was repeated at these locations.

After surface profiling was complete, residual debris and dust that might have interfered with the composite bond to the girder surface were removed by water blasting, shown in Figure 4.3. Surfaces were allowed to dry completely before commencing subsequent stages of the FRP installation.

4.4 CRACK INJECTION

Cracks with widths of 0.010 in. or wider may lead to premature failure of bonded FRP composite (ACI Committee 440 2000). ACI Committee 440 suggests epoxy pressure injection of cracks wider than 0.010 in. To determine which cracks required injection, cracks that appeared more than 0.003 in. wide were mapped and measured with a crack comparator. A summary of the locations and widths of measured cracks is included in Appendix A. All cracks 0.010 in. or wider were pressure injected with epoxy. A total of seven crack groups in Span 10 were pressure injected with epoxy. The original construction joints in all three end spans and the center span had cracked, and these cracks were also injected (sixteen total construction joints). Cracks located in the end spans were less than the limit outlined by ACI 440 and therefore did not require injection. Several crack groups located near the one-third-span sections of the center span were

larger than the 0.010-in. limit and required injection. Some additional center span locations were also injected. The locations, given in approximate distances, are as follows:

- Girder 1, Span 10—one group located 45–47 ft north of Bent 10,
- Girder 2, Span 10—two groups, located 18–19 ft north of Bent 10 and 45 ft north of Bent 10,
- Girder 3, Span 10—one group, located 18–20 ft north of Bent 10, and
- Girder 4, Span 10—three groups, located 17 ft north of Bent 10, 19–20 ft north of Bent 10, and 31 ft north of Bent 10.

ACI Committee 224 (1993) outlined a procedure for epoxy injection, which consists of installing injection ports at close intervals, sealing the crack along its length and around the port, and pressure injecting epoxy into the cracks. The same procedure can be used for crack groups and construction joints. Injection of a crack group is shown in Figure 4.4. First, the crack surface was sealed along the crack length on both sides of the girder. Venting ports were installed every 6–8 in. along the length of the crack. The ports were bonded flush with the surface of the concrete and sealed around the base. Seals were allowed to harden for 24 hours before injection. Injection was performed by mechanical means from both sides of the girder starting at the bottom port. Once epoxy became visible in the port immediately above the port being injected, the port being injected was capped. Injection then began in the port immediately above. This procedure continued until all ports had been injected.

Figure 4.3: Hydroblasting the War Memorial Bridge

4.5 FRP System Preparation

All components of the FRP system were shipped as one unit on a single pallet (Figure 4.5). The FRP composite was delivered in several large rolls of 2-in. and 4-in. strips. Each epoxy type necessary for application was shipped as two parts in pre-measured quantities within five-gallon containers. Required amounts of epoxy were measured and mixed at the bridge site daily, and required lengths of FRP were cut from the larger rolls in the field.

All FRP preparation was performed on site. Composite strips were unrolled, and strips were cut to required lengths using a circular saw with a carbide-tipped blade. To prevent the composite from splitting or fraying during cutting, the ends of the FRP strips were temporarily wrapped in duct tape. Once cut, the abraded (lackluster) side of the composite was thoroughly cleaned with lint-free rags soaked in acetone or methyl-ethyl-ketone (MEK). The cleaning solvent was allowed to dry thoroughly before proceeding with the application.

4.6 Installation Description

Though messy and sometimes awkward to handle, the FRP system installs relatively quickly and requires minimal equipment. Because of the relative ease of installation, repairing a structure with a composite laminate strip system is a worthwhile option to consider over other methods such as steel plate bonding or total bridge replacement. If suitable for the application, installing a composite laminate strip system can be a very effective repair method while saving large amounts of time and money relative to other methods.

Figure 4.4: Crack Injection of the War Memorial Bridge

Figure 4.5: FRP System Components, Shown as Shipped

A team comprised of ALDOT bridge maintenance personnel and Auburn University researchers performed installation. This team typically consisted of about eight members. Four to five men applied the composite to the girder soffit while two or three additional crewmen handled operations on the bridge deck. Team numbers should be adjusted for the size of the installation, and crews familiar with the installation procedures will be easily able to adjust for differing project sizes. Once surface preparation was complete, installation was performed during the month of November 2001, over a period of about three weeks. Weather was rather warm and somewhat dry as compared to a typical November in Alabama, with an average low of 51.6°F and an average high of 72.1°F for the month of installation. Traffic control and ambient temperature concerns were addressed each day. Tools and supplies required for application were purchased at a local home improvement store and did not comprise a significant portion of the project budget. Work was performed from scaffolding suspended under the bridge. I-beams were hung by steel cable from the bridge guardrails where scaffolding was laid perpendicular to the beams to provide a working surface under the bridge deck from which to install the FRP.

Installation of the composite laminate strip system requires several tools, most being generic tools that can be purchased at a general hardware or discount store. Specific needs may vary from each application, but a typical list would include the following:

Drill w/ paint stirrer bit (to mix epoxy)
Utility knife
Paint rollers and trays
Drop cloths
Trowels (notched to the width of the FRP strips)
J-rollers
Methyl Ethyl Ketone (MEK)
Utility pails or 5-gallon buckets
Shop rags

A safety equipment list should include, but is not limited to:

Respirator
Protective Eyewear
Chemical Suit
Chemical-resistant rubber gloves

For the War Memorial Bridge repair, target application time of FRP to one girder was from 45 minutes to one hour. This timeframe was the same for interior and exterior girders. Based upon this estimate, installation was scheduled to be completed by installing FRP on three girders per day for a total of four days. Due to limited experience with FRP installation, this target pace was not realized at the outset but was achieved after the experience of a few girder installations. The installation was ultimately performed in six working days. The installation team managed only one girder on an end span the first day. Subsequent days saw an increase in familiarity and the completion of two or three girders per day until the installation was finished.

A typical installation schedule should require an early start to prepare for and plan the installation activities. Proper time should be allotted to set out materials, tools, and organize the strategy for FRP application. This is especially true in cases similar to the War Memorial Bridge application, where the Tyfo TC Epoxy was applied to the FRP strip on the bridge deck and then handed down to personnel on scaffolding to be applied to the girder. It is necessary to have all tools ready and anticipate potential problems in order to minimize downtime when the Tyfo TC Epoxy has been mixed and is waiting to be applied. Lost time might lead to a situation where the epoxy has set before it can be applied. Because of the high unit cost of the epoxy, economics dictate that as little should be wasted as possible.

After preparations are made, the epoxy components should be mixed and then applied to the substrate and to the FRP strip. Tyfo TC Epoxy should be applied to liberally coat both the substrate and FRP strip in a manner that will promote complete adhesion of the FRP to the substrate and avoid trapping air between the two. If air is trapped between the substrate and the FRP, this may provide a point from which delamination may initiate under service level loads. Local delamination is undesirable for two reasons: it disrupts the transfer of forces between the FRP and the concrete substrate, and its propagation creates the potential for complete bond failure.

The installation of FRP composite for the strengthening of exterior and interior girders consisted of three major steps: priming epoxy application, application of bonding epoxies to required surfaces, and application of the composite strips to the concrete surface. To ensure optimum compatibility, the entire epoxy and FRP composite strip system was purchased from Fyfe Company.

Manufacturer specifications require that the ambient temperature be above 40ºF (4ºC) for epoxy use. Temperatures below that threshold decrease epoxy workability and increase curing time. Though temperatures for November 2001 were above average, ambient air temperature occasionally fell below this critical temperature at night. To remedy this problem, plastic and canvas sheeting was draped along the sides of the exterior girders of all three spans. These tarpaulins were used as thermal insulation to trap heat underneath the bridge deck. Five kerosene space heaters with a 155,000 BTU output were placed at several locations on the scaffolding to maintain a temperature of 40°F or greater. The heaters typically operated overnight for up to 12 hours. Outside air temperature and temperature beneath the bridge were checked with a digital thermometer

before daily work began. Heater operation ceased once an ambient temperature above 40ºF was observed. The heaters could also serve to accelerate the cure of epoxy.

Due to traffic demand on State Highway 81 and the War Memorial Bridge, the bridge could not be completely closed to traffic during installation. However, vibration during curing could cause a strength reduction in the epoxy bond strength, with larger amplitudes of vibration having the potential to cause greater strength loss (Barnes and Mays 2001). Therefore, careful attention had to be given to how installation could proceed while traffic continued to use the bridge. Installing FRP to an exterior girder would be easier and less critical than installing FRP to an interior girder since any traffic crossing the bridge would be required to travel in the lane opposite installation and, therefore, further away from the exterior girder than the interior girder. Installation of the composite to all exterior girders was completed before installing composite to any interior girder. For composite installation to an exterior girder on the west side (Girder 1 for all spans), the southbound lane was closed to traffic. For composite installation to an exterior girder on the east side (Girder 4 for all spans), the northbound lane was closed to traffic. It was determined that traffic moving on the opposite side of the bridge deck would have minimal effect on the girder undergoing application. All truck traffic was restricted from using the bridge during daylight hours of installation days.

Lane closures and traffic control during FRP application to an interior girder was similar to that for an exterior girder. However, during application of composite to an interior girder, the single lane open to traffic was shifted as close as possible to the farthest curb and all heavy traffic was detoured to prevent damaging load effects to the FRP application. Traffic control was maintained for approximately 9 hours daily after

installation began to allow time for application and epoxy cure. Typically, a period of 5–6 hours was available for epoxy cure after installation procedures had been completed. After having installed FRP on six exterior girders, installers became more comfortable with the installation procedure; therefore, the time required for interior girder FRP installation was minimal—thus maximizing the time allowed for curing during the duration of the traffic shift and truck detour.

According to Fyfe Company recommendations, a prime coat of Tyfo Saturant (Tyfo S) Epoxy should be applied to the concrete surface before adhesive application. On the War Memorial Bridge, this was the girder soffit of both interior and exterior girders in regions defined in Figures 4.1 and 4.2. Next, Tyfo Tack-Coat (Tyfo TC) Epoxy should be applied to the primed areas of the concrete substrate. A thin layer of Tyfo TC Epoxy should also be applied to the abraded side of the FRP after having cleaned it with an approved solvent. Once the Tyfo TC Epoxy achieves optimum tackiness, the composite strips may be applied.

Priming was accomplished by applying Tyfo S Epoxy with a paint roller. The Tyfo S Epoxy should be applied such that holes in the concrete are filled and a smooth surface is created. Holes, bumps, and other imperfections may trap air in the application of the Tyfo TC Epoxy or prevent flush contact between the FRP strip and the substrate. Before application of the Tyfo TC Epoxy and FRP, the Tyfo S Epoxy was cured to a “tacky” condition, best defined as the condition where the epoxy should be sticky to the touch but should leave no more than a slightly distinguishable fingerprint on the surface. By applying the Tyfo S Epoxy during the afternoon of the day prior to application of the Tyfo TC Epoxy and FRP, the Tyfo S Epoxy was allowed to cure to sufficient tackiness.

To remedy any over-cured conditions with the Tyfo S Epoxy, the primed substrate was abraded with a wire brush within a few hours of losing tackiness to the touch. This exposed the uncured Tyfo S Epoxy under the surface, which was used to properly bond the Tyfo TC Epoxy and composite to the girder. Additionally, due to the from-below application process of the War Memorial Bridge project, the Tyfo S Epoxy was applied thinly to the underside of the girders in order to prevent drip spots from forming during curing. If drip spots formed, they had to be removed before installation proceeded.

The portions of the girders being strengthened with FRP were marked on both the girder sides and soffits. This made application of the prime coat of Tyfo S Epoxy easier, and ensured that adequate coverage would be obtained. The amount of coverage provided by a single sealed, pre-measured unit of Tyfo S Epoxy was in excess of that required for application to a single girder. In order to avoid mixing more than needed, portions of the two-part epoxy were rationed at a volumetric ratio of 100 parts A component to 42 parts B component. Mixing was done for five minutes using a hand-held drill with a paint mixing attachment. Once a uniform blend was achieved, the Tyfo S Epoxy was applied to the required locations using a standard 9-in. paint roller. Before application of Tyfo TC Epoxy began, the primed girder surfaces were inspected to ensure the Tyfo S Epoxy had been applied uniformly, that no bumps or drips had formed, and that the proper tackiness had been achieved.

In several cases, the application of the Tyfo S Epoxy to the girder surface was observed to be substandard. A common error made was the application of an excessively thick coat of Tyfo S Epoxy. When dry, this condition was characterized by the semblance of droplets on the girder soffit. These nonuniformities in the application were removed

using a bubble scraper as typically used in paint removal. In one extreme case (Span 10 Girder 3), the remedy process removed almost all Tyfo S Epoxy from the girder surface. The soffit of Span 10 Girder 3 was subsequently reprimed and allowed to cure for about 45 minutes prior to proceeding.

Another problem occurred when an application of Tyfo S Epoxy was allowed to overcure before FRP adhesion. Tyfo S Epoxy was applied to Girder 3 in Span 9 and 11 two days prior to Tyfo TC Epoxy and FRP application. Upon inspection for tackiness before Tyfo TC Epoxy application, a near complete cure was observed. To remedy the overcured condition, the surface was roughened with a wire brush to attempt to provide a better bond.

After the prime coat of Tyfo S Epoxy had been applied, Tyfo TC Epoxy was applied simultaneously to the girder soffit and to the composite strips. The two-component epoxy was mixed at a volumetric ratio of 100 parts A to 30 parts B using the same method described in the Tyfo S Epoxy mixing procedure. For application of Tyfo TC Epoxy to the girder soffit and composite strips, at least one complete pre-measured, pre-packaged unit was mixed per day. Application of this epoxy to the girder soffit was performed from scaffolding suspended below the bridge deck. The preparation of the composite strips and application of epoxy to the composite strips was completed on the bridge deck.

Application of Tyfo TC Epoxy to the concrete substrate was performed by means of two different methods. The manufacturer required a thickness of 1/16 in. be applied to the girder soffit. Layers thicker than 1/16 in. may increase curing times and mar the visual appearance of the installation. For the first application, the Tyfo TC Epoxy was applied to girder soffit using a paint roller. This method proved to have little control over the

applied thickness of epoxy, resulting in an excess amount being applied. An alternative Tyfo TC Epoxy application procedure was to use an 8-in. taping knife to apply epoxy to the girder soffit (Figure 4.6). The thickness of the application was controlled by finishing the surface with a V-notched trowel with a 3/16-in. notch depth. This method resulted in an initial (3/32-in. average) thickness 50 percent larger than the thickness recommended. While this was greater than specified, it compensated for slightly less epoxy than specified being applied to the FRP strips (described below) and proved to be the ideal application method. This method was used for application of Tyfo TC Epoxy to all but the first girder.

Application of epoxy to the FRP composite was performed on the bridge deck. Preparation of the composite—including measuring, cutting, and cleaning the composite surface—was completed before epoxy application. After the cleaning solvent had evaporated, Tyfo TC Epoxy was applied to the surface of the composite (Figure 4.7). A minimum thickness of 1/16 in. was recommended. Tyfo TC Epoxy was applied with a modified V-notched trowel (Figure 4.8). The trowels were modified by cutting V-shaped notches of 1/8-in. depth at the peak and tapering to 1/16-in. depth at the edges. This was done for both 2- and 4-in. strip application. Use of this tool resulted in slightly less than 1/16 in. epoxy thickness. However, the recommended amount of epoxy was applied in combination with the Tyfo TC Epoxy on the strip and girder.

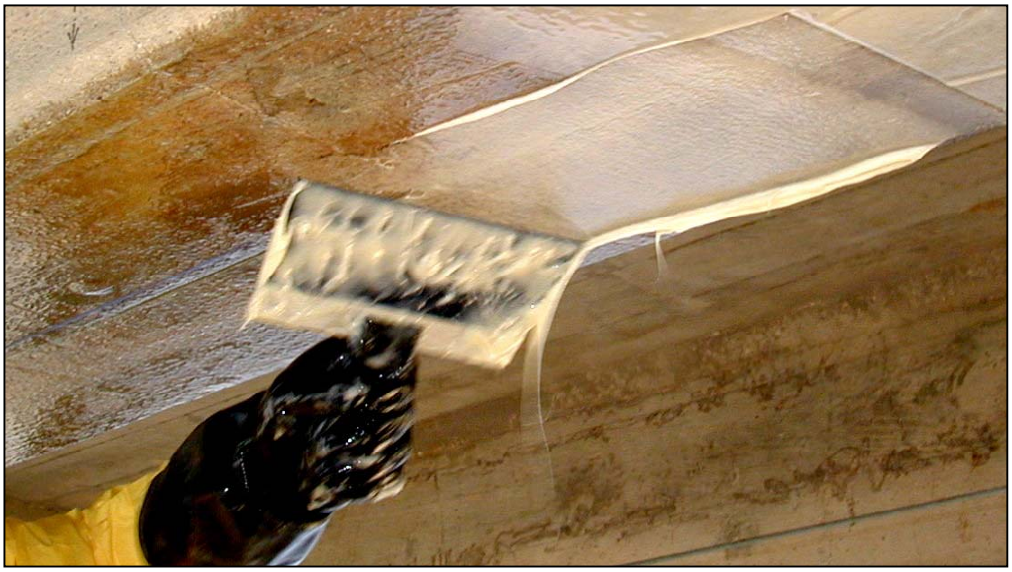

Figure 4.6: Application of Tyfo TC Epoxy Using an 8-inch Taping Knife

Figure 4.7: Application of Tyfo TC Epoxy to the Composite Strip

After Tyfo TC Epoxy was applied to all surfaces, the composite strip was applied to the girder soffit. The installation procedure for each single composite strip was identical, regardless of strip width or girder type. The epoxy consistency was monitored, and FRP application began as soon as the epoxy reached a level of tackiness to support the FRP strip once it was placed. Personnel on the bridge deck handed the epoxy-coated strip over the deck railing to personnel on the scaffolding below (Figure 4.9).

The crew performing FRP installation to the girder soffit typically consisted of five men. Application began at one end of the strip. Firm palm pressure was applied along the length of the strip, as shown in Figure 4.10. After initial contact was made at all points along the strip, the longitudinal alignment of the strip was examined and adjustments were made as necessary. The strip could be easily repositioned by sliding the composite in the correct direction using only fingertips. Adjustments were within two inches or less.

Figure 4.8: Modified 4-inch V-notched Trowel

After placing and aligning the FRP strip, excess epoxy was troweled off the surface of the composite using firm pressure. Next, the composite was seated along its length using a 3-in. J-roller. Figure 4.11 shows the seating of an FRP strip using a J-roller. A firm back-and-forth motion was employed to guarantee complete contact and remove any voids beneath the surface of the strip. For aesthetic purposes, the composite surface was finished by a final removal of excess epoxy with a trowel. Subsequent visual inspection of the composite edges was performed to check for voids. If voids were indeed present along these edges, excess Tyfo TC Epoxy from the girder soffit was utilized to fill them.

The installation of composite to a typical exterior girder consisted of a single 2-in. Tyfo UC Strip (2UC55) and a pair of 4-in. Tyfo UC Strips (4UC55), resulting in a 10-in. total width. The Tyfo 2UC55 Strip was applied first along the center of the girder soffit, aligning the primary fiber direction with the longitudinal axis of the girder. Next the two Tyfo 4UC55 Strips were applied parallel on each side of the Tyfo 2UC55 Strip. A gap of approximately 1/16–1/8 in. was left between strips for excess epoxy to escape.

The installation of composite to a typical interior girder consisted of two Tyfo 4UC55 Strips resulting in an eight-inch total width. The two 4-in. strips were centered on the girder soffit again leaving a gap of approximately 1/16–1/8 in. between strips. Figure 4.12 shows the finished installation of the Tyfo UC Composite to the soffit of the center span girders.

Figure 4.9: Transfer of Epoxy-Coated Strip from Bridge Deck to Scaffolding

Figure 4.10: Application of the Composite Strip to a Girder

The installation process is a relatively easy process. For the War Memorial Bridge installation, the limiting factor was the crew's inexperience with handling the materials. That issue was quickly overcome after a day or two of working with the components. All personnel found the system to be straightforward. However, the installation process is exceptionally messy. All personnel wore chemical resistant suits, but ALDOT personnel found that they preferred full non-porous, non-breathable raingear to the chemical suits provided. The Tyfo S and TC Epoxies found their way into and onto most equipment that was used, and most of that equipment became ruined and had to be thrown away as a result. The installation crew had an aversion to wearing proper fall protection. Though it was provided, it was noted that wearing fall protection would make the from-below installation exceedingly difficult. Had fall protection been properly worn, the job duration would have likely doubled. At the conclusion of the job, ALDOT maintenance personnel concluded that they would rather contract out the installation rather than perform it with their own crews.

Figure 4.11: Seating an FRP Strip Using a J-roller

Figure 4.12: Completed Installation of Composite to Center Span Girders

4.7 INSPECTION OF COMPLETED INSTALLATION

Once FRP composite had been installed on all girders, the FRP was inspected for bond quality. Researchers accomplished this by searching for any voids and determining their size related to surface area. A void is defined as a location between the FRP composite and concrete substrate that was not filled with epoxy during installation through air being present or other mechanism. ACI Committee 440 (2002) recommends guidelines for evaluation of wet lay FRP systems. Voids less than 2 in^2 are acceptable, provided that the total void surface area is less than 5 percent of the total bonded area and the frequency is less than 10 voids per 10 ft^2. Based on these guidelines, the integrity of the system was evaluated with the tap test. The tap test is a method for locating voids or delaminations based upon the sound produced when the composite surface is struck with a blunt object. A U.S. quarter-dollar coin was used to tap the surface of all FRP composite installed on the girders. When tapped, an air void beneath the surface of the composite will produce a hollow sound. The results of the tap test proved that less than 0.1 percent of the evaluated surface area contained air voids. Small voids beneath the composite surface detected by the tap test are indicated in Figure 4.13. The largest void measured was approximately 3–4 in^2. While larger than recommended, this single void should not have significantly affected the overall performance of the composite system as it lay within a few inches of the end of the FRP strip. Based on tap test results, repairs to the installed FRP were deemed unnecessary.

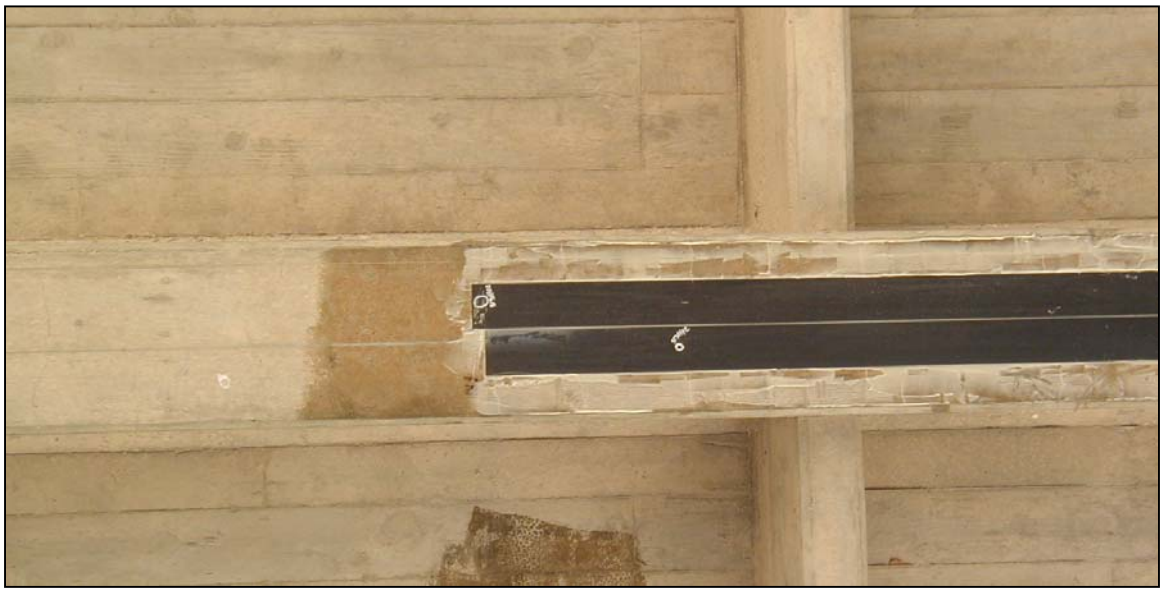

Figure 4.13: Voids (Marked with White Circles) on FRP

CHAPTER 5: TESTING DESCRIPTION

5.1 GENERAL

Field live load tests of the War Memorial Bridge were conducted four times: the first test was performed before the FRP installation, the second immediately after FRP installation, and the third and fourth six months after FRP installation. Testing consisted of static and dynamic tests in northbound and southbound directions. Results from each test are presented later in this report. A description of the instrumentation scheme, the data acquisition system, and the static and dynamic tests are included in this chapter.

5.2 INSTRUMENTATION

Electrical resistance strain gauges (ERSGs) and deflectometers—used to measure live load deflection—were used to measure the response of the bridge to live loads. Gauges were installed at critical locations in Span 9 and Span 10 for Girder 3 and Girder 4. Strain gauges were bonded to the positive moment reinforcing bars as well as the FRP surfaces. Deflectometers were installed flush with the girder soffit using removable brackets at the critical section. Deflections were measured for both the Existing and Repaired Load Tests in the manner described in following sections. Figure 5.1 shows the locations of all deflectometers and ERSGs on the primary steel reinforcement and the FRP reinforcement.

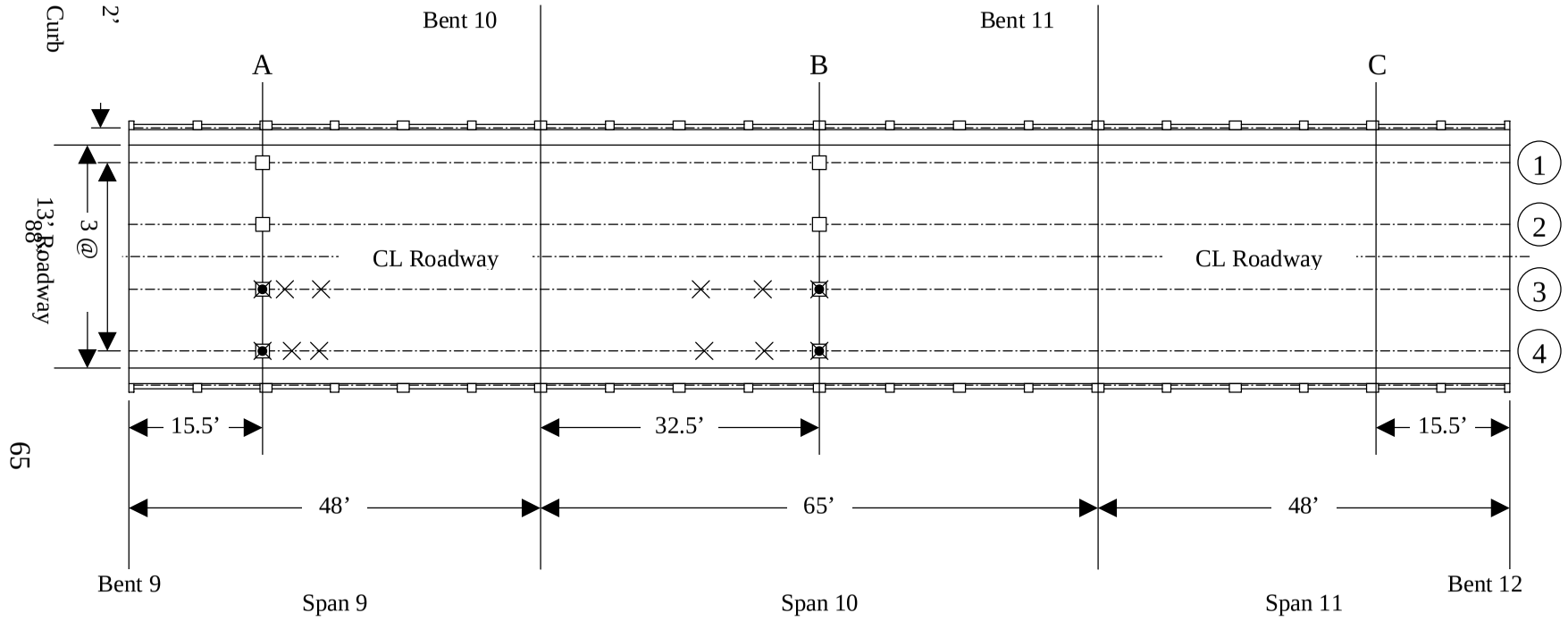

Quantity Measured
□ Deflection
• Steel Strain
× Composite Strain

Figure 5.1: Plan View with Sensor Locations

Each strain gauge used for measurement had a nominal resistance of 350 Ω. The actual resistance of each installed gauge should be within +/- 0.3 percent of the manufacturer's listed 350-Ω nominal resistance value. Deviation of actual resistance from nominal resistance was measured immediately after installation and approximately two weeks prior to load testing of the strengthened bridge.

The deflectometers used were made of a tongue-like piece of aluminum attached to a steel bracket. A typical deflectometer installation at the critical section is shown in Figure 5.2. The bracket was attached to the girder soffit at the critical section—the point of interest for measuring deflections. The other end of the tongue was attached to a cable, and the cable was tensioned and attached to a tie-down point located directly below the tongue. Therefore the tip end of the tongue remained relatively fixed when the bridge girder deflected. Four strain gauges were mounted on the tongue in a full-bridge, bending strain configuration. For each deflectometer, the output of this full-bridge circuit was calibrated in the laboratory to indicate the deflection of the bracket relative to the tip end of the tongue.

When the girder deflected, the bracketed end of the tongue would move relative to the fixed end, increasing or decreasing the amount of bending strain on the tongue. If a load caused a downward deflection of the object, strain was reduced on the tongue, and the gauge measured a decrease. If a load created an upward deflection, strain was increased, and the gauge measured an increase. From having measured an initial at-rest reference voltage (zero voltage) of the strain gauge and calibrating the voltage change to a deflection, real-time deflections could be measured.

Prior to FRP installation and initial load testing, portions of the girder soffit concrete cover at critical sections were cut and removed. This procedure was completed for Girders 3 and 4 in Spans 9 and 10. This procedure exposed the bottom-most layer of reinforcing steel so that strain gauges could be installed. ERSGs were installed on only four cross sections due to the symmetry of the bridge. Six reinforcing-bar strain gauges were placed at each critical location for a total of 24 gauges within the constant-depth portion of each span where the largest live load strain was expected to occur. Only four gauges were actually used for data acquisition at each critical location for all the tests; the extra gauges were installed for redundancy and only monitored in the first (pre-strengthening) test. All reinforcing steel strain gauges had a gauge length of 1/4 in.

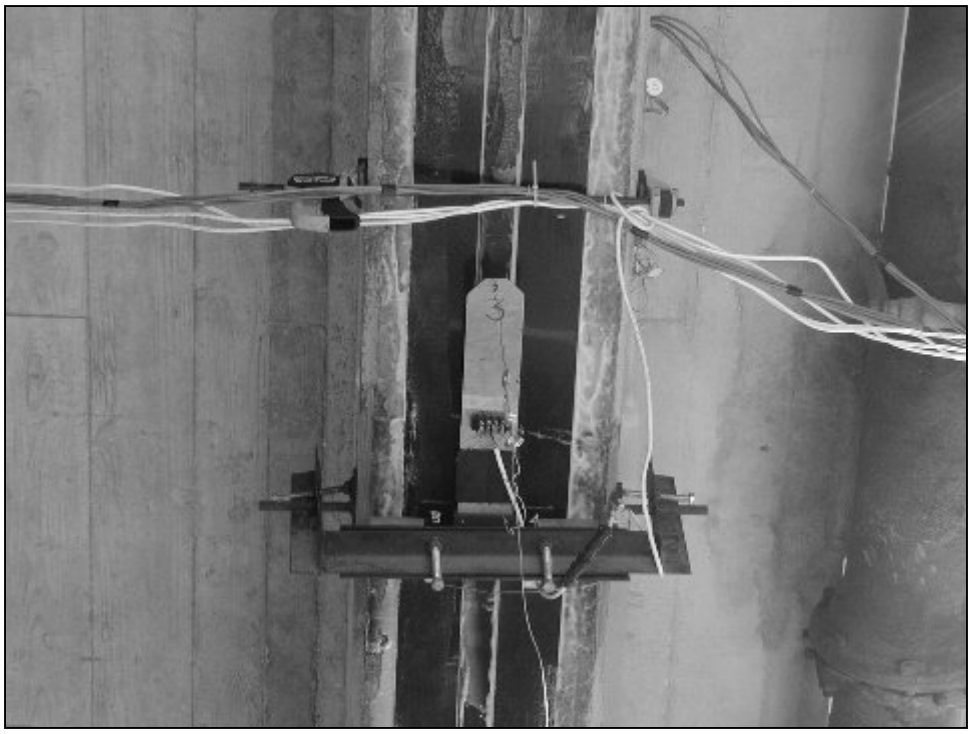

Figure 5.2: Typical Deflectometer Installation

Locations of steel strain gauges are shown in Figure 5.1. For both instrumented girders in Span 9, the location of the critical design section was 186 in. from the noncontinuous end of the bridge. For both instrumented girders in Span 10, the location of the critical design section was at midspan (966 in from the end of the bridge). Figure 5.3 shows a typical strain gauge installation at the exposed layer of steel reinforcement. Each piece of bar was instrumented with one strain gauge at the critical location. Two redundant gauges were installed on the two interior bars, approximately 2 in. north of the critical locations. Figures 3.4 and 3.5 show cross sections with reinforcing details for the 186 in. and 966 in. sections, respectively. After gauges were installed and coated, the sections were patched using Thoro Roadpatch DOT, a cement-based, fiber-reinforced, fast-setting repair material. This was done in order to protect the reinforcing steel, prepare for testing, and provide a smooth surface for FRP installation.

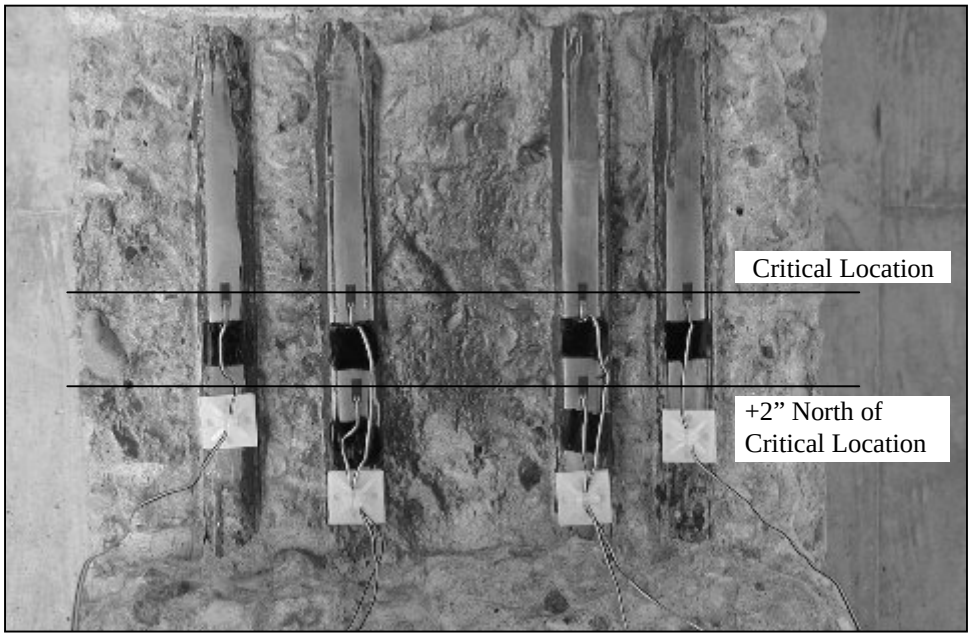

Figure 5.3: Typical Strain Gauge Installation to Steel Reinforcement

After FRP installation, strain gauges were bonded to the surface of the FRP composite strips. Strain gauges were installed at the critical design sections and directly below cracked sections on the instrumented girders over which FRP had been installed. Two gauges were installed at each critical section location—one gauge installed at the center of each 4-in. strip. This configuration allowed comparisons to be made between FRP strains alongside strains measured in the reinforcing steel. Gauges installed on the FRP surface at critical locations had a gauge length of 1/2 in.

For the Repair 3 Load Test, additional FRP gauge locations were selected based on concrete cracking near the critical locations but beyond the extent of the post-instrumentation concrete patching. For Girders 3 and 4 in Span 9, one gauge was installed per cracked section at locations approximately 18–19 ft and 22–23 ft north of Bent 9. For Girders 3 and 4 in Span 10, one gauge was installed per cracked section at locations approximately 18–19 ft and 25–26 ft north of Bent 10. Each gauge was installed at the center of a 4–in. FRP strip at a point where it was estimated that the gauge would span the crack on the girder soffit. FRP gauges installed at cracked sections had a gauge length of 1/8 in. Figure 5.4 and Figure 5.5 show typical FRP strain gauge installations for an exterior and interior girder, respectively.

Figure 5.4: Typical Strain Gauge Installation to FRP Surface for Exterior Girder

Figure 5.5: Typical Strain Gauge Installation to FRP Surface for Interior Girder

Vertical deflections were measured at the critical locations for all four girders in Spans 9 and 10. Deflectometers were mounted at the eight locations indicated in Figure 5.1. Figure 5.2 shows a typical deflectometer installation at a critical location. The deflectometers were mounted flush with the girder soffit and measured the girder displacement relative to a fixed reference. The displacement of a girder is the sum of the deflection of the instrumented girder and the bridge bents; however, bent deflection was considered to be negligible. Measured deflections could be used as an alternative means to quantify the service load performance of the FRP composite system, as well as to verify symmetric response about the centerline of the roadway (when loads are applied symmetrically).

5.3 DATA ACQUISITION

In order to process the electrical signals generated by strain gauges on the reinforcing steel, FRP, and deflectometers, a MEGADAC 3415AC high-speed data acquisition system, manufactured by OPTIM Electronics, was employed. The strain gauges output a voltage signal. The MEGADAC can be programmed to correlate a voltage to a corresponding value of strain or deflection. When the MEGADAC receives a voltage signal from an instrument, it converts it to a strain or deflection. It displays and stores the strains and deflections as they occur. MEGADAC data was filed electronically using a notebook computer and OPTIM's TCS Windows-based software. Data sets were archived to the computer after conducting each test.

Scan rates used in the live load testing of the bridge differed between tests. A scan rate of 200 scans per second was used for all static tests in the Existing Load Test and the Repair 1 Load Test, and for all tests (static and dynamic) in subsequent tests. A scan rate

of 500 scans per second was used for all dynamic tests in the Existing Load Test and the Repair 1 Load Test. The 200 scans-per-second rate was used for quasi-static tests to limit the file size of these long duration tests. Once trucks were positioned for each static test, data acquisition was triggered manually. Each static test was approximately three seconds in duration. The duration of a dynamic test was typically five to six seconds (the amount of time required for the trucks to cross the bridge and for the bridge response to return to negligible levels). The strain and deflection for each location and data set during a static test was determined by averaging the respective sensor values over the duration of the data set. The strain and deflection recorded for dynamic tests and quasi-static tests correspond to the peak sensor values over the test duration.

Because the rate of change of strain and deflection for a dynamic test is much larger than for a static test, it was believed that increased resolution from a higher scan rate was needed to obtain adequate accuracy in peak values of dynamic test results. However, between the Repair 1 and Repair 2 Load Tests, it was discovered that this was not the case for this bridge, and a scan rate of 200 scans per second would suffice for all tests.

In order to account for voltage drift in the circuits as well as temperature-dependent deformations, a zero reference point for each sensor was established for each test. Two complimentary methods were used to accomplish this task: (1) eliminating the offset by balancing all sensors prior to a set of measurements and (2) measuring a data set immediately after the conclusion of each set of measurements to establish a no-load "zero" reference. If the zero reference data taken at the end of each set of measurements were of significant magnitude, the value for each sensor was halved and subtracted from the recorded average measurement. In this manner, the final recorded data value for each

sensor represents the difference between the actual sensor output and the average of the outputs before and after the load was applied.

5.4 LOAD-TESTING PROCEDURE

Static and dynamic tests were performed before and after FRP composite installation. Personnel from ALDOT Maintenance Bureau and Auburn University conducted tests according to AASHTO design truck transverse spacings as well as worst-case spacing scenarios.

Field live load tests were performed with two identical load test trucks owned and operated by ALDOT. ALDOT load truck block configuration LC-5 was used in all static and dynamic tests for the Existing, Repair 1, and Repair 2 Load Tests, and load truck block configuration LC-6 was used for the Repair 3 Load Test. The LC-5 loading configuration was chosen because its moment demand curve best duplicates that of the tri-axle dump truck used by ALDOT for maximum load posting on the War Memorial Bridge. Based on analysis, the live load moments at all critical sections due to the LC-5 truck loading are larger than the live load moments due to the tri-axle dump truck loading by less than 7 percent. Each load truck has a three-axle configuration. LC-5 has a gross vehicle weight of 85,700 lbs while LC-6 has a gross vehicle weight of 93,275 lbs. Figures 5.6 and 5.7 illustrate the approximate axle spacing and weight distribution for each truck.

Actual load test truck transverse positions were chosen given truck wheel spacing information provided by ALDOT based on AASHTO design lane configurations and more demanding worst-case lane loading scenarios. The design configurations were referred to as AASHTO and Tight configurations, respectively. Eight different transverse locations were used in the static live load testing of the bridge for the Existing Load Test

and the Repair 1 Load Test. Ten different transverse locations were used in static live-load testing for the subsequent strengthened live load tests (Repair 2 and Repair 3 Load Tests). The transverse locations were selected at positions where the critical girder would experience the maximum load effect. The common eight locations are shown in Figures 5.8–5.15. The two additional configurations used in the Repair 2 and Repair 3 Load Tests were similar to the AASHTO configuration for Girders 1 and 4, except that a second truck was added at a distance governed by AASHTO specifications. The two additional configurations are shown in Figures 5.16 and 5.17, and are referenced as AASHTO Old and AASHTO New for the one- and two-truck AASHTO configuration, respectively, on Girders 1 and 4. Three different longitudinal positions—A, B, and C—were used per transverse line location and are shown in Figure 5.1. Trucks were positioned on the bridge deck with a tolerance of 3 in. in the transverse and longitudinal directions.

For each transverse location, the middle truck axle was positioned at three different longitudinal positions—labeled A, B, and C, as indicated in Figure 5.1—corresponding to gauged critical section locations for each span (the Span 11 critical section location mirrors the critical section location of Span 9). For the Existing and Repair 1 Load Tests, trucks were positioned as if traveling either northbound or southbound. For the Repair 2 and Repair 3 Load Tests, only northbound orientations were employed.

Since eight common truck positions were determined based on AASHTO recommended design lane loadings and worst-case loading scenarios, this resulted in two truck configurations per girder for lateral placement of wheel lines. The AASHTO design configuration—AASHTO—can be seen in Figures 5.8, 5.10, 5.12, 5.14, and 5.16 for Girders 1–4, respectively. AASHTO (1996) recommends 12-ft design lanes be used for

design. In addition, the center of each wheel group is placed no closer than 2 ft. from the lane boundaries. Following those recommendations, trucks were positioned within these moveable design lanes in a position that Auburn researchers believed would produce the maximum live load effect for the critical girder. The worst-case loading configuration, Tight, can be seen in Figures 5.9, 5.11, 5.13, 5.15, and 5.17 for Girders 1–4, respectively. These configurations were determined by placing the two trucks as close together as safely possible (ignoring the limits on distances from lane boundaries). A static test set consisted of data taken at three longitudinal positions for a single transverse position.

Critical transverse load positions, as shown in Figures 5.8–5.17, were identical for northbound and southbound static tests. The southbound test was eliminated from the test battery for the Repair 2 and Repair 3 Load Tests. Tests were executed for a particular transverse position by beginning at one end span and successively testing the other two spans in the same position. For example, consider a typical northbound load test sequence for critical loading on Girder 4. First, load test trucks were transversely positioned for the AASHTO design lanes on Span 9 Girder 4, as shown in Figure 5.8. A data set was recorded at each longitudinal position on Span 9, and the truck then moved to Span 10 and then Span 11, with data sets recorded at each position. A final data set was recorded for the unloaded bridge to establish a zero reference point making a total of four data sets per transverse position. Test trucks were then repositioned transversely on the bridge deck for the next design loading configuration. Data sets were again recorded at each longitudinal position, with a final data set recorded for the unloaded bridge to establish a zero reference point. Northbound and southbound static tests corresponding for all girders were completed in a similar manner.

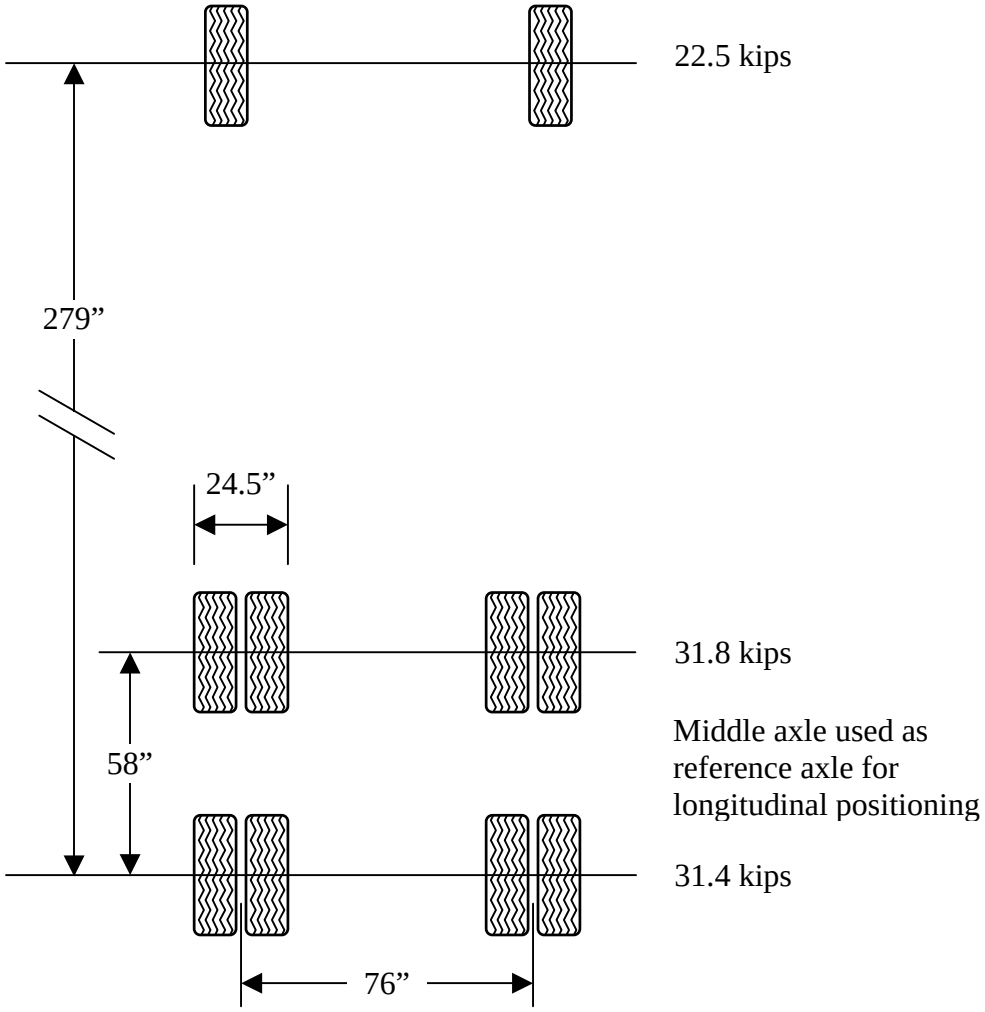

Figure 5.6: Weight and Axle Configuration for LC-5 Truck

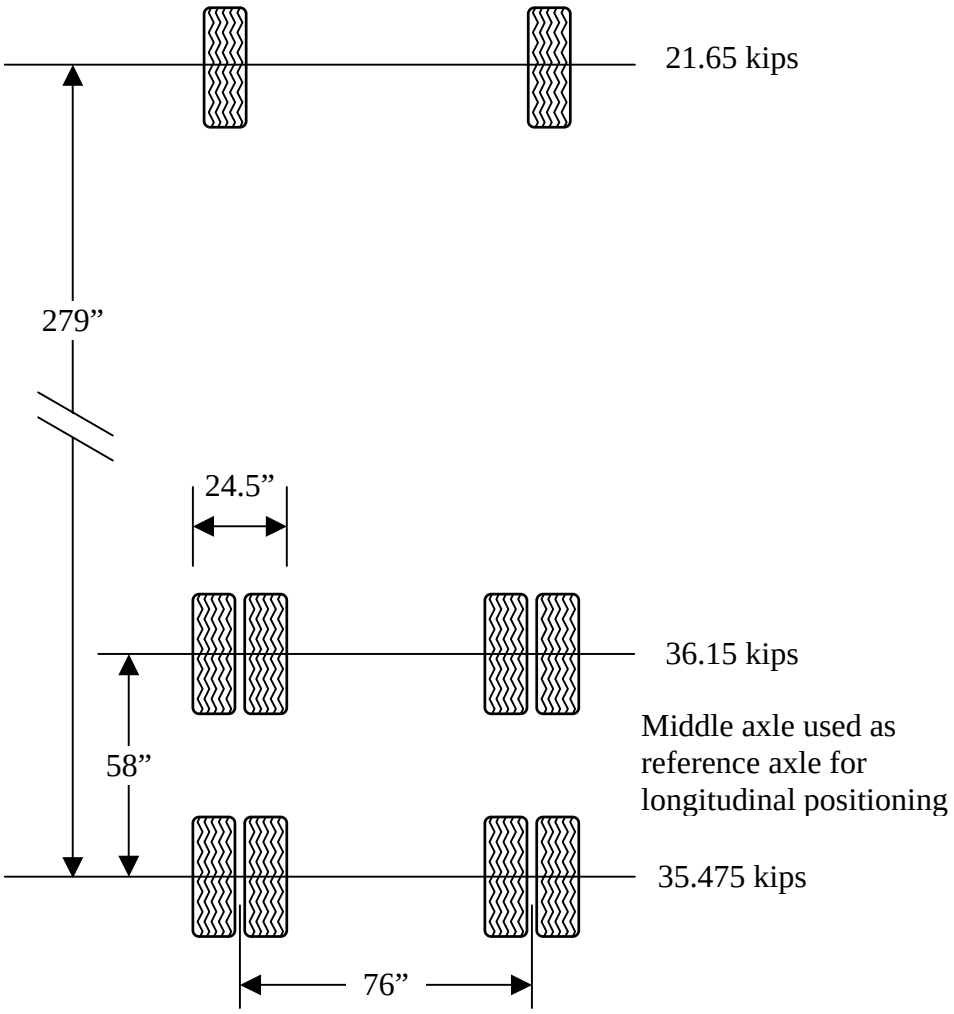

Figure 5.7: Weight and Axle Configuration for LC-6 Truck

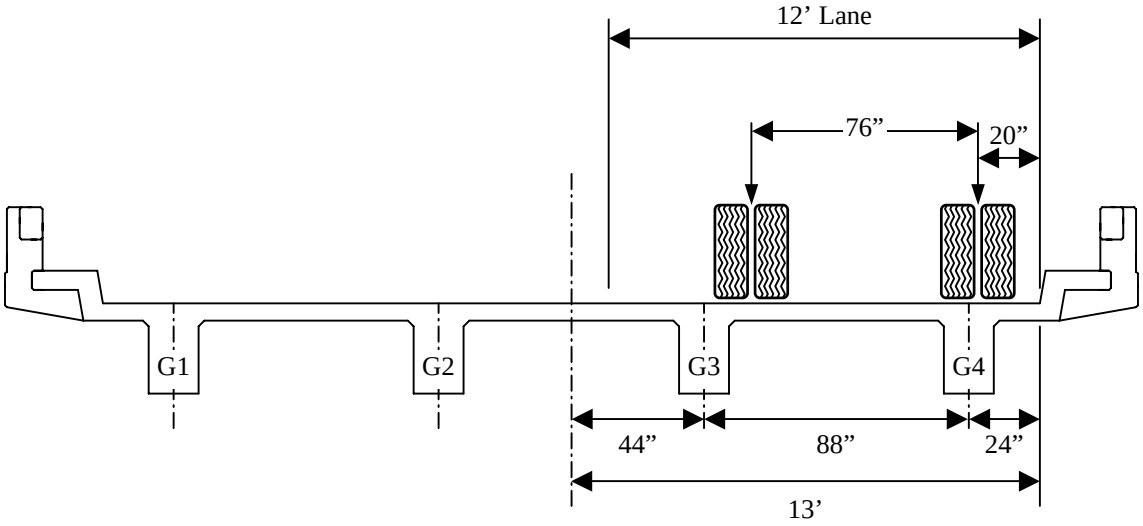

Figure 5.8: AASHTO Critical Loading for Girder 4 (AASHTO Old)

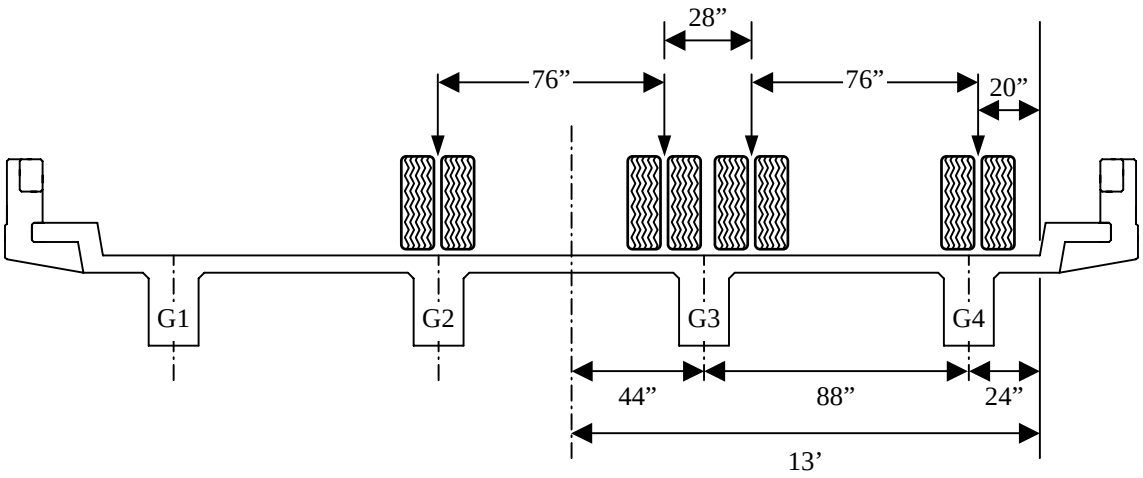

Figure 5.9: Worst-case Critical Loading for Girder 4 (Tight)

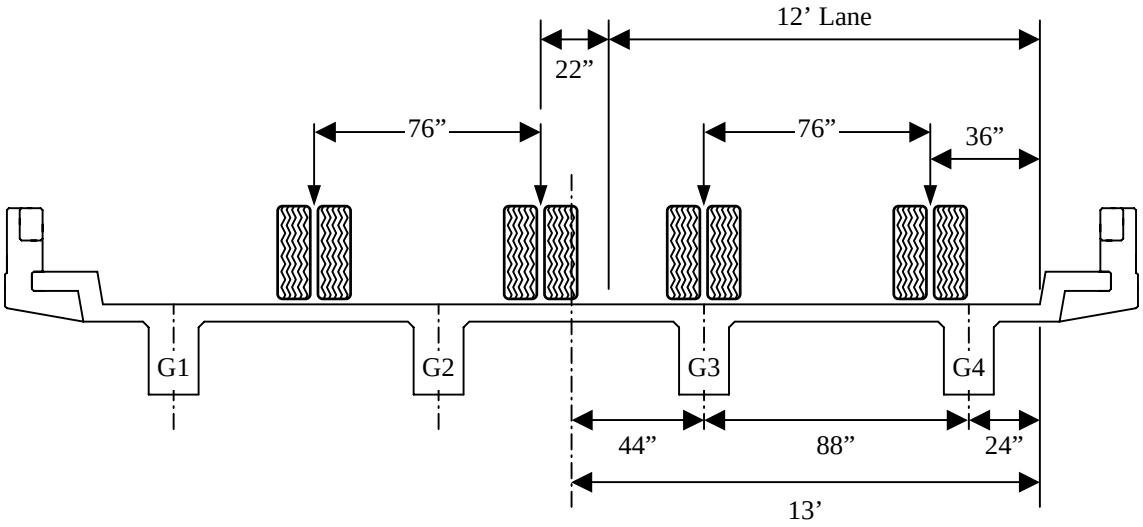

Figure 5.10: AASHTO Critical Loading for Girder 3 (AASHTO)

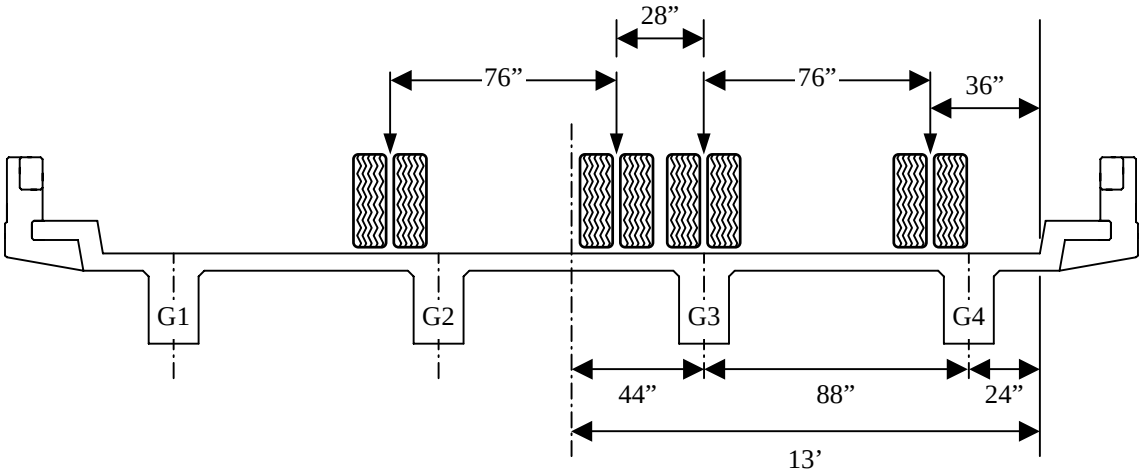

Figure 5.11: Worst-case Critical Loading for Girder 3 (Tight)

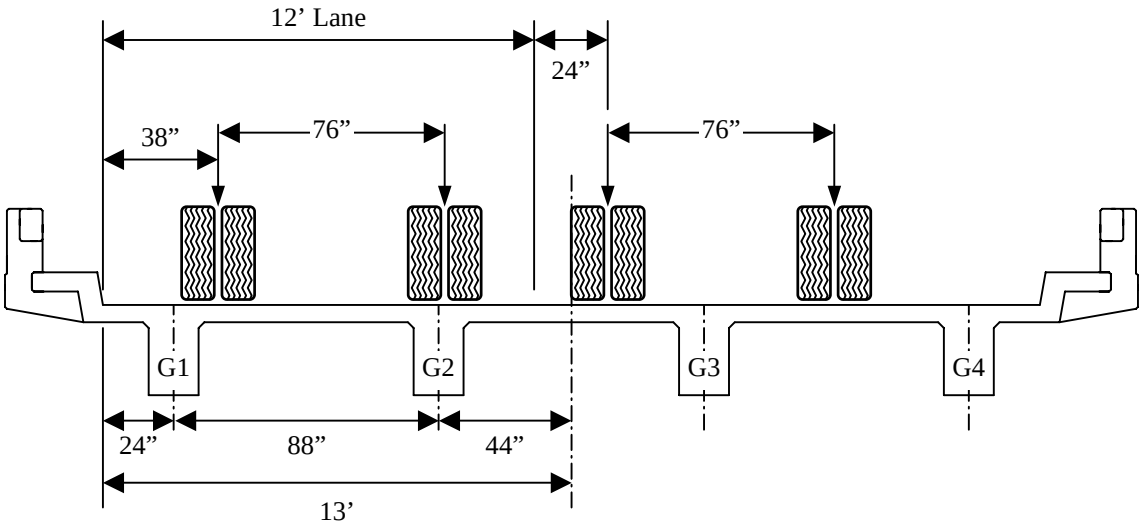

Figure 5.12: AASHTO Critical Loading for Girder 2 (AASHTO)

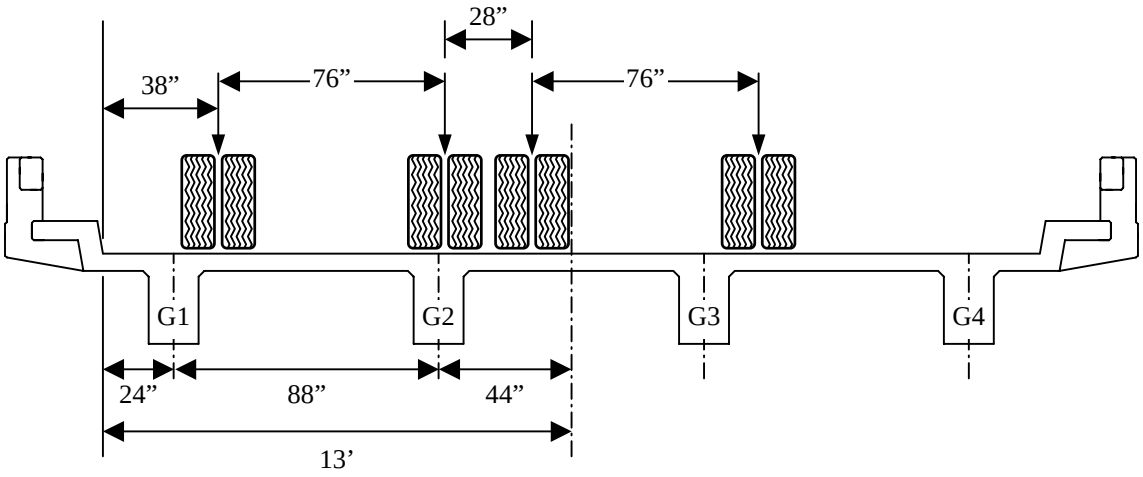

Figure 5.13: Worst-case Critical Loading for Girder 2 (Tight)

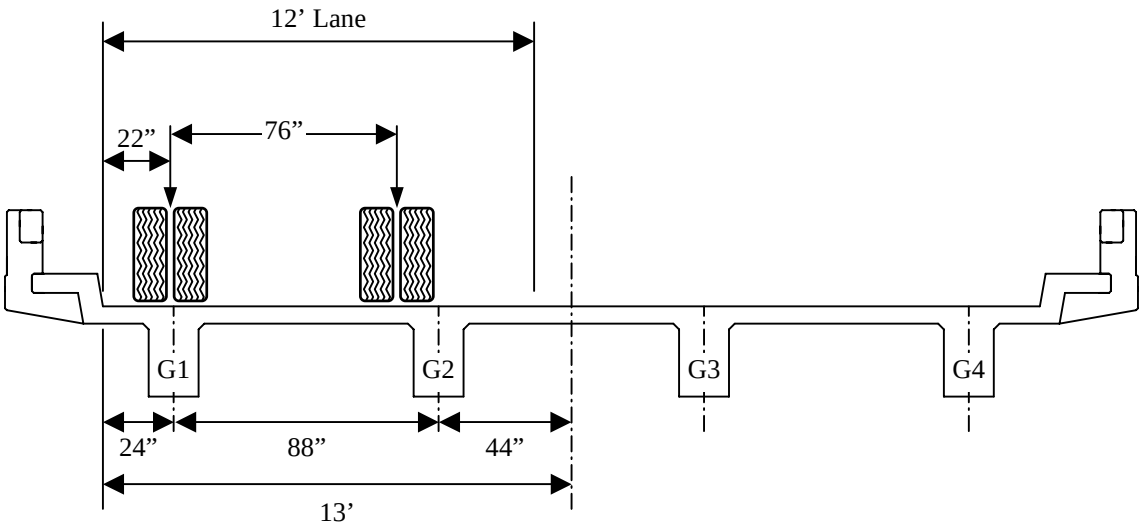

Figure 5.14: AASHTO Critical Loading for Girder 1 (AASHTO Old)

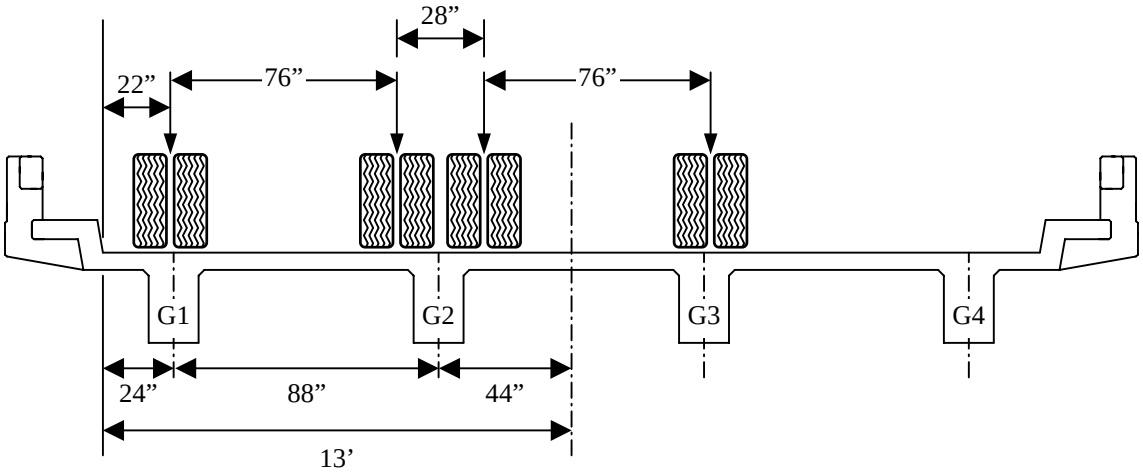

Figure 5.15: Worst-case Critical Loading for Girder 1 (Tight)

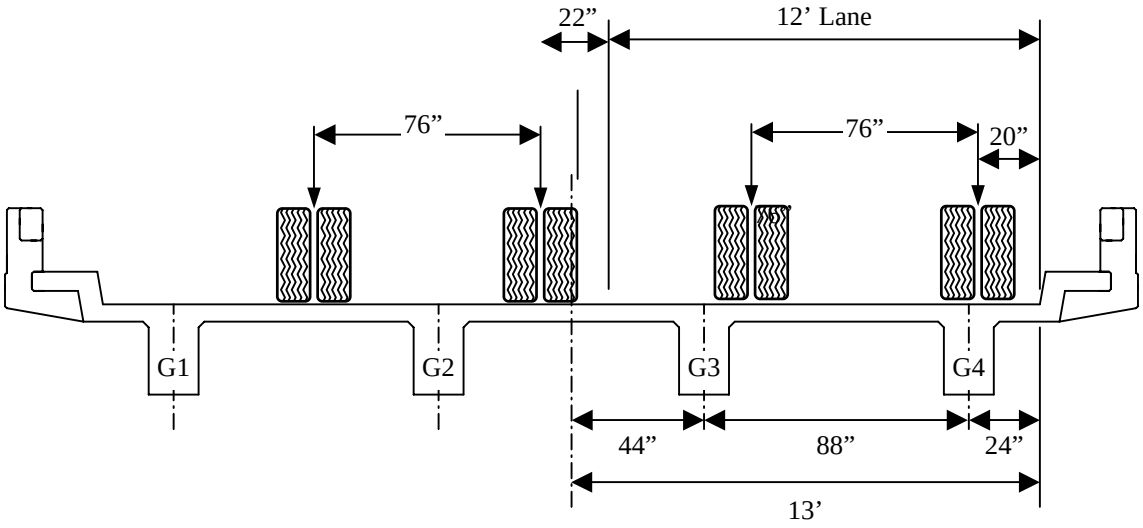

Figure 5.16: AASHTO Critical Loading for Girder 4 (AASHTO New)

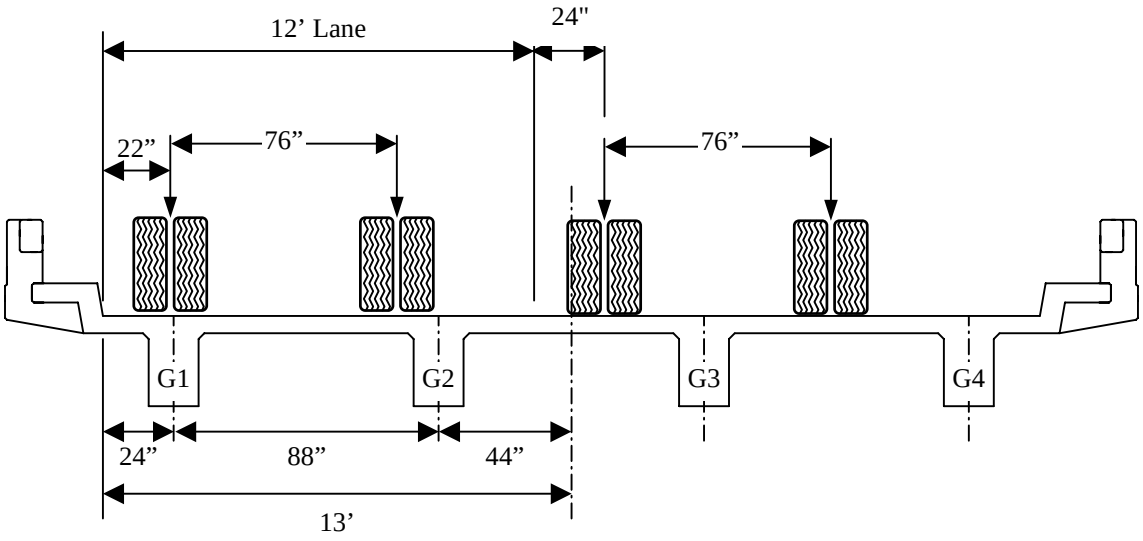

Figure 5.17: AASHTO Critical Loading for Girder 1 (AASHTO New)

Two repetitions of northbound static tests for critical loadings on Girder 3 and Girder 4 were performed for both the Existing and Repair 1 Load Tests. Only a single repetition of each northbound static test for critical loadings on Girder 1 and Girder 2 was performed due to time constraints. Only one repetition of southbound tests was conducted for Girders 3 and 4 only. For the Repair 2 Load Test, three repetitions of northbound static tests for Girders 3 and 4 were performed, while two repetitions of static tests for Girders 1 and 2 were performed. For the Repair 3 Load Test, two repetitions of northbound static tests were performed for each girder.

Dynamic live load tests were performed with the load test trucks traveling side-by-side over the bridge at a target constant speed of 45 mph. The load test trucks were positioned in the center of each traffic lane as shown in the midlane configuration in Figure 5.18. The number of dynamic tests performed in each direction was dependent on the quality of the tests. Load test truck position within the lanes was a difficult parameter to control for dynamic tests, and the test was repeated until adequate (transverse and longitudinal) alignment was achieved. Actual truck speeds for dynamic tests ranged from 42–55 miles per hour for both the northbound and southbound directions.

For comparison purposes, static and quasi-static tests were also performed with the trucks placed in the midlane transverse position used for the dynamic tests (Figure 5.18). For each static test, strains and deflections were measured with the trucks positioned in each longitudinal position used for AASHTO and Tight load configurations. For the quasi-static tests, strains and deflections were measured as the trucks passed over the bridge at a slow speed of approximately 5 miles per hour.

Midlane static tests were performed two times for northbound trucks and one time for southbound trucks for the Existing and Repair 1 Load Tests. Midlane static tests produced data sets at critical cross sections for all three spans. Prior to the installation of FRP composite, a total of three northbound tests and two southbound tests were performed. After completion of the strengthening process, a total of three northbound tests and three southbound tests were performed for the Repair 1 Load Test, three northbound sets for the Repair 2 Load Test, and two northbound sets for the Repair 3 Load Test.

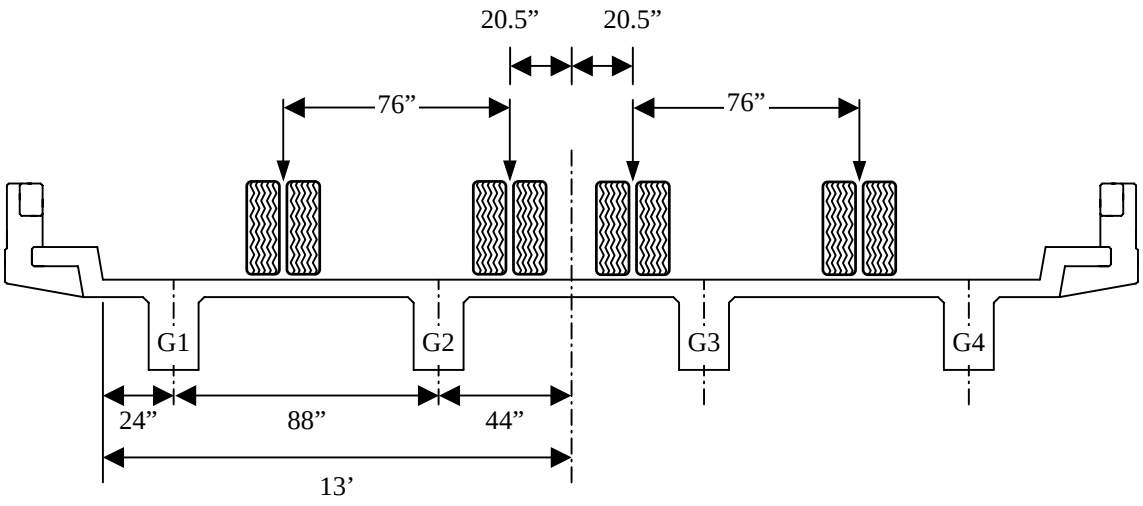

Figure 5.18: Midlane Loading Truck Configuration

During the Existing Load Test, it was discovered that the gauge (transverse wheel group spacing) of the ALDOT load test trucks was approximately 2 in. larger than the value shown in documents used to plan the test locations. However, the truck placement lines had already been painted onto the bridge deck before recognition of this problem. Placement lines corresponded to the back axle tread of the driver's side for northbound tests and the passenger's side for southbound tests. For this reason, symmetry of truck positions about the centerline of the roadway did not exist during the actual "midlane" tests. Actual transverse positions used are shown in Figures 5.8–5.17. However, based on the specified tolerances, the assumption of approximate symmetry is reasonable.

CHAPTER 6: ANALYSIS METHODS

6.1 General

In order to gain a better understanding of the effects of the FRP on bridge strength as well as the impact of time on the FRP adhesion, an analytical model of the War Memorial Bridge was created and used as an integral component of this study. This model provides a theoretical basis for comparison to the experimental data collected in the series of load tests described in previous chapters. This chapter includes a description of the selection of the finite element analysis procedure and program, modeling assumptions, and programming techniques.

6.2 Selection of Finite Element Analysis

Finite element analysis was chosen because of the robust techniques that it employs. Finite element programs can provide many relevant engineering measures at discrete points, or nodes, along a model. Each of these nodes is constitutive of the area or volume surrounding it and yields data that are functions of the conditions taken across the entire area or volume. Smaller areas or volumes, which are created out of the nodes, yield greater accuracy by defining a more precise area or volume for which analysis is performed. More nodes means more points of data collection where information about the model's behavior can be discerned. Therefore, it is advantageous to refine the mesh—that is, to create a model with as many nodes per given space as practical. One must keep in mind the law of diminishing returns—as well as the limitations of the program

processor—when deciding how many nodes will define the mesh, since too many nodes will consume too much processing capacity while generating only insignificant additional data.

The ADINA (Automatic Dynamic Incremental Nonlinear Analysis) program was chosen for modeling the War Memorial Bridge. While ADINA is frequently used for its fluid flow modeling properties, it has a concrete modeling tool that can account for many of the nonlinearities involved with cracked concrete. Using the concrete modeler to simulate the concrete in the bridge and truss elements as the reinforcing steel, the properties of cracked reinforced concrete could potentially be well simulated. However, due to constraints on time and resources, the concrete modeler was not employed and reinforced concrete section properties from cracked-section analysis were used for the purposes of this study.

6.3 Modeling Assumptions

To initiate the model design, some assumptions were made that would simplify the modeling process but would not have a significant impact on the behavior of the bridge model as compared to the actual bridge. The first assumption was to model the bridge deck as completely horizontal. In actuality, the roadway is crowned along the centerline of the roadway which cause the interior to be 1.125” higher than the outside of roadway and interior curb. In reality, the bottoms of the girders terminate at common lower vertical positions; their depths, however, vary due to the crown in the roadway. Due to the assumption of a perfectly horizontal roadway, the bottoms of the girders in the model vary 1.125” between interior and exterior girders, with the interior girders being the deeper than the exterior.

The second assumption was the decision to leave out the curb, pedestrian walk area, and guardrails from the model. It was decided that the additional stiffness due to these elements is generally negligible in the bridge's performance, especially given the loading positions employed for the load testing.

The third assumption concerned the connections between the bents and the bridge. The south ends and north ends of the four continuous girders rest upon rollers and were modeled as such. The interior connections between the continuous span and the two interior bents are pins. Though the behavior of the interior bents therefore has an effect on the overall bridge behavior, the bents were not included directly in the model. Therefore, modifications were needed to accurately account for the north-south movement of the pin supports due to the movement in the interior bents. This is discussed in a following section.

A fourth assumption involved load distributions in the bridge structure. The analysis would have to account for the load distribution in the non-linear cracked concrete material. It was judiciously decided that using linear-elastic material should simulate the load distributions appropriately while greatly reducing the time and complications that would arise from using a non-linear material in the finite-element model to account for the cracked concrete. The cracked concrete would be considered via an ACI 318 prescribed cracked section analysis following the finite-element analysis using the stresses determined in the finite-element analysis.

The final assumption is related to the loading applied by ALDOT load test trucks. In practice, some contact area transfers the load between the tire and the bridge deck. This contact area had a transverse dimension (Y-direction) dictated by the width of the tire.

For simplification, the gap of a few inches between the dual rear wheels was ignored and one transverse segment dimension, equal to the width of the tires plus the gap, was assumed at each dual wheel location. The longitudinal dimension is governed by the truck's weight distribution and the tire pressure. For simplicity and ease of calculation, this dimension was assumed to be approximately six inches, which is the surface nodal element dimension in the longitudinal (X-) direction.

6.4 Modeling Techniques and Data Processing

The first step in the modeling process was to reference the bridge in a Cartesian coordinate system. It was decided that the travel direction of the roadway—essentially north-south—would be the X-direction. The horizontal direction perpendicular to the longitudinal axis would be the Y-direction. The vertical direction would be the Z-direction, with upwards as positive. The origin was taken to be the most southeastern point that is in the plane of the intersection of the bottom of the bridge deck and the top of the girders. X-coordinates increased in a south to north direction. Y-coordinates increased in a east to west direction. Z-coordinates increased from bottom to top.

After assuming a reference system, the second step in modeling the War Memorial Bridge was to create a base of points to create the bridge volume. While the bridge deck and some parts of the girders in Span 9 and Span 11 have prismatic geometries, all of Span 10 and the balance of Span 9 and Span 11 girders have curved profiles as the bridge is haunched. To define the prismatic geometries, few points were required. To accurately model the haunches, curved lines were created to define the geometry of the haunch. ADINA has a curved-line modeler, which could have been employed to correctly model the slope of the haunch. However, when comparing the benefits to precisely modeling the

slope of the haunch through the curved-line modeler or modeling the haunches using a series of short, straight line segments, the simplicity of defining and processing a series of straight line segments made it the preferred modeling method. The distances between points defining the curve needed to be as short as possible to create accurate geometry but the number of points used needed to be kept to a reasonable minimum for processing purposes.

Approximately 14,500 points were used to define the basic volume of the War Memorial Bridge superstructure. A computer spreadsheet tool developed using Microsoft Excel was used to generate the points that defined the volume. By using formulas on a spreadsheet, the creation of the points was performed both expeditiously and in a regular manner, while errors were minimized and quickly fixed when they were discovered. A spreadsheet was also employed to generate the code from which an input (.in) file could be written for analysis in ADINA. Because points were defined in a discernable, regular fashion, formulas were written that quickly created volumes from the defined points. Furthermore, a formulaic approach to writing program code to create the mesh density and perform the meshing function could quickly be developed. Support fixities were also written and defined using a spreadsheet to expedite their inclusion in the code. Similarly, loads were assigned on elements using a spreadsheet. Similarities in the load cases made it possible to quickly alter the spreadsheet to define all load conditions. A typical Excel input spreadsheet can be found as Appendix B.

The typical volume defined in the model was approximately 6 in. long by 6 in. wide by 3 in. high. All volumes were rectangular elements having 8-nodes and six faces. The bridge was modeled with a compressive strength of 5,000 psi and a modulus of elasticity

of $4.031x10^3$ ksi. A linear elastic material was used in the modeling analysis. The cracked concrete would be considered in the post-processing calculations.

In order to model the movement of the continuous span supports at the top of the interior bents in the North-South (X-) direction, differing fixities were incorporated into the model simulating different stiffness of the pier-supported bents. Three models were created: a Stiff Model, a Flexible Model, and a Spring Model. Lines of fixity at bents between the piers at the intersection of the continuous-span portion of the bridge and the simple-span portion were modeled as ideal rollers for all models. While this restrained the connections in the east-west (Y-) direction, it still allowed for movement along the north-south direction. For the interior bents, each model used a different fixity condition at the intersection of the girders and the bents. For the Stiff Model, an ideal pinned condition was created with infinite stiffness at both bents by restraining all movement in the horizontal plane. For the Flexible Model, the south bent was modeled a an ideal roller with zero stiffness by restraining movement in the y-direction and allowing free translation in the x-direction. The north bent in the Flexible Model was modeled again as in ideal pin. Upon examining the behavior of the Stiff and Flexible Models, it was determined that restraint in the north-south direction was needed as a function of the movement of the top of the bents under the lateral load caused by bridge traffic. To accomplish this for the Spring Model, nodes at the fixity lines of the interior bent connections were joined with nodes aligned in the span's north-south direction through spring elements placed between these nodes. The spring elements were given spring constants determined by modeling the bent at the south end of Span 10 using ADINA and measuring the deflection in inches under a 1-kip load of the top of a model of the bridge

bent. For this bent model, all parameters were identical to the larger model except for the moment of inertia, which was taken to be 70 percent of the uncracked moment of inertia according to ACI 318-02 10.11.1 (2002). From the bent model, a spring constant of 1.86 k/in. was found for the movement of the pier in the north-south (X-) direction. The resulting spring constant in inches per kip could be entered as a parameter for the springs in the model. Therefore, movement in the x-direction of the bridge was restrained by the spring elements simulating the movement of the bents under load applied in the longitudinal (X-) direction.

Loading patterns were created for the load cases described in Chapter 5. Loadings for LC5 and LC6 trucks were simulated for all span and girder combinations, including Girder 1 and Girder 4 AASHTO Old and New configurations. To accurately model the loads as they would appear on the bridge, half of the appropriate truck axle weight was divided by the contact area for each wheel group. This yielded a weight per unit area which was then input into ADINA as a surface pressure upon an element face. A spreadsheet was used to create the code for the different loadings, and those codes could be imported into a *.in* file of the basic bridge model. From that, the ADINA processor could run the *.in* file of the bridge with that particular loading to yield nodal load effects that could be converted into strains for comparison with experimentally obtained strain measurements.

The stresses generated at the nodes by ADINA were organized and extracted by their location in the model. Nodal stresses at critical cross sections of the four girders were extracted, multiplied by the appropriate area surrounding the node, and then multiplied by the area's distance from the section centroid to find the bending moment associated with

that nodal stress. Moments were summed over the critical cross sections for further analysis. The cracked section moment of inertia of each girder cross section was determined and, along with the determined moments, the known modulus of elasticity, and the distance from the centroid to the strain gauge location, were used to determine the strain at the position on the model congruent to the strain gauge locations on the actual bridge. Two sets of cracked-section analyses were performed which corresponded to the existing bridge and the repaired bridge. The contribution of the FRP to the bridge was considered in this analysis by determining the modulus of elasticity and neutral axis location for both the unstrengthened and strengthened bridge through transformed section analysis. The effect of the FRP was not investigated in the ADINA analysis.

CHAPTER 7: RESULTS AND DISCUSSION

7.1 GENERAL

To evaluate service load performance of the strengthened bridge girders, static and dynamic live load tests were performed before and after FRP installation. One unstrengthened load test, referred to as the Existing Load Test, and three strengthened load tests, referred to as the Repair 1 Load Test, Repair 2 Load Test, and Repair 3 Load Test, were performed. The response of the bridge was assessed by measurements at the critical locations and cracked section locations described in Chapter Four. Chapter Five includes specific details on the live load tests performed and the instrumentation scheme utilized.

From the analysis of the finite element model, bridge behavior was extracted through stress and displacement values at the nodes generated by ADINA. Displacements from the model were used to aid in verification of bridge model behavior, while the stresses were converted to strains and compared against experimental results to gauge the benefit of the addition of FRP to the positive moment section of the War Memorial Bridge.

This chapter will demonstrate that the use of spring elements at the bridge-to-interior-bent interface best simulates the bridge support behavior and yields sufficiently accurate results. Comparisons using the “spring” model are made between analytical and experimental data to develop conclusions about the effectiveness of the FRP immediately after installation and six-months after installation.

7.2 Experimental Data Collection

The values of experimental strains used in comparisons are strains averaged over the number of data sets recorded for a given position and test date. As outlined in Chapter Five, six strain gauges were installed on the steel reinforcement at each critical location, of which two were installed for redundancy. Redundant gauges were not monitored during strengthened-bridge load tests and are not included in evaluating the effectiveness of the strengthening procedure. For each critical cross section, the four steel gauges monitored for both unstrengthened-bridge and strengthened-bridge load tests were used in evaluation.

Strains in the FRP composite were measured at critical and cracked locations for Girders 3 and 4 in Span 9 and 10 during all strengthened-bridge load tests. For the Repair 3 Load Test, FRP strains were also measured at critical and cracked locations on Girders 1 and 2 in Spans 9 and 10. No steel strains were measured during the Repair 3 Load Test.

Though data were collected for all instrumented locations, only sensor data particular to the loaded span were large enough to be significantly useful in evaluating the service-load performance of the strengthened girders. For example, for Span 9 loading, strains measured at critical locations in Span 9 girders are most relevant and reliable. Therefore, only these strains are included in the Span 9 comparisons presented in this thesis. Likewise, for Span 10 loading, only strains measured at critical locations in Span 10 girders are included in comparisons. Because Span 11 behavior should mirror that of Span 9 due to symmetry, Span 11 was not instrumented and is therefore not included in comparisons. Due to symmetry in the transverse direction, Girders 1 and 2 should behave similarly to Girders 3 and 4. Therefore, they are not included in comparisons either.

Only results from northbound tests are considered for this report. An average was taken of measured strains for identical iterations of load tests for more accurate comparison, except where the difference was significant. In these cases, it was judged that an erroneous signal resulted in the aberrant result, and the value that was representative of typical data was used. Since southbound static tests were performed in one set per load test, an average could not be obtained, making a reliable comparison for those tests more difficult. Additionally, southbound FRP strain comparisons could not be made because only one set of FRP data was collected for southbound tests. Dynamic tests most often produced data that were incongruent and random, which is attributed to the difficulties in maintaining correct truck placement in the design lanes as the load-test trucks rolled onto the bridge at 45 mph. Therefore, strain response results from northbound and southbound dynamic tests were not analyzed for this report.

Deflections were measured for each girder at critical locations in Span 9 and Span 10. Upon examination of the recorded data, it was determined that the measured quantities do not reliably reflect actual girder deflections. With the exception of the Repair 2 and Repair 3 Load Test results obtained from the Span 9, Girder 1 deflectometer, all results appear invalid. An examination of data from the two tests shows that no pattern of deflection reduction similar to steel strain reduction can be deduced. In fact, the results seem somewhat random.

For the Existing and Repair 1 Load Tests, a significant vibration was typically present in the deflection results from dynamic tests. The same periodic motion is apparent in the Repair 1 and Repair 2 Load Tests, but smaller in magnitude. The vibration is not representative of the girder deflections because this periodic motion is not present in any

of the strain response histories. The likely source of this vibration was a fixity flaw discovered during setup for the Repair 2 Load Test, performed in June 2002. When loaded, the removable deflectometer mounting brackets used in both previous load tests, allowed considerable rotation of the deflectometer. Shims were used to correct this problem before conducting the Repair 2 and Repair 3 Load Tests. For these reasons, the measured deflections are not included for comparison here.

7.3 DATA EXTRAPOLATION FROM ADINA

Finite element programs return results at nodes. ADINA will return an array of results, including stresses, displacements, and reactions, at discretized nodes. In order to be beneficial for comparison, the location at which strain data is extracted from the model must be at the same location as the strain gauge location on the bridge. Therefore, there must be a node on the model at the same coordinate as the gauged location on the model, or either the nodal data must be taken and reduced to find the resultant behavior at the gauge location.

For this study, nodal data was taken at the cross sections of Span 9, Span 10, and Span 11 given in Chapter 5. From the vertical, planar node map on each of those cross sections, areas of element cross sections were ascertained, discretized for reassignment as nodal areas, and used to find the resultant bending moment on the cross section as a function of the nodal stresses and areas. Bending moments were determined for each cross section in this manner. A cracked-section analysis of the bridge was performed, and the moment of inertia and neutral axis location were determined that corresponded to the cracked cross section (both before and after FRP strengthening). In accordance with engineering beam theory, these properties were used in conjunction with the bending

moment extracted from the ADINA results to determine the flexural strains at the reinforcing bar and FRP gauge locations. Thus, the analytically determined strains were obtained by (1) performing a linear-elastic analysis of the uncracked structure and (2) modifying the results to include the incorporate the effects of flexural cracking. Comparisons could then be made between the analytically and experimentally determined strains.

7.4 Selection of Support Restraint Model for Continuous Supports

As discussed in the previous chapter, the basic bridge was modeled using three different support conditions at the bents between Spans 9 and 10 and Spans 10 and 11. The positive-moment results from the analysis of the bridge under LC5 AASHTO loading of Spans 9 and 10, Girders 3 and 4, are given in Figures 7.1 through 7.4 on the following page. In those graphs, some trends can be seen that will emerge as all data are considered as a whole. The analytical results from the Flexible and Spring Models differ from each other within a range of 0.5-7%. The difference between the values of either the Flexible or Spring Model result and the Stiff Model result is much more marked, varying by 5-12% for the Span 9 critical loading results, but varying by up to 45% for Span 10 critical loading. Agreement between Flexible and Spring Models and the experimental data is better for Span 10 critical loadings than for Span 9 critical loadings. However, when the load cases were analyzed with the Stiff Model, loadings critical to Span 9 resulted in a deflected shape with double curvature in Span 10. With this in mind and comparing results from all three models against the experimental data, the viability of the Stiff Model is not as great as that of either the Flexible or Spring Model. Therefore, the behavior of the bridge cannot be accurately estimated by assuming the support condition

at the bent between Spans 9 and 10 and Spans 10 and 11 as a pinned condition. Some account must be made of the bridge's longitudinal translation due to the piers.

The Flexible Model and Spring Model yield similar results. It can be observed that results from Girder 3 critical loadings are closer between the Flexible and Spring Models than for loadings critical to Girder 4, and results from Span 10 critical loadings are closer between the two models than for Span 9. For Span 10 critical loadings, the Spring Model comes slightly closer to the experimental data. For Span 9 critical loadings, both models vary by roughly the same percentage, with the exception of the Span 9, Girder 4 critical loading where the Spring Model overestimates strain more than the Flexible model. While both models should lead to valid analytical results, the decision was made to proceed with the Spring Model based on the consideration it makes to account more completely for the longitudinal translation of the piers. The Spring Model was used exclusively in determining analytical results for comparison to the experimental data. However, the Flexible Model is sufficiently accurate for design purposes, especially given its ease of applicability in an analysis compared to that of the Spring Model as no extra effort need be taken to determine the lateral stiffness of the piers.

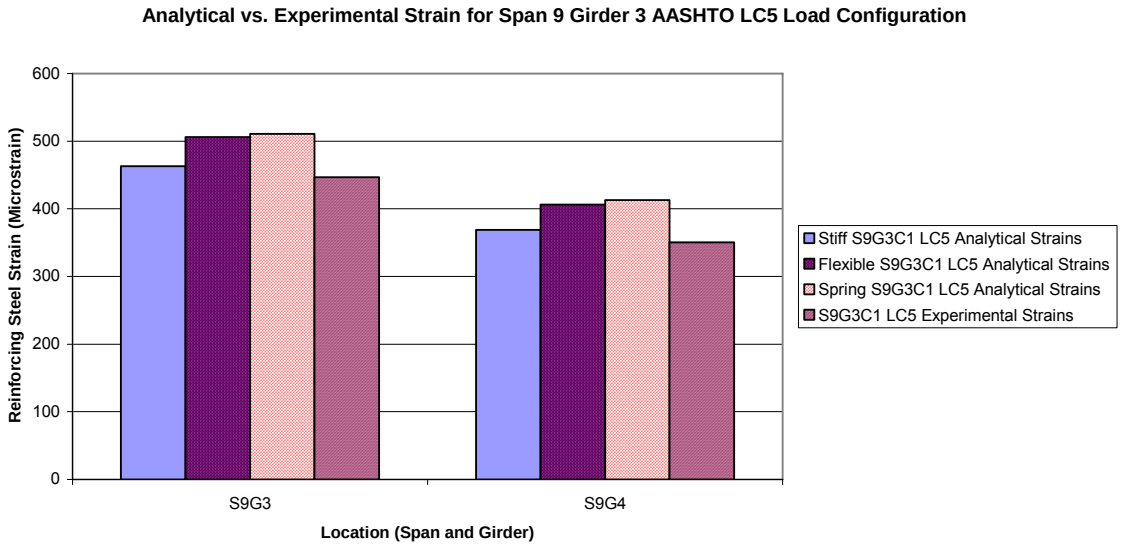

Figure 7.1: Model Comparison for Span 9 Girder 3 AASHTO Loading

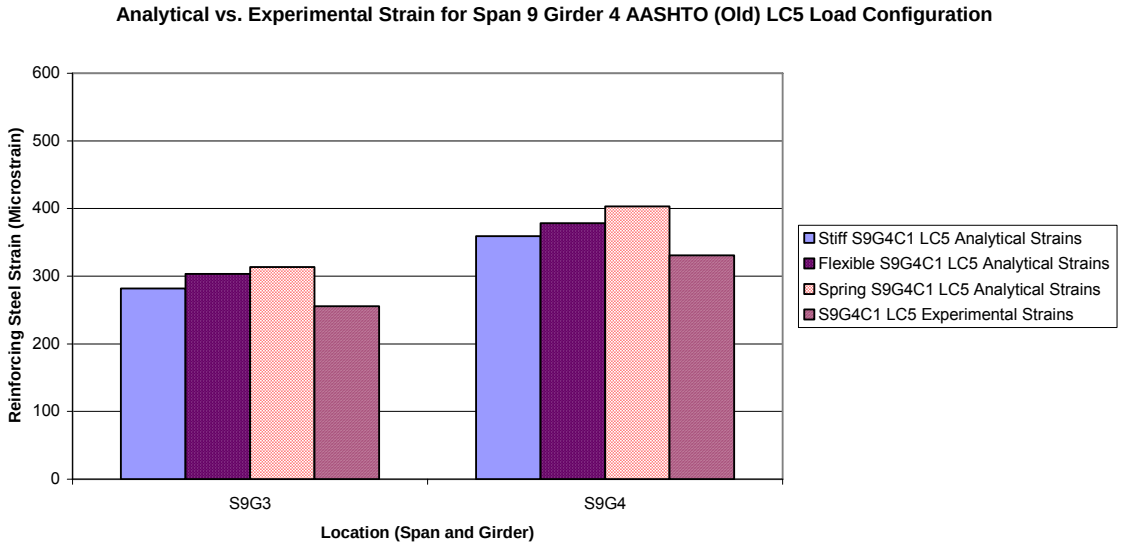

Figure 7.2: Model Comparison for Span 9 Girder 4 AASHTO (Old) Loading

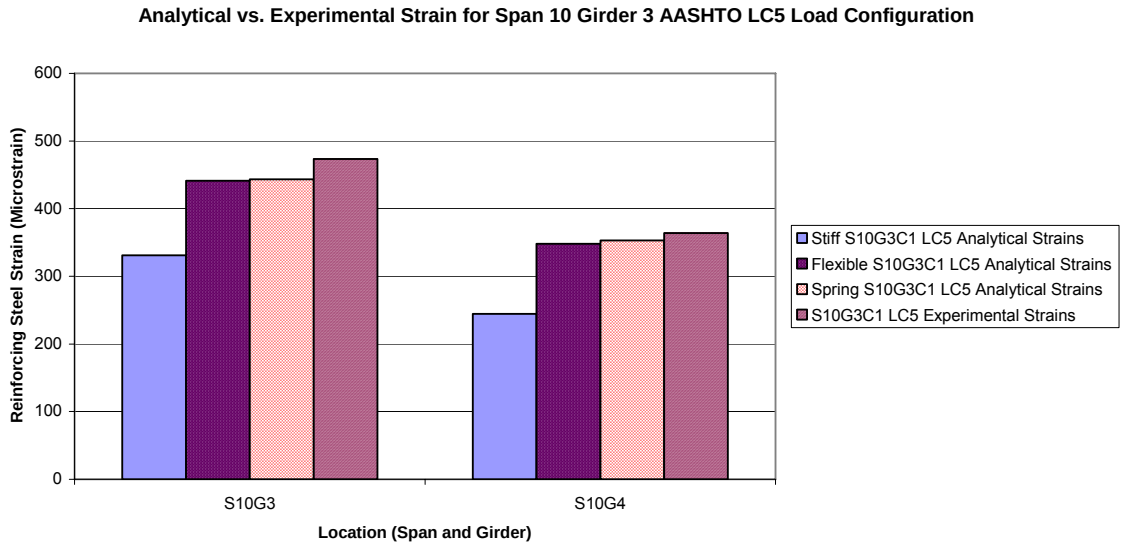

Figure 7.3: Model Comparison for Span 10 Girder 3 AASHTO Loading

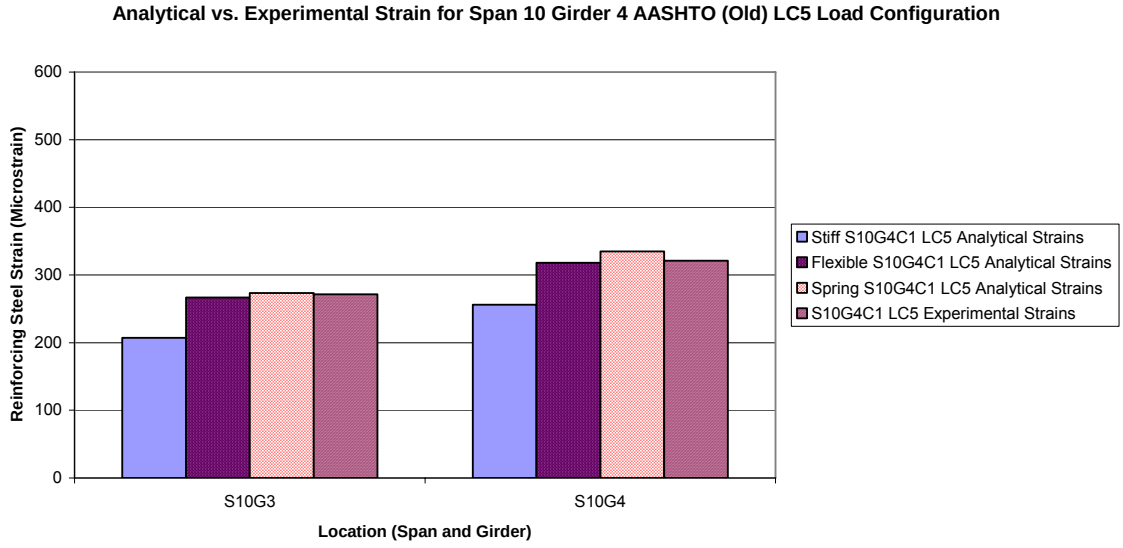

Figure 7.4: Model Comparison for Span 10 Girder 4 AASHTO (Old) Loading

7.5 Steel Strain Comparisons and Results

A total of four load tests were performed on the War Memorial bridge: a pre-repair load test, an initial test of the repaired bridge, a load test six months after repair which used trucks with the same weight as the previous two tests, and a load test six months after repair which used trucks with a heavier weight than the previous three tests. For reference, these four load tests are referred to as the Existing Load Test, Repair 1 Load Test, Repair 2 Load Test, and Repair 3 Load Test, respectively. From comparisons of the experimental data to the analytical data, observations can be made regarding the performance of the FRP in strengthening the deficiencies of the bridge, and the feasibility of utilizing this method as a plausible repair for failing infrastructure in Alabama and beyond.

Figures 7.5 through 7.12 show the comparisons made between analytical and experimental strains for Span 9 and Span 10 Girder 3 and Girder 4 loadings in both the AASHTO and Tight load test configurations. All steel strain comparisons are made using the LC5 loading, as no steel strains were measured during the Repair 3 Load Test and therefore using the LC6 loading. More comparisons are given for the Girder 4 AASHTO configuration than other configurations due to the addition of a two-truck loading on that girder during Repair 2. The single truck loading is referred to as AASHTO Old while the two-truck loading is referred to as AASHTO New.

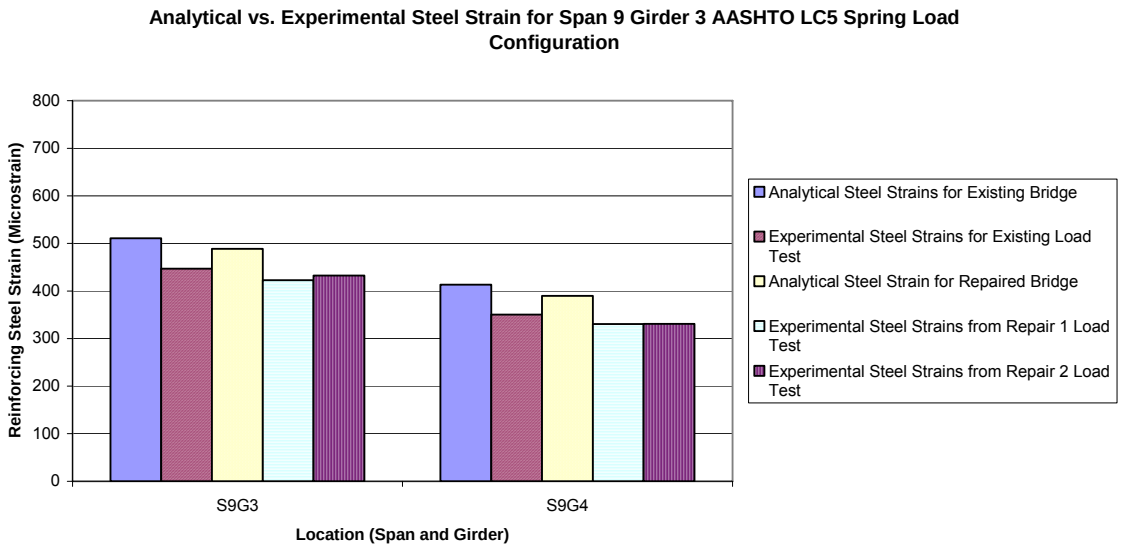

Figure 7.5: Steel Strain Comparison for Span 9 Girder 3 AASHTO Loading

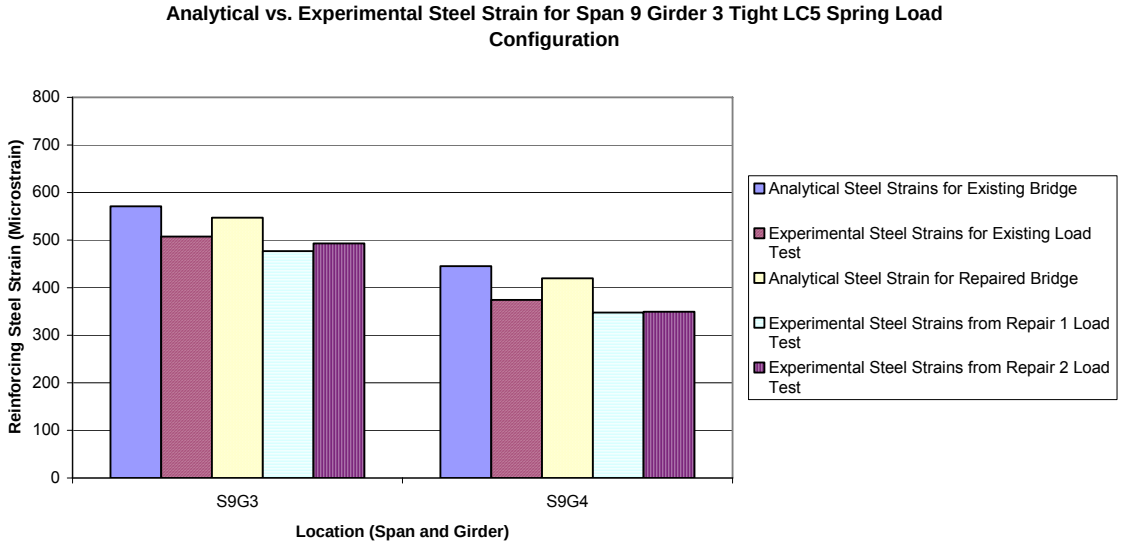

Figure 7.6: Steel Strain Comparison for Span 9 Girder 3 Tight Loading

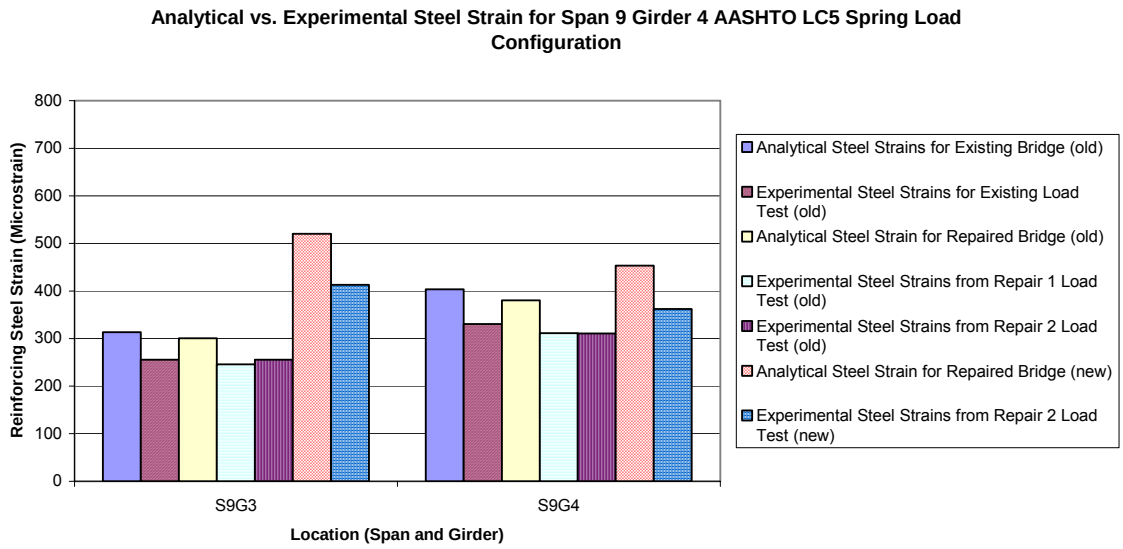

Figure 7.7: Steel Strain Comparison for Span 9 Girder 4 AASHTO Loading

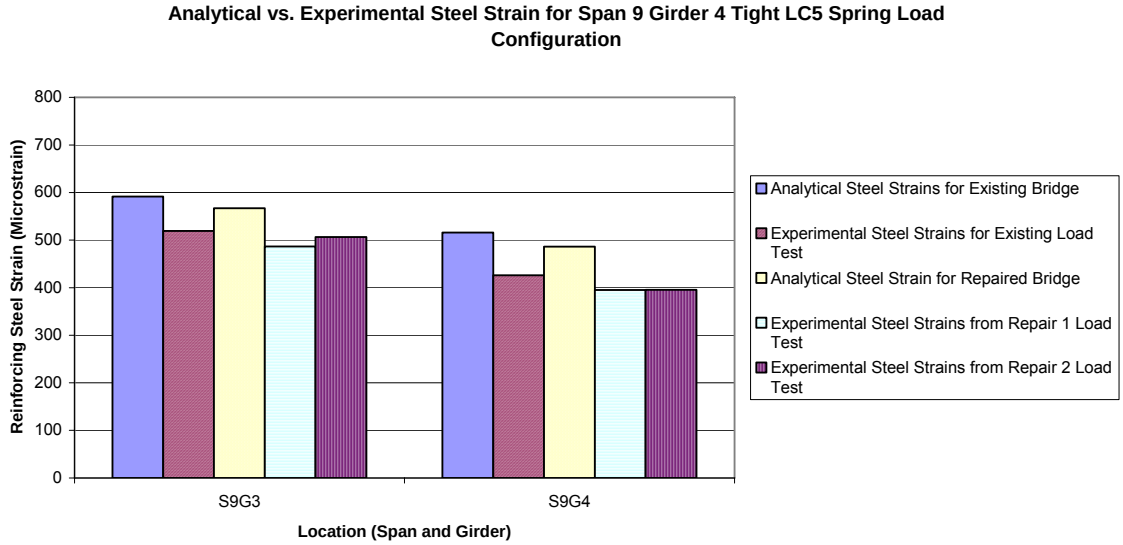

Figure 7.8: Steel Strain Comparison for Span 9 Girder 4 Tight Loading

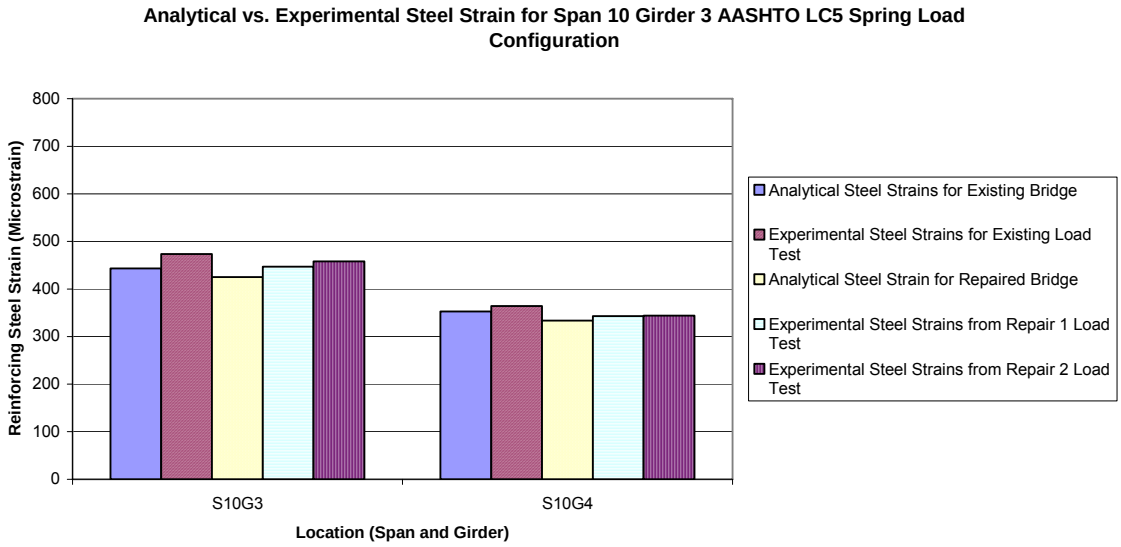

Figure 7.9: Steel Strain Comparison for Span 10 Girder 3 AASHTO Loading

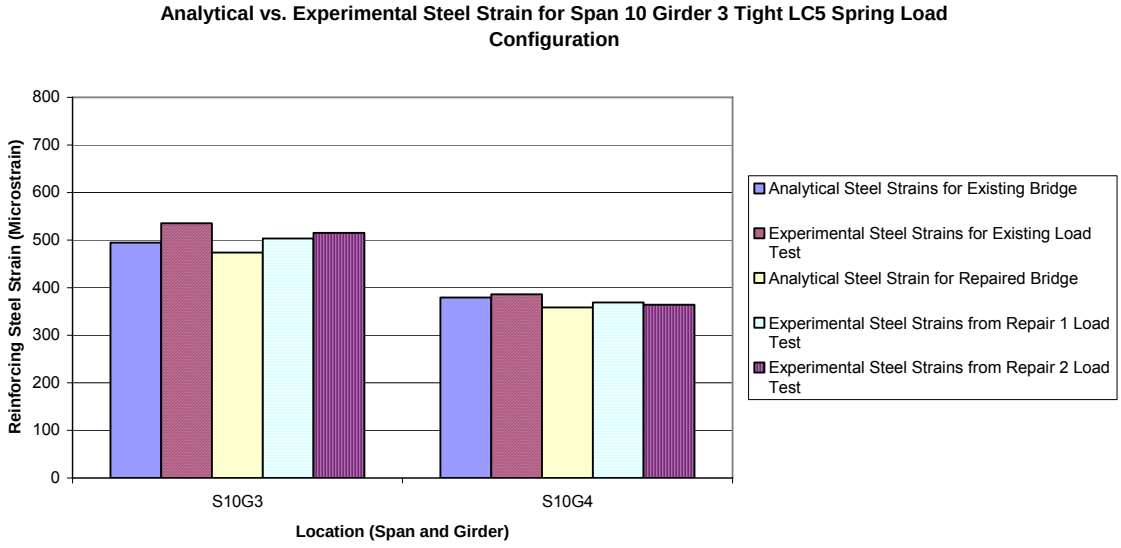

Figure 7.10: Steel Strain Comparison for Span 10 Girder 3 Tight Loading

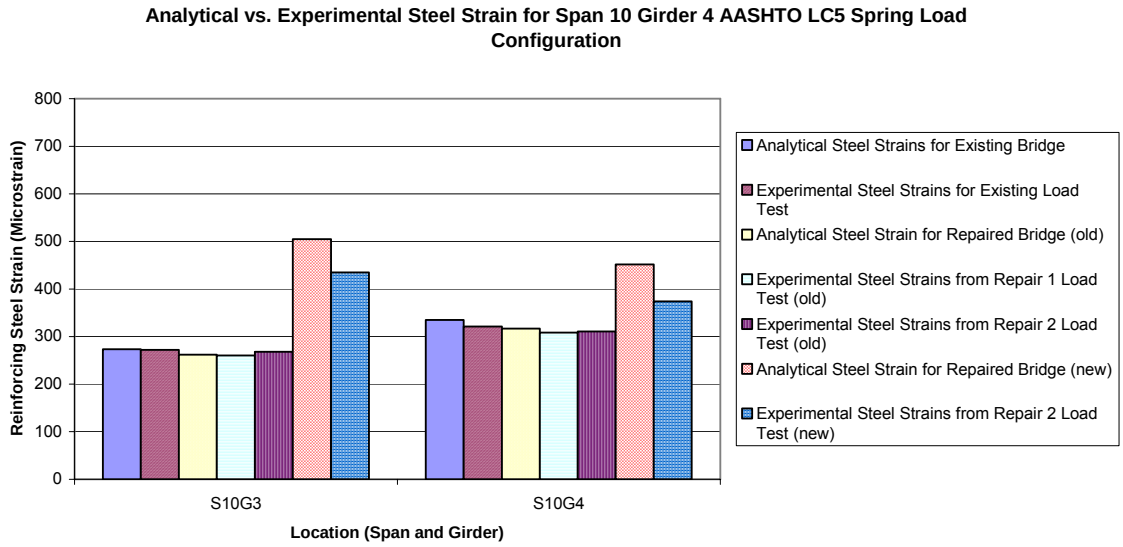

Figure 7.11: Steel Strain Comparison for Span 10 Girder 4 AASHTO Loading

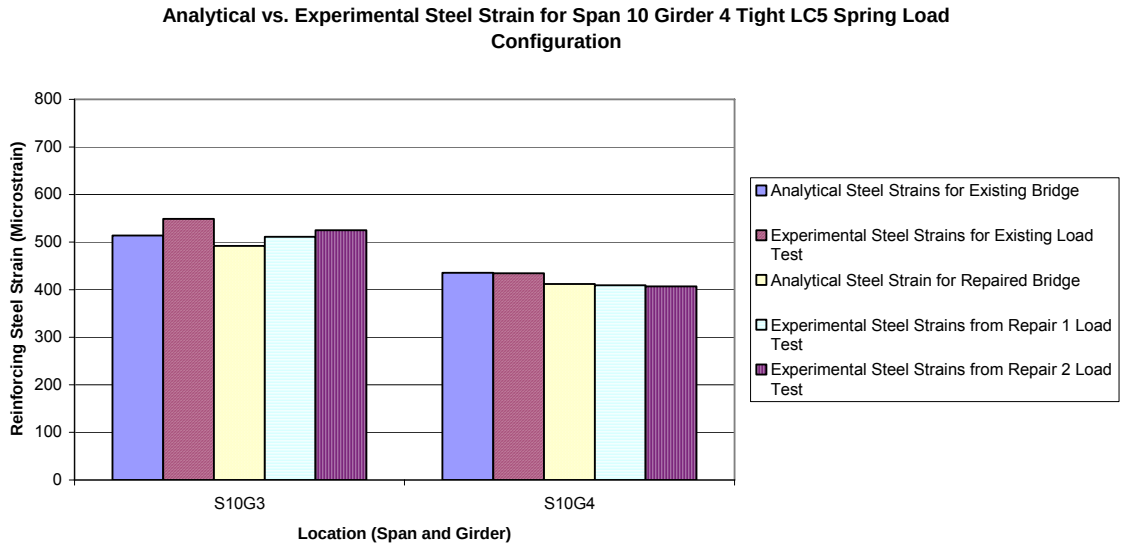

Figure 7.12: Steel Strain Comparison for Span 10 Girder 4 Tight Loading

Strains measured on the primary reinforcing steel in Girder 3 and Girder 4 were reduced during the Repair 1 Load Test relative to the values measured during the Existing Load Test. Analytically, a strain reduction of 4.5% was expected on Span 9 Girder 3 reinforcing steel, while a 6% reduction was expected on Span 9 Girder 4 reinforcing steel. Likewise, a strain reduction of 4.5% was expected on Span 10 Girder 3 reinforcing steel, and a strain reduction of 6% was expected on the Span 10 Girder 4 reinforcing steel. For the Repair 2 Load Test, the experimental reductions ranged from 4-7% for Girder 3 and 6-8% percent for Girder 4. During the Repair 2 Load Test, measured strains were still observed to be reduced relative to those in the Existing Load Test, but the reductions were often not as great as observed during the Repair 1 Load Test. That was most true for Girder 3, where the reductions ranged from 0-3% for the Repair 2 Load Test and were approximately halved in all cases for strains measured on Girder 3 between the Repair 1 and the Repair 2 Load Tests. After six months, it appeared that Girder 3 reinforcing steel was subject to more demand. For Girder 4, the steel strain reduction remained approximately constant between the Repair 1 and Repair 2 Load Tests. For Girder 4, the Repair 2 Load Test reductions range from 6-8%.

From an examination of Figures 7.8 and 7.12, one can see that the strain measured on Girder 3 is higher than for Girder 4 in both graphs. This is unusual since the Girder 4 Tight load configuration is designed to place the most demand on Girder 4 for both the Span 9 and 10 load configurations. However, it can be seen that demand is clearly higher on Girder 3 than Girder 4 in the Tight load configuration. An examination of the design lanes reveals that the limits imposed on truck placement by the curb on the bridge deck creates a scenario where two side-by-side load test trucks, separated by only a few inches,

cannot physically be placed to create more demand on Girder 4 than Girder 3. Therefore, though not intentional, the Girder 4 Tight load configuration is, in practice, a Girder 3 critical loading. The Tight load configuration for Girder 4 produces the largest strains on both Girders 3 and 4 in Span 9 and Span 10, as seen in Figures 7.8 and 7.12.

Agreement between analytical and experimental values is much better for Span 10 results under Span 10 critical loadings than for Span 9 results under Span 9 critical loadings. Span 9 results differ within a range of 12-25% of the analytical value, with the analytical value being higher in all cases. However, there is agreement between the analytically predicted percentage of strain reduction and the amount of reduction observed experimentally on Span 9, suggesting that the model overestimated the actual strains on the bridge. There is negligible difference between the Repair 1 and Repair 2 Load Test data for Girder 4, suggesting that whatever phenomenon resulted in additional measured strain on Girder 3 after six months was not also at work on Girder 4. There is between a 2-4% increase from the Repair 1 Load Test to the Repair 2 Load Test for all measured strain from Span 9 Girder 3. This is nearly half of the stiffness gained initially, and might suggest that some degree of degradation may be occurring.

All analytical results from Span 10 behave in concert with Span 9 results, and, as expected, a 4-6% reduction in reinforcing bar strain can be observed analytically between the Existing Load Test results compared to the Repaired Load Test results. However, for Span 10, the model underestimates by 6-8% strains for loadings that are critical to Girder 3 (Figures 7.9, 7.10, and 7.12), which includes the Span 10 Girder 4 Tight Load Configuration. Though the model underestimates bridge response, performance is generally consistent analytically and experimentally. Furthermore, the same phenomenon

of increased demand seen on Girder 3 in Span 9 is seen in Span 10 from the Repair 1 Load Test to the Repair 2 Load Test. This could suggest an FRP-system issue, though an examination of the FRP strains in the following section will downplay that concern. Additionally, the results of tap tests prior to Repair 1 and Repair 2 Load Tests indicate very minimal voids and no extensive bond failure, which leads to the conclusion that the FRP-system integrity is not in question. An additional demand on Girder 3 may occur for three reasons: the limitations the curb imposes on placing the load test trucks directly over exterior girders may create incongruence in testing, the trucks may have been slightly off-position in one or more of the tests, or there may be a crack that is outside of the limits of repair on Girder 3 which accentuates the effects of the loading.

7.6 FRP Strain Comparisons and Results

FRP strains were gauged for the Repair 1, Repair 2, and Repair 3 Load Tests. The FRP strain comparisons are made for both LC5 and LC6 loadings, as LC5 was used for the Repair 1 and Repair 2 Load Tests while LC6 was used on the Repair 3 Load Test. While useful for determining whether the rehabilitative effects of the FRP retain integrity within six months after application, they are not particularly useful for ascertaining whether or not a benefit has been made to the overall strength capacity of the bridge.

An examination of FRP strains for the Repair 1, Repair 2, and Repair 3 Load Tests is less informative than examination of the reinforcing steel strains. Shown in Figures 7.13 through 7.20, it is seen immediately that the model overestimated actual FRP strains. However, a narrow range of difference between analytical and experimental FRP strains is not discernible as it is for the steel strains. This is most likely due to the nature of the gauged locations for FRP measurements. To be most beneficial, FRP gauges need to

bridge a crack in the concrete. This proved to be a problem in the War Memorial Bridge instrumentation, as discussed below.

For the first two repaired bridge tests, FRP gauges were located at the critical sections defined as Cross Sections 9, 10, and 11. Therefore, these gauges were applied to the FRP where it was bonded to the concrete used to patch the reinforcing bar gauge sections. After the tests, it was discovered that the cracks passed around the patch material, rather than through it. Thus, these FRP gauges did not bridge actual cracks. The analytical strains are computed based on the assumption that the concrete carries no tension. However, the gauged sections were not completely cracked, and the concrete can be expected to carry a portion of the tension. Thus, the experimental FRP strains are significantly less than predicted by the analytical model. As proximity of these gauges to the actual cracks varied, so too did the variance between analytical and experimental results.

Prior to the Repair 3 Load Test, new gauges were installed at locations close to the critical sections but where a crack was actually located. From crack maps and interpolation, attempts to place the gauges on the FRP where they would span a crack were made. Still, because the FRP covered the actual crack path, it is not certain that any FRP gauge actually spans a crack. Therefore, FRP results are not as reliable for making conclusions regarding the effectiveness of the FRP in positive moment reinforcement.

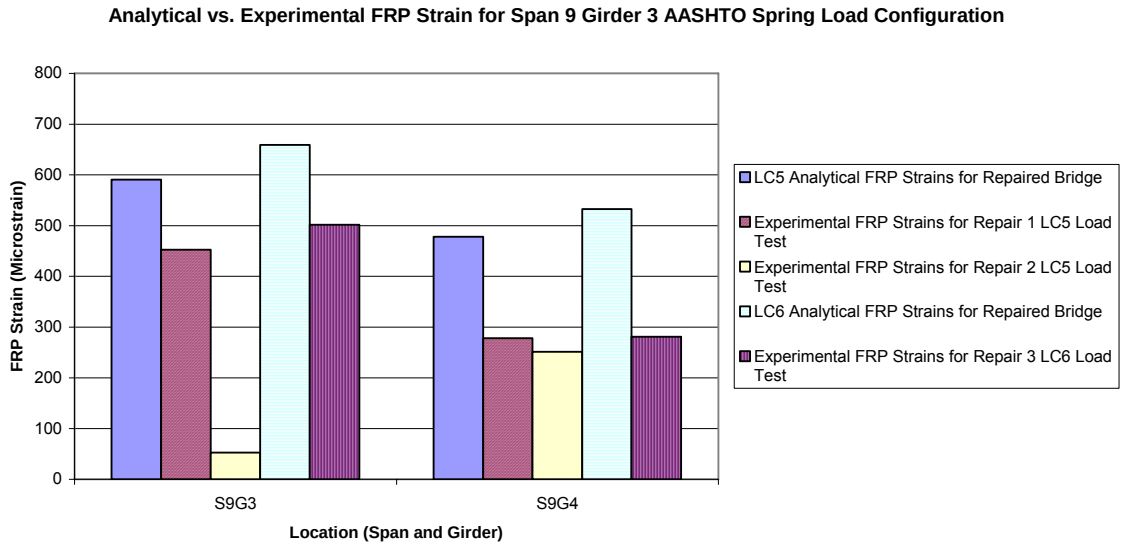

Figure 7.13: FRP Strain Comparison for Span 9 Girder 3 AASHTO Loading

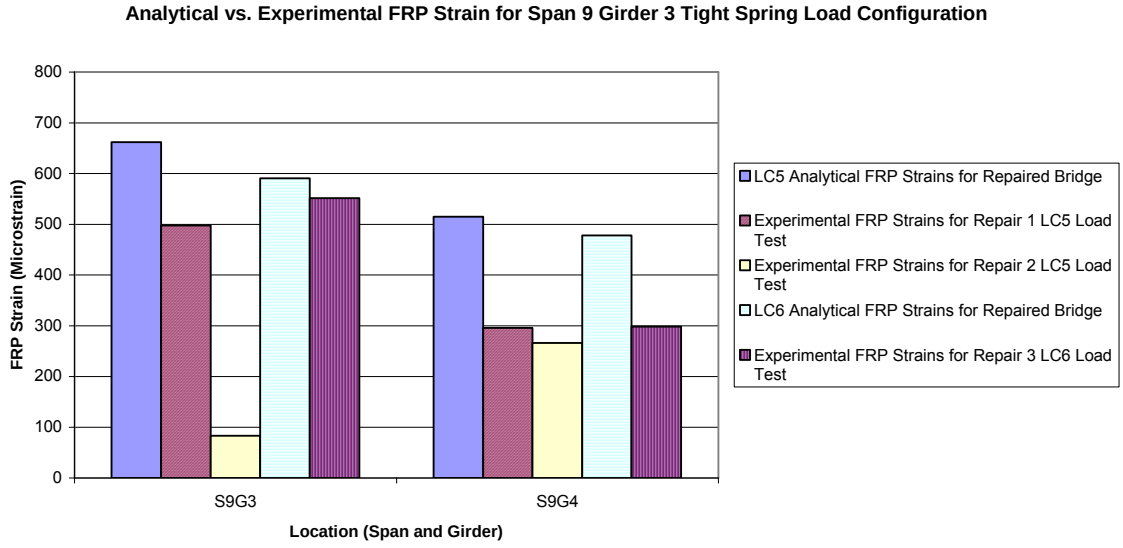

Figure 7.14: FRP Strain Comparison for Span 9 Girder 3 Tight Loading

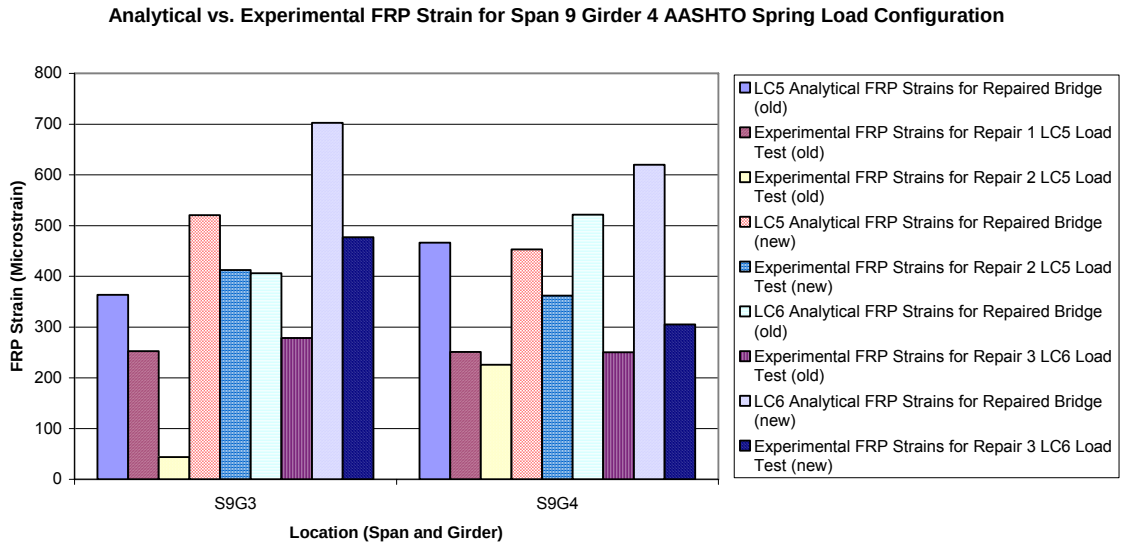

Figure 7.15: FRP Strain Comparison for Span 9 Girder 4 AASHTO Loading

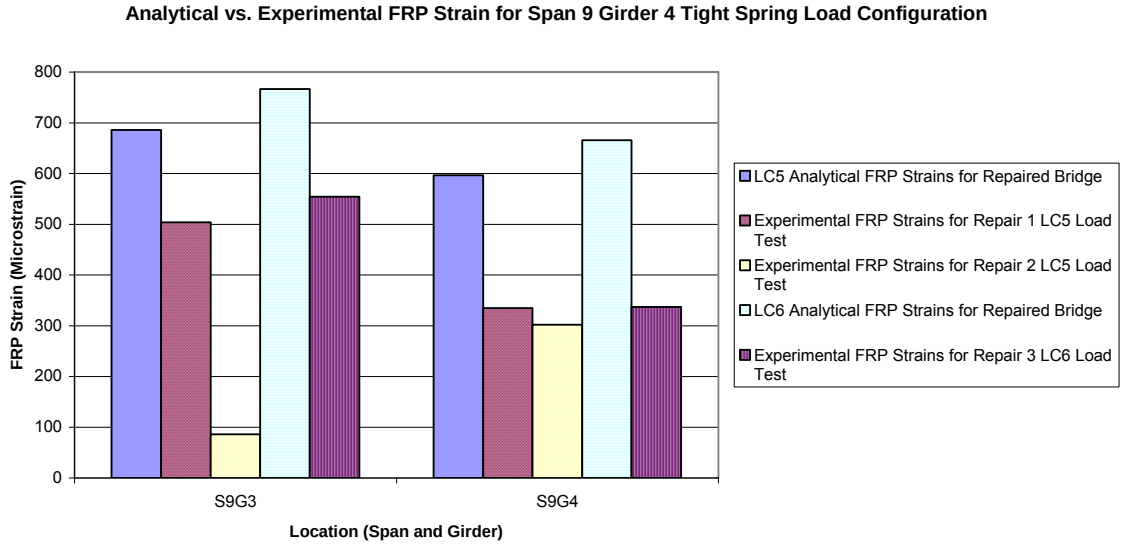

Figure 7.16: FRP Strain Comparison for Span 9 Girder 4 Tight Loading

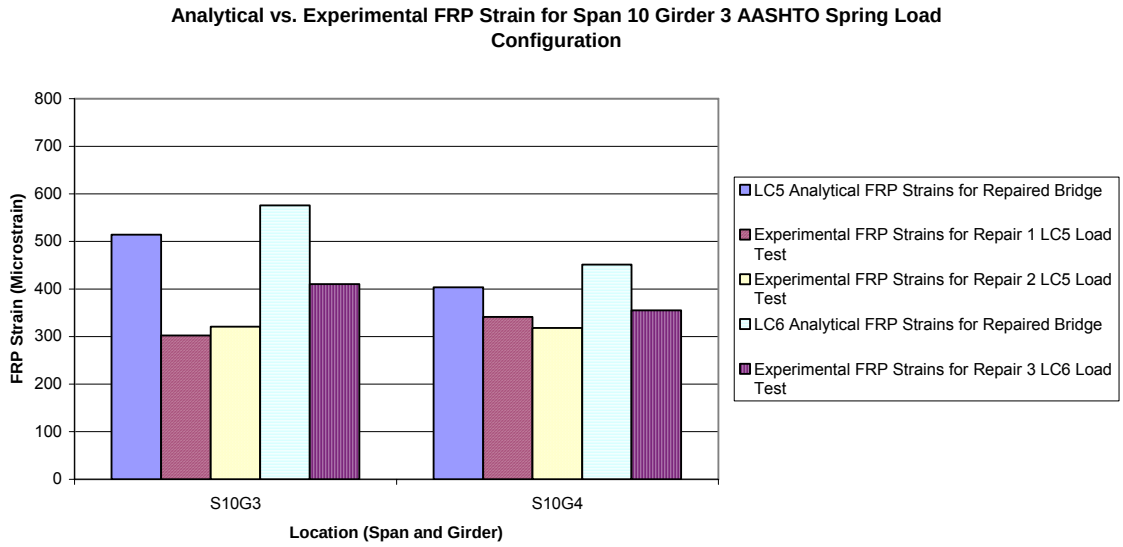

Figure 7.17: FRP Strain Comparison for Span 10 Girder 3 AASHTO Loading

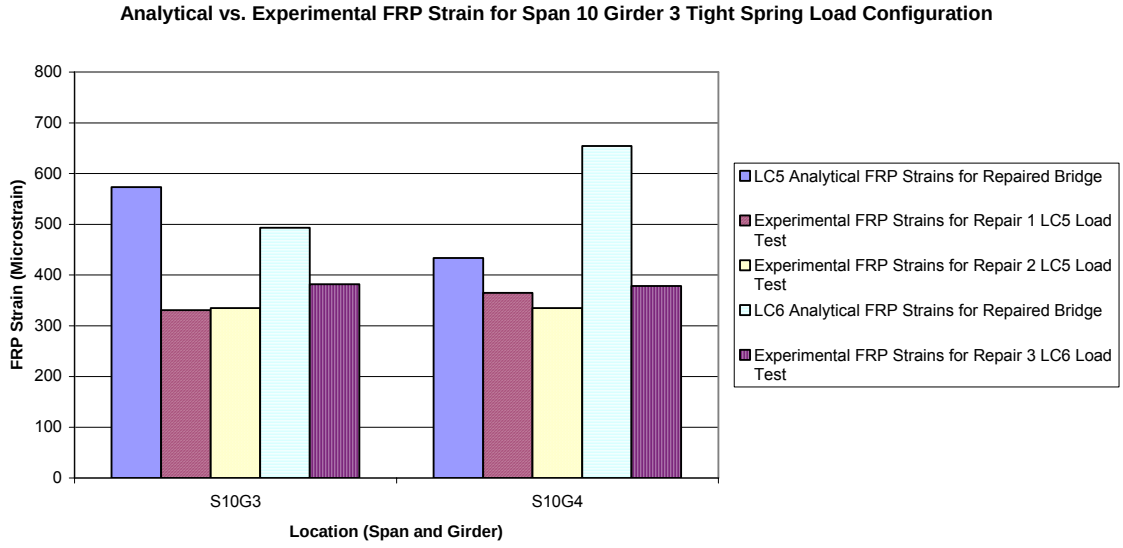

Figure 7.18: FRP Strain Comparison for Span 10 Girder 3 Tight Loading

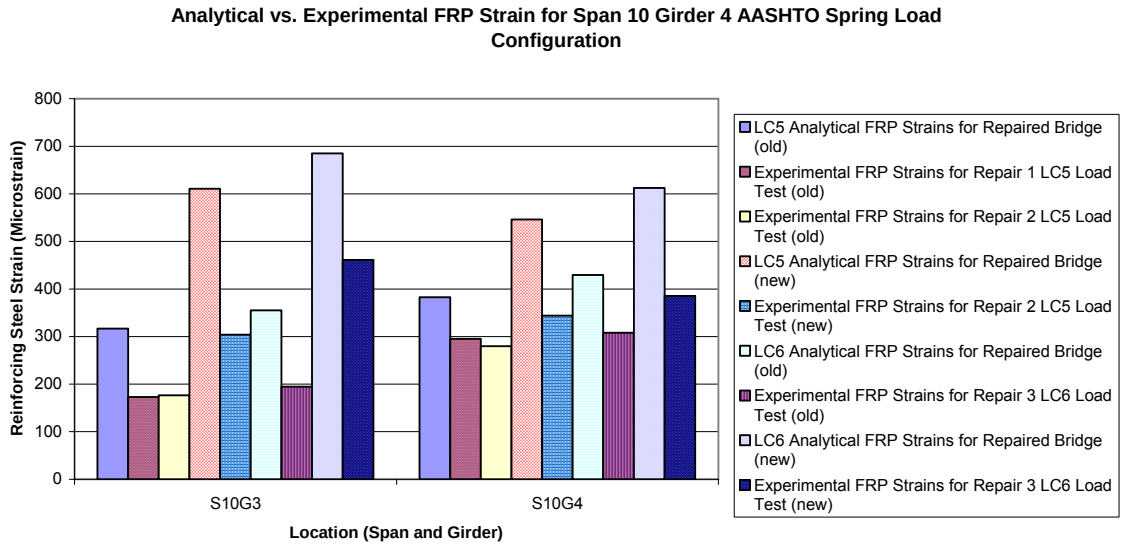

Figure 7.19: FRP Strain Comparison for Span 10 Girder 4 AASHTO Loading

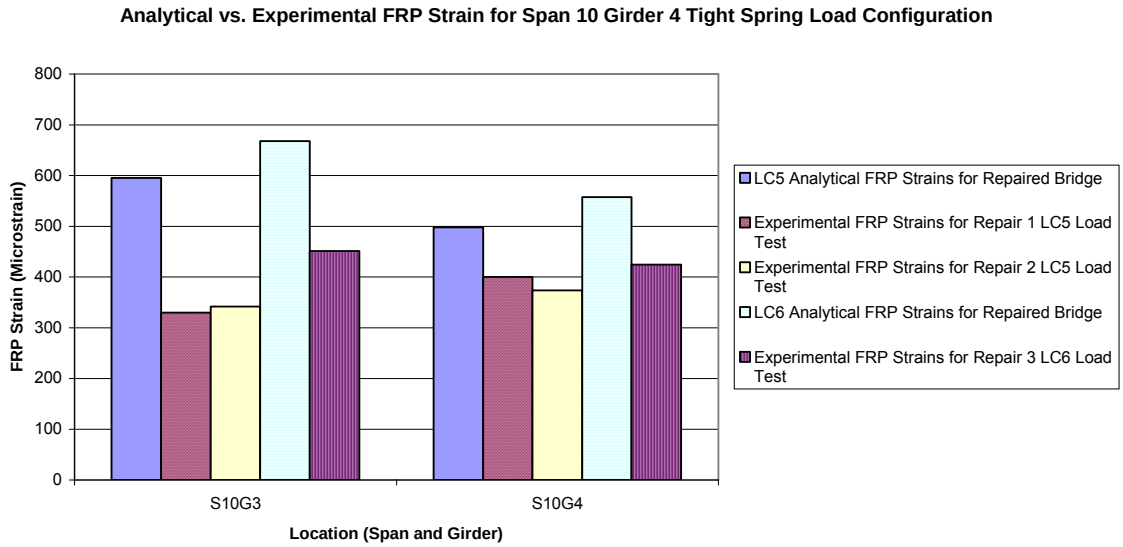

Figure 7.20: FRP Strain Comparison for Span 10 Girder 4 Tight Loading

Some useful information can be still gleaned from the FRP results. By comparing the values from the Repair 1 and Repair 2 Load Tests, it is more evident that some phenomenon exists which created more demand on Girder 3 in the Repair 2 Load Test, as discussed previously in this chapter. It is noteworthy that for Span 10 critical loadings, all FRP strain values on Span 10 Girder 4 were less for the Repair 2 Load Test than the Repair 1 Load Test. At the same time, all FRP strains on Span 10 Girder 3 were greater for the Repair 2 Load Test than the Repair 1 Load Test. The occurrence of this strain increase, though curious, should not warrant concern with the repair. It does indicate that the girder is carrying more moment, which suggests that something has created more demand on Girder 3 in the Repair 2 and Repair 3 Load Test. Some reasons for this demand increase are given at the conclusion of Section 7.5. Comparisons between the Repair 1 and Repair 2 Load Tests cannot be made for Span 9 Girder 3 values due to the appearance of erroneous results from the critical strain gauge. This can be seen in Figures 7.13-7.16. A poor electrical connection is the most likely source of the suspiciously low values output from this sensor. Span 9 Girder 4 data may be useful where instruments record a reduction in FRP strain for Span 9 critical loading from Repair 1 Load Test to Repair 2 Load Test, closely imitating results for Span 10 Girder 4 under Span 10 critical loading.

7.7 SUMMARY OF RESULTS

The integrity of the FRP strengthening system is necessarily of primary concern to potential users. Of the two instrumented girders on the War Memorial Bridge, testing indicates no strong evidence of delamination on either girder. While there are some variations in strain reduction between the Repaired Load Tests, it is most likely due to an

increase in demand on Girder 3. In the short term, it appears that the bond integrity remains sufficient to provide adequate FRP performance for providing additional capacity. The overall reduction in steel strain is approximately 5%. Agreement between behavior predicted by the model and that observed in the field was good. The model was found to be conservative in prediction of actual strains on the bridge by up to 25% except in Span 10 Girder 3 critical loadings, where the model underestimates actual strains by up to 8%. A tap test indicated no serious delamination in the FRP bond. The integrity of the installation appeared to be sound six months after installation. As the bond is the critical element in the life of the repair, long term tests regarding the epoxy's ultimate life span would need to be conducted.

CHAPTER 8: SUMMARY AND CONCLUSIONS

8.1 GENERAL

A study was performed to analyze the performance of carbon fiber-reinforced polymer (FRP) laminate strips on the War Memorial Bridge and to gauge the practicality of utilizing this technique to rehabilitate additional deficient infrastructure in the Alabama transportation system. The War Memorial Bridge, whose construction was completed in 1945, spans the Uphapee Creek in Macon County on Alabama Highway 81 and was determined to be structurally deficient in the positive moment regions of the three-span continuous portion of the bridge. FRP was applied to the girder bottom in the positive moment regions of the three-span section. The study consisted of a control load test, the Existing Load Test, of the bridge in its pre-strengthened state, and three load tests, the Repaired Load Tests, of the repaired bridge to determine the effectiveness of the FRP repair. The repair was studied and evaluated and conclusions made regarding the effectiveness of the repair.

8.2 DESIGN AND INSTALLATION

A design was formulated and proposed by Swenson and Barnes (2002) in a previous report, and the repair was implemented based on that design. The Tyfo UC brand composite system from Fyfe Company, LLC., was utilized as the basis of design. Materials were procured, and beginning in late October 2001, installation was performed by Auburn University personnel working with an Alabama Department of Transportation

bridge maintenance crew. The preparatory work duration, including preparation of the concrete surfaces of the girder, instrumentation of existing reinforcing steel, and crack injection was approximately one month. Total duration for the actual FRP installation was six working days. A suspended scaffolding system was necessary from which to work to install the FRP to the girder bottoms. Tools required for the installation are readily available for any state DOT crew and in any hardware store. Light chemical resistant suits should be used as a minimum requirement for workers in order to prevent prolonged skin contact to the epoxy for health reasons.

8.3 TESTING AND ANALYSIS

Four load tests were performed on the War Memorial Bridge—one on the unrepaired bridge and three on the repaired bridge, referenced as the Existing Load Test, Repair 1 Load Test, Repair 2 Load Test, and Repair 3 Load Test, respectively. On the Existing Load Test, the positive moment reinforcing steel strains and girder deflections were measured at cross sections located on Spans 9 and 10. On the Repair 1 and Repair 2 Load Tests, the positive moment reinforcing steel strains, FRP strains, and girder deflections were measured on Spans 9 and 10 in the same critical locations. For the Repair 3 Load Test, only FRP strains and girder deflections were measured. Load test trucks of identical weights which simulated the tri-axle dump truck that is restricted from using the War Memorial Bridge were used in the first three load tests. A heavier load test truck was used in the Repair 3 Load Test. Strain values from the load tests were used for comparison to a finite-element computer model of the bridge.

For the computer model, a finite-element model was created using the ADINA program. Three models were created with different interior supports, defined by using

varying spring stiffness at the intersection of the girders and bents to simulate the support conditions. The model neglected the effect of the guardrails and raised curbs on the roadway. The Spring Model, which used a spring constant determined from a finite-element model of the bent to model the effect of the lateral movement of the piers at interior bents, was determined to most closely model bridge behavior. Nodal data were extracted at critical cross sections from the model that corresponded to the instrumented cross sections on the actual bridge, and the nodal data were converted to strain values at locations of the reinforcing steel and FRP through a cracked-section property analysis.

8.4 RESULTS

Strains from the model were compared with strains from the four load tests to validate bridge performance immediately after FRP installation and after a period of six months of use. Additionally, the usefulness of the FRP model as a design and evaluation aid was examined.

The model was found to be conservative in prediction of actual strains on the bridge by up to 25%. However, behavior on the bridge was well predicted by the model. The model predicted a reduction in strain of about 4-6% in the reinforcing steel; the experimental data collected supported this prediction. Some increase can be seen in the reinforcing steel strain between the Repair 1 Load Test and Repair 2 Load Test. A likely cause of this is more moment on the girder as a result of some slight shifting of truck positions between tests. It was found that comparisons made between FRP strain values were not reliable for determining conclusions regarding the FRP benefit to the bridge. However, the trends that are evident in the FRP strain data support the model's behavioral predictive abilities. A tap test indicated no serious delamination in the FRP

bond between tests. Overall, the integrity of the installation seems to be sound six months after installation.

8.5 CONCLUSIONS

From the finite element analysis and four load tests of the War Memorial Bridge, some observations can be made regarding the practicality of adopting FRP on a large scale as a rehabilitative method for aging infrastructure. For FRP laminates to be attractive for repairs, the installation process must be efficient and economical for state DOT's, and the repair must remain effective for many years after installation. Relative to many other methods of bridge rehabilitation, installing FRP is very cost-effective. Resources are minimal; a typical installation should consist of no more than the following:

- access to the area of repair through scaffolding, boom truck, etc.
- a crew of four to six men, depending on FRP size
- job truck with a portable work surface (e.g., plywood and sawhorses), a small generator, and miscellaneous small tools
- personal protective equipment, such as a chemical suit, gloves, safety glasses, etc.

The scope of work for FRP installation is much smaller than for most other contemporary repair work. However, the work is excessively messy, and many of the tools used in the FRP application will have to be thrown away upon job completion. Unless a state DOT wishes to devote a crew solely to the installation of FRP laminates to ailing reinforced concrete members, it might be an attractive option for the agency to contract out installation, as ALDOT did after installation on the War Memorial Bridge.

The integrity of the installation is necessarily of primary concern to potential users. Of the two measured girders on the War Memorial Bridge, load tests and tap tests indicate

no evidence of serious delamination on either girder. Some small isolated spots of delamination are present, but their size and the load test results indicate that they are not a problem. Through attention during the FRP installation to ensure a liberal amount of epoxy coverage on both the FRP strip and the substrate, as well as proper pressure on the FRP to promote complete bonding, the bond integrity remained effective over six months of use. As the bond is the critical element in the life of the repair, long term tests regarding the epoxy's ultimate life span would need to be conducted to determine long-term performance. However, if expected life of the epoxy is even as short as ten years, many state DOT's might find it more economical to repair a structure in this manner every ten years rather than pay for labor-intensive and material-intensive repairs or total replacement.

For predicting and interpreting the behavior of a rehabilitated structure, the use of a finite element analysis model proves to be a useful tool. The model is conservative in predicting actual steel strain values, but appears to be correct in predicting behavior and provides a reference for deducing problems in the bridge from the experimental data. It was seen in the load test results that overall initial reduction in steel strain is approximately 4-8% and is predicted by the model. Agreement between behavior predicted by the model and that observed in the field was good. Based on comparisons and the tap tests, cases where the model and the experiment were not in accord point to issues that are most likely not related to bond failure. The finite element model could be refined to include phenomena such as concrete cracking, reinforcement (steel and FRP) bond, etc., which could yield more precise and accurate predictions. The inclusion of these phenomena in refining the model is not in the scope of this report.

When considering the costs involved with this repair, states will no doubt see a dramatic difference in overall project costs and duration when compared to traditional methods of bridge repair or rehabilitation. They should also note a difference in resources needed to complete the work, with FRP repairs having the advantage over traditional methods. Consequently, use of FRP as a repair method has great promise for continued infrastructure repair. Providing that the amount of FRP installed is properly designed and dimensioned for prescribed design loads, using FRP for rehabilitation can be an attractive and viable option for state DOT's in future years to help meet capacity demands by revitalizing aging infrastructure.

REFERENCES

AASHTO. 1994. *Manual for Condition Evaluation of Bridges*. American Association of State Highway and Transportation Officials. Second Edition. Washington D.C.

AASHTO. 1996. *Standard Specifications for Highway Bridges*. American Association of State Highway and Transportation Officials. Sixteenth Edition. Washington, D.C.

ACI Committee 224. 1993. *ACI 224.1R-93 - Causes, Evaluation, and Repair of Cracks in Concrete Structures*. American Concrete Institute. Farmington Hills, MI.

ACI Committee 318. 2002. *Building Code Requirements for Structural Concrete (318-02) and Commentary (ACI 318R-02).* American Concrete Institute. Farmington Hills, MI.

ACI Committee 440. 1996. *ACI 440R-96 - State of the Art Report on Fiber Reinforced Plastic Reinforcement for Concrete Structures*. American Concrete Institute. Farmington Hills, MI.

ACI Committee 440. 2002. *ACI 440R-02 - Design and Construction of Externally Bonded FRP Systems for Strengthening Concrete Structure*. American Concrete Institute. Farmington Hills, MI.

Aprile, A., E. Spacone and S. Limkatanyu. 2001. Role of Bond in RC Beams Strengthened with Steel and FRP Plates. *Journal of Structural Engineering* (December): 1445-52.

Arduini, M., A. Nanni, and M. Romagnolo. 2002. Performance of Decommissioned Reinforced Concrete girders strengthened with Fiber-Reinforced Polymer Laminates. *ACI Structural Journal* 99, no. 5 (September-October): 652-9.

Barnes, R.A. and G.C. Mays. 2001. The Effect of Traffic Vibration on Adhesive Curing During Installation of Bonded External Reinforcement. *Structures & Buildings* 146, no. 4: 403-10.

Collins, M.P. and D. Mitchell. 1991. *Prestressed Concrete Structures*. Prentice Hall. Englewood Cliffs, NJ.

El-Mihilmy, M. and J.W. Tedesco. 2000. Analysis of Reinforced Concrete Beams Strengthened with FRP Laminates. *Journal of Structural Engineering* (June): 684-91.

Frosch, R.W. 1999. Another Look at Cracking and Crack Control in Reinforced Concrete. *ACI Structural Journal* 96, no. 3 (May–June): 437–42.

Mayo, R., A. Nanni, S. Watkins, M. Barker, and T. Boothby. 1999. *Strengthening of Bridge G-270 with Externally Bonded Carbon Fiber Reinforced Polymer (CFRP).* University of Missouri – Rolla: Center for Infrastructure Engineering Studies. Research Investigation R198-012.

Mapquest, Inc. 2005. October 2, 2005. <url:http://www.mapquest.com>

Monti, G. and E. Spacone. 2000. Reinforced Concrete Fiber Beam Element with Bond-Slip. *Journal of Structural Engineering* 126, no. 6: 654-61.

National Bridge Inventory. 2005. October 25, 2005. <url:http://www.nationalbridgeinventory.com/structurally_deficient.htm>

Nystrom, H.E., S.E. Watkins, A. Nanni, and S. Murray. 2003. Financial Viability of Fiber-Reinforced Polymer (FRP) Bridges. *Journal of Management in Engineering* (January): 2-8.

Petrou, M.F., K.A. Harries, and C. Papakonstantinou. 1999. *Bridge Rehabilitation Using Fiber Reinforced Polymer (FRP) Composites.* University of South Carolina. Report No. ST99-01.

Quantrill, R.J., L.C. Hollaway, and A.M. Thorne. 1996. Experimental and analytical investigation of FRP strengthened beam response: Part I. *Magazine of Concrete Research* (December): 331-342.

Rahami, H. and A. Hutchinson. 2001. Concrete Beams Strengthened with Externally Bonded FRP Plates. *Journal of Composites for Construction* (February): 44-56.

Reed, M. and R.W. Barnes. 2004. *Effects of Traffic Loads During FRP Strengthening of War Memorial Bridge*. Auburn, AL: Auburn University Highway Research Center. Interim Report RP-930-466-1.

Schiebel, S., R. Parretti, A. Nanni, and M. Huck. 2002. Strengthening and Load Testing of Three Bridges in Boone County, Missouri. *Practice Periodical on Structural Design and Construction* (November).

Shahrooz, B.M., S. Boy, and T.M. Baseheart. 2002. Flexural Strengthening of Four 76-Year-Old T-Beams with Various Fiber-Reinforced Polymer Systems: Testing and Analysis. *ACI Structural Journal* 99, no. 5 (September-October): 681-90.

Spacone, E. and S. Limkatanyu. 2000. Response of Reinforced Concrete Members Including Bond-Slip Effects. *ACI Structural Journal* 97, no. 6 (November-December).

Swenson, K.S. and R.W. Barnes. 2002. *Design Procedure for FRP Strengthening of War Memorial Bridge*. Auburn, AL: Auburn University Highway Research Center. Interim Report 930-466.

Tedesco, J.W., J.M. Stallings, and M. El-Mihilmy. 1999. *Finite Element Method Analysis of a Concrete bridge with Fiber Reinforced Plastic Laminates*. *Computer and Structures* 72.

Vecchio, F.J. and F. Bucci. Analysis of Repaired Reinforced Concrete Structures. *Journal of Structural Engineering* 125, no. 6 (June): 644-52.

Wong, R.S.Y. and F.J. Vecchio. 2003. Towards Modeling of Reinforced Concrete Members with Externally Bonded Fiber-Reinforced Polymer Composites. *ACI Structural Journal* 100, no. 1 (January-February): 47-55.

Ziraba, Y.N., M.H. Baluch, I.A. Basunbul, A.M. Sharif, A.K. Azad, and G.J. Al-Sulaimani. 1994. Guidelines toward the Design of Reinforced Concrete Beams with External Plates. *ACI Structural Journal* 91, no. 6 (November-December): 639-46.

APPENDICES

APPENDIX A: STEEL STRAIN COMPARISON TABLES

For the following tables, the table values are determined from the following formula:

$$\%\ \text{Difference} = \left(\frac{\text{A - B}}{\text{B}} \right) \times 100$$

where
A = test iteration on vertical column
B = test iteration on horizontal column

Key to Table Headings
A – Analytical
E – Existing Bridge Load Test
R – Repaired Bridge Load Test
1, 2, 3 – Repaired Bridge Load Test Iteration (Repair 1, Repair 2, Repair 3)
Old – AASHTO “Old” Load Configuration
New – AASHTO “New” Load Configuration

S9G3C1 Strains			S9G3 Differences				
	S9G3	S9G4	A-E	E	A-R	R1	R2
A-E	511	413	0.0%	14.3%	4.6%	20.9%	18.1%
E	447	350	-12.5%	0.0%	-8.5%	5.7%	3.3%
A-R	488	389	-4.4%	9.3%	0.0%	15.5%	12.9%
R1	423	331	-17.3%	-5.4%	-13.4%	0.0%	-2.3%
R2	433	331	-15.4%	-3.2%	-11.4%	2.3%	0.0%
			S9G4 Differences				
			A-E	E	A-R	R1	R2
			0.0%	17.9%	6.1%	24.9%	24.8%
			-15.2%	0.0%	-10.0%	6.0%	5.9%
			-5.7%	11.1%	0.0%	17.7%	17.7%
			-19.9%	-5.6%	-15.1%	0.0%	-0.1%
			-19.9%	-5.6%	-15.0%	0.1%	0.0%

Table A.1: Steel Strain Comparison for Span 9 Girder 3 AASHTO Load Configuration

S9G3C2 Strains			S9G3 Differences				
	S9G3	S9G4	A-E	E	A-R	R1	R2
A-E	571	445	0.0%	12.6%	4.3%	19.7%	15.9%
E	507	374	-11.2%	0.0%	-7.3%	6.4%	2.9%
A-R	547	420	-4.2%	7.9%	0.0%	14.8%	11.1%
R1	477	348	-16.5%	-6.0%	-12.9%	0.0%	-3.2%
R2	493	349	-13.7%	-2.9%	-10.0%	3.3%	0.0%
			S9G4 Differences				
			A-E	E	A-R	R1	R2
			0.0%	19.0%	6.1%	28.0%	27.5%
			-15.9%	0.0%	-10.8%	7.6%	7.2%
			-5.7%	12.2%	0.0%	20.7%	20.2%
			-21.9%	-7.0%	-17.1%	0.0%	-0.4%
			-21.6%	-6.7%	-16.8%	0.4%	0.0%

Table A.2: Steel Strain Comparison for Span 9 Girder 3 Tight Load Configuration

S9G4C1 Strains			S9G3 Differences						
	S9G3	S9G4	A-E	E	A-R-Old	R1	R2-Old	A-R-New	R2-New
A-E	313	403	0.0%	22.6%	4.3%	27.4%	22.7%	-39.8%	-24.0%
E	256	331	-18.4%	0.0%	-14.9%	4.0%	0.1%	-50.9%	-38.0%
A-R-Old	300	380	-4.2%	17.5%	0.0%	22.1%	17.6%	-42.3%	-27.2%
R1	246	311	-21.5%	-3.8%	-18.1%	0.0%	-3.7%	-52.7%	-40.4%
R2-Old	256	311	-18.5%	-0.1%	-14.9%	3.9%	0.0%	-50.9%	-38.1%
A-R-New	520	453	66.0%	103.5%	73.2%	111.6%	103.7%	0.0%	26.1%
R2-New	413	362	31.7%	61.4%	37.4%	67.8%	61.5%	-20.7%	0.0%
			S9G4 Differences						
			A-E	E	A-R-Old	R1	R2-Old	A-R-New	R2-New
			0.0%	22.0%	6.1%	29.7%	29.8%	-13.7%	29.8%
			-18.0%	0.0%	-13.0%	6.3%	6.4%	-33.8%	6.4%
			-5.7%	15.0%	0.0%	22.2%	22.4%	-20.1%	22.4%
			-22.9%	-5.9%	-18.2%	0.0%	0.1%	-39.2%	0.1%
			-23.0%	-6.0%	-18.3%	-0.1%	0.0%	-39.3%	0.0%
			12.3%	37.0%	19.1%	45.6%	45.8%	0.0%	45.8%
			-10.3%	9.4%	-4.8%	16.3%	16.5%	-25.2%	16.5%

Table A.3: Steel Strain Comparison for Span 9 Girder 4 AASHTO Load Configuration

S9G4C2 Strains			S9G3 Differences				
	S9G3	S9G4	A-E	E	A-R	R1	R2
A-E	592	516	0.0%	13.9%	4.3%	21.5%	16.9%
E	519	426	-12.2%	0.0%	-8.4%	6.7%	2.6%
A-R	567	486	-4.2%	9.2%	0.0%	16.5%	12.0%
R1	487	395	-17.7%	-6.3%	-14.1%	0.0%	-3.8%
R2	506	396	-14.4%	-2.5%	-10.7%	4.0%	0.0%
			S9G4 Differences				
			A-E	E	A-R	R1	R2
			0.0%	21.1%	6.1%	30.6%	30.4%
			-17.4%	0.0%	-12.4%	7.8%	7.7%
			-5.7%	14.2%	0.0%	23.1%	22.9%
			-23.4%	-7.3%	-18.8%	0.0%	-0.1%
			-23.3%	-7.1%	-18.6%	0.1%	0.0%

Table A.4: Steel Strain Comparison for Span 9 Girder 4 Tight Load Configuration

S10G3C1 Strains			S10G3 Differences				
	S10G3	S10G4	A-E	E	A-R	R1	R2
A-E	444	353	0.0%	-6.3%	4.3%	-0.7%	-3.3%
E	473	364	6.7%	0.0%	11.4%	6.0%	3.2%
A-R	425	334	-4.2%	-10.2%	0.0%	-4.8%	-7.3%
R1	447	343	0.7%	-5.7%	5.1%	0.0%	-2.6%
R2	459	344	3.4%	-3.1%	7.9%	2.7%	0.0%
			S10G4 Differences				
			A-E	E	A-R	R1	R2
			0.0%	-3.1%	5.8%	2.9%	2.6%
			3.2%	0.0%	9.1%	6.1%	5.9%
			-5.4%	-8.4%	0.0%	-2.7%	-3.0%
			-2.8%	-5.8%	2.8%	0.0%	-0.2%
			-2.5%	-5.6%	3.1%	0.2%	0.0%

Table A.5: Steel Strain Comparison for Span 10 Girder 3 AASHTO Load Configuration

S10G3C2 Strains			S10G3 Differences				
	S10G3	S10G4	A-E	E	A-R	R1	R2
A-E	495	379	0.0%	-7.6%	4.3%	-1.8%	-4.0%
E	535	386	8.2%	0.0%	12.9%	6.3%	3.9%
A-R	474	359	-4.2%	-11.4%	0.0%	-5.9%	-8.0%
R1	504	369	1.8%	-5.9%	6.2%	0.0%	-2.2%
R2	515	364	4.1%	-3.8%	8.6%	2.3%	0.0%
			S10G4 Differences				
			A-E	E	A-R	R1	R2
			0.0%	-1.9%	5.8%	2.8%	4.1%
			1.9%	0.0%	7.8%	4.8%	6.1%
			-5.4%	-7.2%	0.0%	-2.8%	-1.5%
			-2.8%	-4.6%	2.8%	0.0%	1.2%
			-4.0%	-5.7%	1.6%	-1.2%	0.0%

Table A.6: Steel Strain Comparison for Span 10 Girder 3 Tight Load Configuration

S10G4C1 Strains			S10G3 Differences						
	S10G3	S10G4	A-E	E	A-R-Old	R1	R2-Old	A-R-New	R2-New
A-E	273	335	0.0%	0.6%	4.3%	5.2%	2.0%	-45.8%	-37.1%
E	272	321	-0.6%	0.0%	3.7%	4.5%	1.3%	-46.2%	-37.5%
A-R-Old	262	317	-4.2%	-3.5%	0.0%	0.8%	-2.3%	-48.1%	-39.8%
R1	260	309	-4.9%	-4.3%	-0.8%	0.0%	-3.1%	-48.5%	-40.2%
R2-Old	268	311	-2.0%	-1.3%	2.3%	3.1%	0.0%	-46.9%	-38.4%
A-R-New	505	452	84.6%	85.8%	92.6%	94.2%	88.3%	0.0%	16.1%
R2-New	435	374	59.1%	60.1%	66.0%	67.4%	62.2%	-13.8%	0.0%
			S10G4 Differences						
			A-E	E	A-R-Old	R1	R2-Old	A-R-New	R2-New
			0.0%	4.3%	5.8%	8.6%	7.7%	-25.9%	-10.5%
			-4.1%	0.0%	1.4%	4.1%	3.3%	-28.9%	-14.1%
			-5.4%	-1.4%	0.0%	2.7%	1.8%	-29.9%	-15.3%
			-7.9%	-4.0%	-2.6%	0.0%	-0.8%	-31.7%	-17.5%
			-7.1%	-3.2%	-1.8%	0.8%	0.0%	-31.2%	-16.9%
			34.9%	40.7%	42.7%	46.5%	45.3%	0.0%	20.8%
			11.7%	16.4%	18.1%	21.3%	20.3%	-17.2%	0.0%

Table A.7: Steel Strain Comparison for Span 10 Girder 4 AASHTO Load Configuration

S10G4C2 Strains			S10G3 Differences				
	S10G3	S10G4	A-E	E	A-R	R1	R2
A-E	514	436	0.0%	-6.4%	4.3%	0.4%	-2.1%
E	549	435	6.8%	0.0%	11.4%	7.2%	4.5%
A-R	492	412	-4.2%	-10.3%	0.0%	-3.8%	-6.2%
R1	512	409	-0.4%	-6.8%	3.9%	0.0%	-2.5%
R2	525	407	2.2%	-4.3%	6.6%	2.6%	0.0%
			S10G4 Differences				
			A-E	E	A-R	R1	R2
			0.0%	0.2%	5.8%	6.4%	7.1%
			-0.2%	0.0%	5.5%	6.2%	6.9%
			-5.4%	-5.2%	0.0%	0.6%	1.3%
			-6.0%	-5.8%	-0.6%	0.0%	0.7%
			-6.6%	-6.4%	-1.3%	-0.7%	0.0%

Table A.8: Steel Strain Comparison for Span 10 Girder 4 Tight Load Configuration

APPENDIX B: FRP STRAIN COMPARISON TABLES

For the following tables, the table values are determined from the following formula:

$$\%\ \text{Difference} = \left(\frac{\text{A - B}}{\text{B}} \right) \times 100$$

where

A = test iteration on vertical column
B = test iteration on horizontal column

Key to Table Headings

A – Analytical
E – Existing Bridge Load Test
R – Repaired Bridge Load Test
1, 2, 3 – Repaired Bridge Load Test Iteration (Repair 1, Repair 2, Repair 3)
Old – AASHTO “Old” Load Configuration
New – AASHTO “New” Load Configuration

S9G3C1 Strains			S9G3 Differences				
	S9G3	S9G4	A-R	R1	R2	A-R3	R3
A-R	591	478	0.0%	30.6%	1022.2%	-10.4%	17.8%
R1	453	278	-23.4%	0.0%	759.6%	-31.3%	-9.8%
R2	53	251	-91.1%	-88.4%	0.0%	-92.0%	-89.5%
A-R3	659	533	11.5%	45.6%	1151.8%	0.0%	31.4%
R3	501	281	-15.1%	10.8%	852.6%	-23.9%	0.0%
			S9G4 Differences				
			A-R	R1	R2	A-R3	R3
			0.0%	71.8%	90.2%	-10.3%	70.3%
			-41.8%	0.0%	10.7%	-47.8%	-0.9%
			-47.4%	-9.7%	0.0%	-52.8%	-10.5%
			11.4%	91.4%	112.0%	0.0%	89.7%
			-41.3%	0.9%	11.7%	-47.3%	0.0%

Table B.1: FRP Strain Comparison for Span 9 Girder 3 AASHTO Load Configuration

S9G3C2 Strains			S9G3 Differences				
	S9G3	S9G4	A-R	R1	R2	A-R3	R3
A-R	662	515	0.0%	33.1%	695.0%	12.1%	20.0%
R1	497	295	-24.9%	0.0%	497.1%	-15.8%	-9.8%
R2	83	266	-87.4%	-83.3%	0.0%	-85.9%	-84.9%
A-R3	591	478	-10.8%	18.8%	609.3%	0.0%	7.1%
R3	552	298	-16.7%	10.9%	562.3%	-6.6%	0.0%
			S9G4 Differences				
			A-R	R1	R2	A-R3	R3
			0.0%	74.4%	93.6%	7.8%	72.7%
			-42.6%	0.0%	11.0%	-38.2%	-1.0%
			-48.3%	-9.9%	0.0%	-44.3%	-10.8%
			-7.2%	61.8%	79.6%	0.0%	60.2%
			-42.1%	1.0%	12.1%	-37.6%	0.0%

Table B.2: FRP Strain Comparison for Span 9 Girder 3 Tight Load Configuration

S9G4C1 Strains			S9G3 Differences								
	S9G3	S9G4	A-R-Old	R1	R2-Old	A-R-New	R2-New	A-R3-Old	R3-Old	A-R3-New	R3-New
A-R-Old	363	467	0.0%	43.8%	728.3%	-30.2%	-12.0%	-10.5%	30.4%	-48.3%	-23.8%
R1	253	251	-30.5%	0.0%	475.9%	-51.5%	-38.8%	-37.8%	-9.3%	-64.0%	-47.0%
R-2-Old	44	226	-87.9%	-82.6%	0.0%	-91.6%	-89.4%	-89.2%	-84.3%	-93.8%	-90.8%
A-R-New	520	453	43.2%	106.0%	1086.3%	0.0%	26.1%	28.2%	86.8%	-25.9%	9.1%
R-2-New	413	362	13.6%	63.4%	840.7%	-20.7%	0.0%	1.7%	48.1%	-41.3%	-13.5%
A-R3-Old	406	521	11.7%	60.7%	825.2%	-22.0%	-1.6%	0.0%	45.7%	-42.2%	-14.9%
R-3-Old	279	251	-23.3%	10.3%	535.1%	-46.5%	-32.5%	-31.4%	0.0%	-60.3%	-41.6%
A-R3-New	702	620	93.3%	178.1%	1501.3%	35.0%	70.2%	73.1%	152.1%	0.0%	47.3%
R3-New	477	305	31.3%	88.8%	987.4%	-8.3%	15.6%	17.5%	71.2%	-32.1%	0.0%
			S9G4 Differences								
			A-R-Old	R1	R2-Old	A-R-New	R2-New	A-R3-Old	R3-Old	A-R3-New	R3-New
			0.0%	86.1%	106.4%	3.0%	28.9%	-10.5%	86.3%	-24.7%	52.9%
			-46.3%	0.0%	10.9%	-44.7%	-30.7%	-51.9%	0.1%	-59.5%	-17.8%
			-51.6%	-9.8%	0.0%	-50.1%	-37.5%	-56.6%	-9.8%	-63.5%	-25.9%
			-2.9%	80.7%	100.4%	0.0%	25.2%	-13.1%	80.8%	-26.9%	48.5%
			-22.4%	44.3%	60.1%	-20.1%	0.0%	-30.6%	44.5%	-41.6%	18.6%
			11.7%	107.9%	130.6%	15.1%	44.1%	0.0%	108.1%	-15.9%	70.9%
			-46.3%	-0.1%	10.8%	-44.7%	-30.8%	-51.9%	0.0%	-59.6%	-17.9%
			32.8%	147.1%	174.1%	36.8%	71.2%	18.8%	147.3%	0.0%	103.1%
			-34.6%	21.7%	35.0%	-32.7%	-15.7%	-41.5%	21.8%	-50.8%	0.0%

Table B.7: FRP Strain Comparison for Span 9 Girder 4 AASHTO Load Configuration

S9G4C2 Strains			S9G3 Differences				
	S9G3	S9G4	A-R	R1	R2	A-R3	R3
A-R	686	597	0.0%	36.1%	697.7%	-10.5%	23.7%
R1	504	335	-26.5%	0.0%	485.9%	-34.3%	-9.1%
R2	86	302	-87.5%	-82.9%	0.0%	-88.8%	-84.5%
A-R3	767	665	11.8%	52.2%	791.6%	0.0%	38.3%
R3	554	337	-19.2%	10.1%	544.8%	-27.7%	0.0%
			S9G4 Differences				
			A-R	R1	R2	A-R3	R3
			0.0%	78.3%	97.6%	-10.3%	77.0%
			-43.9%	0.0%	10.8%	-49.7%	-0.8%
			-49.4%	-9.8%	0.0%	-54.6%	-10.5%
			11.5%	98.8%	120.3%	0.0%	97.3%
			-43.5%	0.8%	11.7%	-49.3%	0.0%

Table B.4: FRP Strain Comparison for Span 9 Girder 4 Tight Load Configuration

S10G3C1 Strains			S10G3 Differences				
	S10G3	S10G4	A-R	R1	R2	A-R3	R3
A-R	514	403	0.0%	69.8%	60.3%	-10.7%	25.3%
R1	303	341	-41.1%	0.0%	-5.6%	-47.4%	-26.2%
R2	321	318	-37.6%	5.9%	0.0%	-44.3%	-21.8%
A-R3	576	451	12.0%	90.1%	79.5%	0.0%	40.3%
R3	410	355	-20.2%	35.5%	27.9%	-28.7%	0.0%
			S10G4 Differences				
			A-R	R1	R2	A-R3	R3
			0.0%	18.2%	26.8%	-10.6%	13.6%
			-15.4%	0.0%	7.3%	-24.3%	-3.8%
			-21.1%	-6.8%	0.0%	-29.5%	-10.4%
			11.9%	32.2%	41.9%	0.0%	27.1%
			-12.0%	4.0%	11.6%	-21.3%	0.0%

Table B.5: FRP Strain Comparison for Span 10 Girder 3 AASHTO Load Configuration

S10G3C2 Strains			S10G3 Differences				
	S10G3	S10G4	A-R	R1	R2	A-R3	R3
A-R	573	434	0.0%	73.3%	71.3%	16.3%	50.1%
R1	331	365	-42.3%	0.0%	-1.2%	-32.9%	-13.4%
R2	335	335	-41.6%	1.2%	0.0%	-32.1%	-12.4%
A-R3	493	654	-14.0%	49.1%	47.3%	0.0%	29.1%
R3	382	378	-33.4%	15.5%	14.1%	-22.6%	0.0%
			S10G4 Differences				
			A-R	R1	R2	A-R3	R3
			0.0%	18.8%	29.4%	-33.7%	14.6%
			-15.8%	0.0%	8.9%	-44.2%	-3.6%
			-22.7%	-8.2%	0.0%	-48.8%	-11.4%
			50.9%	79.4%	95.3%	0.0%	72.9%
			-12.7%	3.7%	12.9%	-42.2%	0.0%

Table B.6: FRP Strain Comparison for Span 10 Girder 3 Tight Load Configuration

S10G4C1 Strains			S10G3 Differences								
	S10G3	S10G4	A-R-Old	R1	R2-Old	A-R-New	R2-New	A-R3-Old	R3-Old	A-R3-New	R3-New
A-R-Old	317	383	0.0%	83.1%	79.6%	-48.1%	4.3%	-10.8%	62.7%	-53.7%	-31.2%
R1	173	295	-45.4%	0.0%	-1.9%	-71.7%	-43.0%	-51.3%	-11.2%	-74.7%	-62.4%
R-2-Old	177	280	-44.3%	2.0%	0.0%	-71.1%	-41.9%	-50.3%	-9.4%	-74.2%	-61.7%
A-R-New	611	546	92.6%	252.8%	245.9%	0.0%	100.9%	71.8%	213.4%	-10.9%	32.5%
R-2-New	304	344	-4.1%	75.6%	72.2%	-50.2%	0.0%	-14.5%	56.0%	-55.6%	-34.1%
A-R3-Old	355	429	12.1%	105.3%	101.3%	-41.8%	16.9%	0.0%	82.4%	-48.1%	-22.9%
R-3-Old	195	308	-38.5%	12.6%	10.4%	-68.1%	-35.9%	-45.2%	0.0%	-71.6%	-57.7%
A-R3-New	685	613	116.1%	295.7%	288.1%	12.2%	125.4%	92.7%	251.6%	0.0%	48.6%
R3-New	461	385	45.4%	166.2%	161.1%	-24.5%	51.6%	29.7%	136.5%	-32.7%	0.0%
			S10G4 Differences								
			A-R-Old	R1	R2-Old	A-R-New	R2-New	A-R3-Old	R3-Old	A-R3-New	R3-New
			0.0%	29.7%	36.9%	-29.9%	11.3%	-10.8%	24.5%	-37.5%	-0.6%
			-22.9%	0.0%	5.5%	-46.0%	-14.2%	-31.2%	-4.0%	-51.8%	-23.4%
			-26.9%	-5.2%	0.0%	-48.8%	-18.7%	-34.8%	-9.1%	-54.3%	-27.4%
			42.7%	85.1%	95.3%	0.0%	58.8%	27.2%	77.6%	-10.8%	41.8%
			-10.2%	16.5%	23.0%	-37.0%	0.0%	-19.9%	11.8%	-43.8%	-10.7%
			12.1%	45.4%	53.5%	-21.4%	24.8%	0.0%	39.6%	-29.9%	11.4%
			-19.6%	4.2%	10.0%	-43.7%	-10.6%	-28.3%	0.0%	-49.8%	-20.1%
			60.0%	107.5%	118.9%	12.1%	78.0%	42.6%	99.1%	0.0%	59.0%
			0.6%	30.5%	37.7%	-29.5%	12.0%	-10.3%	25.2%	-37.1%	0.0%

Table B.7: FRP Strain Comparison for Span 10 Girder 4 AASHTO Load Configuration

S10G4C2 Strains			S10G3 Differences				
	S10G3	S10G4	A-R	R1	R2	A-R3	R3
A-R	595	498	0.0%	80.5%	74.3%	-10.9%	31.9%
R1	330	400	-44.6%	0.0%	-3.5%	-50.6%	-26.9%
R2	342	374	-42.6%	3.6%	0.0%	-48.9%	-24.3%
A-R3	668	557	12.2%	102.5%	95.5%	0.0%	48.0%
R3	451	424	-24.2%	36.8%	32.1%	-32.4%	0.0%
			S10G4 Differences				
			A-R	R1	R2	A-R3	R3
			0.0%	24.6%	33.3%	-10.6%	17.4%
			-19.7%	0.0%	7.0%	-28.3%	-5.7%
			-25.0%	-6.6%	0.0%	-33.0%	-11.9%
			11.9%	39.4%	49.2%	0.0%	31.4%
			-14.8%	6.1%	13.6%	-23.9%	0.0%

Table B.8: FRP Strain Comparison for Span 10 Girder 4 Tight Load Configuration